Year : 2010

GLUTAMATERGIC REGULATION OF MITOCHONDRIAL ION DYNAMICS IN ASTROCYTES

Guillaume AZARIAS

Département de Biologie Cellulaire et Morphologie

GLUTAMATERGIC REGULATION OF MITOCHONDRIAL ION DYNAMICS IN ASTROCYTES

Thèse de doctorat en Neurosciences

présentée à la Faculté de Biologie et de Médecine de l'Université de Lausanne

par

Guillaume AZARIAS

Biologiste diplômé de l'Université de Paris VI, France

Jury

Prof. Jean-Pierre Hornung, Président
P.D. Dr. Jean-Yves Chatton, Directeur
Prof. Anita Lüthi, Expert interne
Prof. Luca Scorrano, Expert externe

Lausanne 2010

Programme doctoral interuniversitaire en Neurosciences des Universités de Lausanne et Genève

Imprimatur

Vu le rapport présenté par le jury d'examen, composé de

Président	Monsieur	Prof.	Jean-Pierre **Hornung**
Directeur de thèse	Monsieur	Dr	Jean-Yves **Chatton**
Co-directeur de thèse			
Experts	Madame	Prof.	Anita **Lüthi**
	Monsieur	Prof.	Luca **Scorrano**

le Conseil de Faculté autorise l'impression de la thèse de

Monsieur Guillaume Azarias

Master en Neurosciences Université de Paris VI, France

intitulée

**GLUTAMATERGIC REGULATION OF MITOCHONDRIAL
ION DYNAMICS IN ASTROCYTES**

Lausanne, le 30 juillet 2010

pour Le Doyen
de la Faculté de Biologie et de Médecine

Prof. Jean-Pierre Hornung

It Don't Mean a Thing (If It Ain't Got that Swing)

Duke Ellington, 1931

Résumé grand public

REGULATION GLUTAMATERGIQUE DES DYNAMIQUES IONIQUES DE MITOCHONDRIES DANS LES ASTROCYTES

GUILLAUME AZARIAS

Université de Lausanne, Département de Biologie Cellulaire et Morphologie

Le cerveau se compose de cellules nerveuses appelées neurones et de cellules gliales dont font partie les astrocytes. Les neurones communiquent entre eux par signaux électriques et en libérant des molécules de signalisation comme le glutamate. Les astrocytes ont eux pour charge de capter le glucose depuis le sang circulant dans les vaisseaux sanguins, de le transformer et de le transmettre aux neurones pour qu'ils puissent l'utiliser comme source d'énergie. L'astrocyte peut ensuite utiliser ce glucose de deux façons différentes pour produire de l'énergie : la première s'opère dans des structures appelées mitochondries qui sont capables de produire plus de trente molécules riches en énergie (ATP) à partir d'une seule molécule de glucose ; la seconde possibilité appelée glycolyse peut produire deux molécules d'ATP et un dérivé du glucose appelé lactate. Une théorie couramment débattue propose que lorsque les astrocytes capturent le glutamate libéré par les neurones, ils libèrent en réponse du lactate qui servirait de base énergétique aux neurones. Cependant, ce mécanisme n'envisage pas une augmentation de l'activité des mitochondries des astrocytes, ce qui serait pourtant bien plus efficace pour produire de l'énergie.

En utilisant la microscopie par fluorescence, nous avons pu mesurer les changements de concentrations ioniques dans les mitochondries d'astrocytes soumis à une stimulation glutamatergique. Nous avons démontré que les mitochondries des astrocytes manifestent des augmentations spontanées et transitoires de leur concentrations ioniques, dont la fréquence était diminuée au cours d'une stimulation avec du glutamate. Nous avons ensuite montré que la capture de glutamate augmentait la concentration en sodium et acidifiait les mitochondries des astrocytes. En approfondissant ces mécanismes, plusieurs éléments ont suggéré que l'acidification induite diminuerait le potentiel de synthèse d'énergie d'origine mitochondriale et la consommation d'oxygène dans les astrocytes. En résumé, l'ensemble de ces travaux suggère que la signalisation neuronale impliquant le glutamate dicte aux astrocytes de sacrifier temporairement l'efficacité de leur métabolisme énergétique, en diminuant l'activité de leurs mitochondries, afin d'augmenter la disponibilité des ressources énergétiques utiles aux neurones.

Résumé

REGULATION GLUTAMATERGIQUE DES DYNAMIQUES IONIQUES DE MITOCHONDRIES DANS LES ASTROCYTES

GUILLAUME AZARIAS

Université de Lausanne, Département de Biologie Cellulaire et Morphologie

La remarquable efficacité du cerveau à compiler et propager des informations coûte au corps humain 20% de son budget énergétique total. Par conséquent, les mécanismes cellulaires responsables du métabolisme énergétique cérébral se sont adéquatement développés pour répondre aux besoins énergétiques du cerveau. Les dernières découvertes en neuroénergétique tendent à démontrer que le site principal de consommation d'énergie dans le cerveau est situé dans les processus astrocytaires qui entourent les synapses excitatrices. Un nombre croissant de preuves scientifiques a maintenant montré que le transport astrocytaire de glutamate est responsable d'un coût métabolique important qui est majoritairement pris en charge par une augmentation de l'activité glycolytique. Cependant, les astrocytes possèdent également un important métabolisme énergétique de type mitochondrial. Par conséquent, la localisation spatiale des mitochondries à proximité des transporteurs de glutamate suggère l'existence d'un mécanisme régulant le métabolisme énergétique astrocytaire, en particulier le métabolisme mitochondrial.

Afin de fournir une explication à ce paradoxe énergétique, nous avons utilisé des techniques d'imagerie par fluorescence pour mesurer les modifications de concentrations ioniques spontanées et évoquées par une stimulation glutamatergique dans des astrocytes corticaux de souris. Nous avons montré que les mitochondries d'astrocytes au repos manifestaient des changements individuels, spontanés et sélectifs de leur potentiel électrique, de leur pH et de leur concentration en sodium. Nous avons trouvé que le glutamate diminuait la fréquence des augmentations spontanées de sodium en diminuant le niveau cellulaire d'ATP. Nous avons ensuite étudié la possibilité d'une régulation du métabolisme mitochondrial astrocytaire par le glutamate. Nous avons montré que le glutamate initie dans la population mitochondriale une augmentation rapide de la concentration en sodium due à l'augmentation cytosolique de sodium. Nous avons également montré que le relâchement neuronal de glutamate induit une acidification mitochondriale dans les astrocytes. Nos résultats ont indiqué que l'acidification induite par le glutamate induit une diminution de la production de radicaux libres et de la consommation d'oxygène par les astrocytes. Ces études ont montré que les mitochondries des astrocytes sont régulées individuellement et adaptent leur activité selon l'environnement intracellulaire. L'adaptation dynamique du métabolisme énergétique mitochondrial opéré par le glutamate permet d'augmenter la quantité d'oxygène disponible et amène au relâchement de lactate, tous deux bénéfiques pour les neurones.

Abstract

GLUTAMATERGIC REGULATION OF MITOCHONDRIAL ION DYNAMICS IN ASTROCYTES

GUILLAUME AZARIAS

University of Lausanne, Department of Cell Biology and Morphology

The remarkable efficiency of the brain to compute and communicate information costs the body 20% of its total energy budget. Therefore, the cellular mechanisms responsible for brain energy metabolism developed adequately to face the energy needs. Recent advances in neuroenergetics tend to indicate that the main site of energy consumption in the brain is the astroglial process ensheating activated excitatory synapses. A large body of evidence has now shown that glutamate uptake by astrocytes surrounding synapses is responsible for a significant metabolic cost, whose metabolic response is apparently mainly glycolytic. However, astrocytes have also a significant mitochondrial oxidative metabolism. Therefore, the location of mitochondria close to glutamate transporters raises the question of the existence of mechanisms for tuning their energy metabolism, in particular their mitochondrial metabolism.

To tackle these issues, we used real time imaging techniques to study mitochondrial ionic alterations occurring at resting state and during glutamatergic stimulation of mouse cortical astrocytes. We showed that mitochondria of intact resting astrocytes exhibited individual spontaneous and selective alterations of their electrical potential, pH and Na^+ concentration. We found that glutamate decreased the frequency of mitochondrial Na^+ transient activity by decreasing the cellular level of ATP. We then investigated a possible link between glutamatergic transmission and mitochondrial metabolism in astrocytes. We showed that glutamate triggered a rapid Na^+ concentration increase in the mitochondrial population as a result of plasma-membrane Na^+-dependent uptake. We then demonstrated that neuronally released glutamate also induced a mitochondrial acidification in astrocytes. Glutamate induced a pH-mediated and cytoprotective decrease of mitochondrial metabolism that diminished oxygen consumption. Taken together, these studies showed that astrocytes contain mitochondria that are individually regulated and sense the intracellular environment to modulate their own activity. The dynamic regulation of astrocyte mitochondrial energy output operated by glutamate allows increasing oxygen availability and lactate production both being beneficial for neurons.

I. Introduction

A. Foreword

The power requirement of a human body has recently been estimated to correspond to that of a light bulb of 116 Watts (Rich, 2003). As the brain accounts for 20% of total human body energy consumption (Magistretti, 2006), we can calculate that a human brain alone represents an energy consumption of ~ 25 Watts. This very high energy consumption is perhaps not surprising regarding the importance of brain size and complexity in the human evolution. However, the way the energy is generated and used remains debated in the scientific community. This thesis work was aimed at challenging some aspects of a 15-year old hypothesis on brain energy metabolism called astrocyte-neuron lactate shuttle.

The purpose of this introductory chapter is to provide a set of basic elements that have driven our experimental work, in order to place our results presented in the second section in their context.

B. Brain cells and energy metabolism

1. Cellular organization of cerebral cortex

The brain is composed of white matter, mainly constituted by conducting axons, and of gray matter. The gray matter is composed of interconnected neurons, blood capillaries and glial cells and represents the main site of energy consumption in the brain.

a) Neurons

Neurons are electrically-excitable cells able to rapidly communicate to each other to encode, store and retrieve information acquired during the life experiences. Neurons generally release either excitatory or inhibitory neurotransmitters. However, particular neurons are noteworthy able to release both excitatory and inhibitory transmitters (e.g. projection neurons from the supramamillary nucleus releasing both GABA and glutamate, Boulland et al., 2009). The inhibitory or excitatory effect of neurotransmitter is mainly determined by the type of receptors expressed at postsynaptic sites. The majority of neurons of the cerebral cortex are excitatory pyramidal neurons (i.e glutamatergic neurons). Although minor in proportion, inhibitory pathways are increasingly recognized as a relevant mechanism for excitability regulation (termed as "balanced inhibition"). Inhibitory neurons typically show high frequency of firing compared with excitatory neurons and are very variable in terms of markers, electrophysiological properties and morphology (Markram et al., 2004; Thomson and Lamy, 2007).

b) Cerebral vascular system

Glucose, which is the primary and almost exclusive source of energy of the brain, is transported in the blood by capillaries and vessels. The blood capillaries originating from carotid and vertebral arteries travel across the meninges, enter the brain cortex and subdivide sequentially down to fine capillaries irrigating the entire volume of gray matter. The blood flow destined to the brain represents over 10% of cardiac output (Magistretti, 2006) and remains extremely stable, even in the case of cardiac rhythm acceleration during physical exercise. Trafficking of glucose and other soluble molecules across vascular system is tightly regulated by endothelial cells constituting the blood-brain barrier together with basal lamina and pericytes (**Fig. 1**, Abbott et al., 2006). Therefore, the macromolecular and molecular composition of the interstitial fluid in the brain parenchyma is maintained different to that of the blood plasma and is regulated by the blood-brain barrier and the non-neuronal cells surrounding neurons called glial cells.
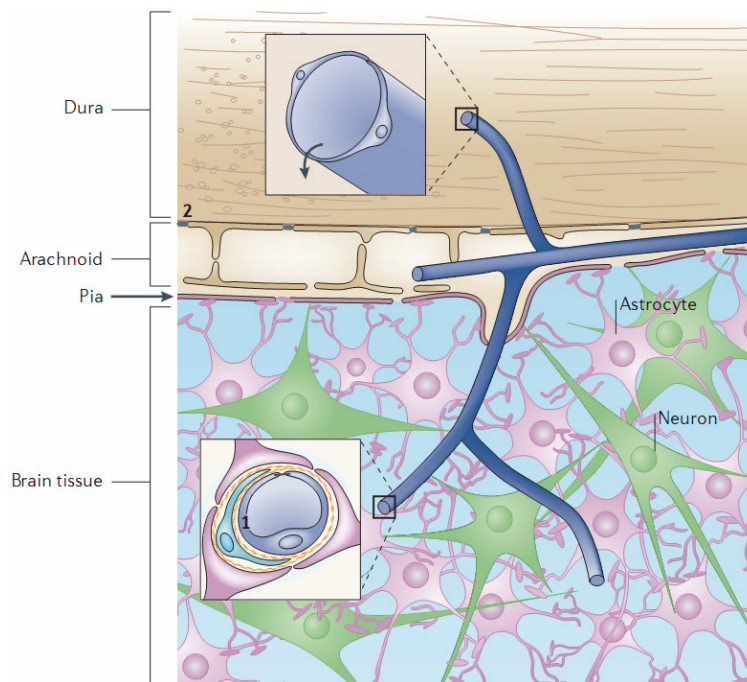
Fig. 1: Blood brain barrier in the central nervous system. Cerebral microvessels (blue) travelling across the meninges (composed of dura mater, arachnoid and pia) are composed of endothelial cells regulating the molecular exchanges with extracelllular space. The inset in the bottom part of the figure shows the detailed composition of blood brain barrier with endothelial cells (in blue), surrounded by basal lamina (yellow) and pericytes (light blue). Astrocytes (purple) physically link blood vessels to neurons (green). Adapted from Abbott et al., 2006.

c) Glial cells

In the central nervous system, glial cells account for half of the volume of human brain (Barres, 2008). Glial cells are categorized in two main groups, microglia and macroglia, based on their structural and functional properties:

- Microglial cells are immune cells of the central nervous system. Microglia play a crucial role in brain diseases such as stroke or multiple sclerosis (Matute and Perez-Cerda, 2005).

- Two different types of macroglia exist: oligodendrocytes and astrocytes:

    - Oligodendrocytes are glial cells whose major function is to electrically insulate neuronal axons to allow a highly reliable conduction of alterations of electrical membrane potential.

    - Astrocytes have been considered as passive cells until recently (Kettenmann and Verkhratsky, 2008). The astrocyte morphology, characterized by cellular protrusions contacting capillaries and neuronal synapses (**Fig. 2**) makes them privileged actors for sensing neuronal activity and adapt the extracellular composition for optimal neuronal activity. New functions of astrocytes are currently emerging such as regulated release of gliotransmitters (Volterra and Meldolesi, 2005) or regulation of sleep (Halassa et al., 2009) but those still remain highly debated (Hamilton and Attwell, 2010).
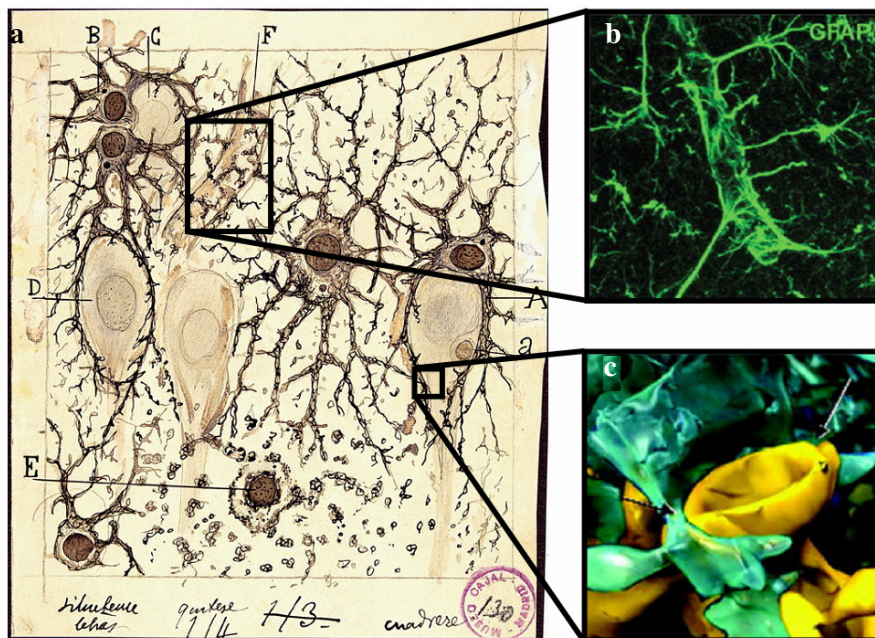
Fig. 2: Astrocyte morphology from endfeet touching capillaries to processes surrounding synapses. (**a**) Cajal's drawing of human hippocampus sublimated with the gold chloride method. Astrocytes (indicated by 'A'), pyramidal neuron (indicated by 'D'), twin astrocytes (indicated by 'B') and a satellite cell (indicated by 'a'). From Ramon y Cajal, 1913. (**b**) Perivascular astrocytes endfeet in GFAP-eGFP mice. From Rouach et al., 2008. (**c**) Three-dimensional reconstruction of a single astroglial process (blue) surrounding a dendrite (yellow). From Witcher et al., 2007.

Astrocytes processes ensheating neuronal synapses express many receptors sensitive to neurotransmitters that enable the astrocytes to establish a neuron to astrocyte communication. At perisynaptic sites, the astrocyte membrane possesses specific transporters that enable astrocytes to regulate extracelllular neurotransmitter and energy equivalent concentrations. As illustrated in **Fig. 3**, the tight distribution of astrocytes and neurons in the brain leaves only small space for the interstitial fluid, suggesting that the composition of interstitial fluid is mainly controlled by astrocytes.
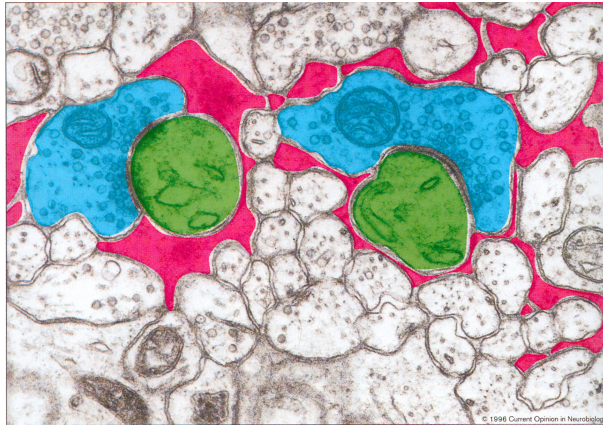
Fig. 3: Astrocytic processes ensheath synapses between CNS neurons. Micrograph of the molecular layer of monkey cerebellum. Presynaptic terminals (blue) ; postsynaptic spines (green) ; astrocytic processes (pink). Magnification 55 000x. From Pfrieger and Barres, 1996.

2. Brain energy metabolism

Until recently, it was believed that most of the energy in the brain was consumed for the propagation of action potentials and postsynaptic effects of glutamate (Attwell and Laughlin, 2001). However, recent advances in neuroenergetics revealed that the propagation of action potentials is energetically optimized, indicating that the proportion energy budget devoted to action potential propagation was overestimated. Thus, postsynaptic potentials dominate the energy requirements for neuronal signalling (Alle et al., 2009; Magistretti, 2009). Although Na^+-dependent glutamate uptake has only a marginal energetic cost, the Na^+ increase provides a signal to promote glucose uptake and a metabolic response in astrocytes (Magistretti, 2006). Importantly, astrocytes are numerically the major cell type of the brain, highlighting the importance of understanding their metabolism, for instance for the proper interpretation of brain imaging signals.

a) Glucose utilization by neurons

Neurons have long been considered as utilizing glucose as a unique source of energy. However, it has been shown that neurons can use lactate as well as a source of energy (Schurr et al., 1988; Izumi et al., 1997; Rouach et al., 2008). In addition, glucose and lactate are equally efficient for activity-dependent synaptic vesicle turnover in purified cortical neurons (Morgenthaler et al., 2006). The question of the dynamic coupling between neuronal energy consumption and increase of metabolic substrate delivery has been addressed 15 years ago by Pierre Magistretti and his colleagues. They proposed a model called the astrocyte-neuron lactate shuttle hypothesis summarized below.

11

b) The astrocyte-neuron lactate shuttle hypothesis

The astrocyte-neuron lactate shuttle hypothesis attempts to explain at the cellular level how energy metabolism is processed in the brain. This hypothesis proposes that astrocytes sense glutamatergic transmission activity and increase their glycolytic activity, even in the presence of oxygen (**Fig. 4**).

Mechanistically, glutamatergic synaptic activity was shown to trigger an energetic demand in astrocytes that generates a diffusion gradient for glucose within a network of astrocytes and that is directly linked to the level of neuronal activity (Rouach et al., 2008). The glutamate uptake through Na^+-coupled transporters induced a cytosolic Na^+ increase that was responsible for a metabolic cost due to increase of Na^+/K^+ ATPase activity by 2 to 3 fold (Chatton et al., 2000). The metabolic cost induced by cytosolic Na^+ increase has been proposed to be met mostly by glycolysis (Pellerin and Magistretti, 1994) although astrocytes contain also a substantial density of mitochondria (see special section below). The glycolysis-derived lactate would be released by astrocytes and transferred to neurons that would use it as metabolic substrate by conversion to pyruvate and utilization by neuronal mitochondria (Magistretti et al., 1999). This mechanism provides a framework for coupling neuronal activity to astrocyte metabolic response (termed "neurometabolic coupling").
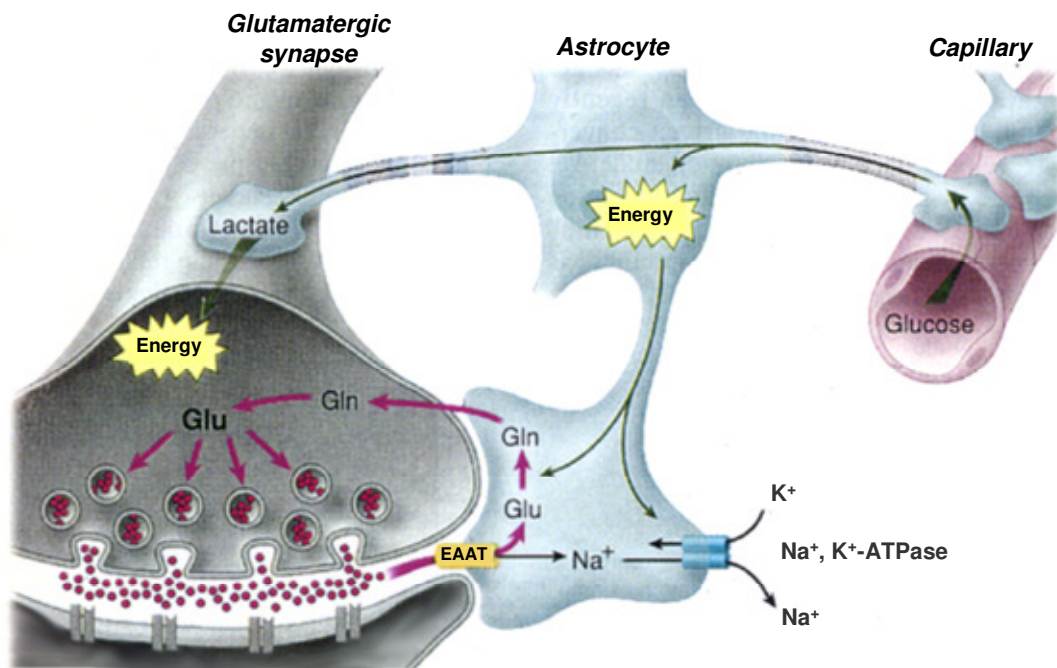
Fig. 4: The astrocyte-neuron lactate shuttle hypothesis. Neuronally released glutamate is taken up by surrounding astrocyte using the Na^+-coupled glutamate transporter EEAT. Glutamate is converted in glutamine and transferred back to neurons. The cytosolic Na^+ rise during glutamate uptake stimulates glucose uptake and "aerobic glycolysis". The glycolysis-derived lactate is transferred to neurons that use it as energy substrate. From Magistretti et al., 1999.

Ultrastructural analysis of cortical astrocytes and neurons indicated that all the elements involved in the astrocyte-neuron lactate shuttle hypothesis are expressed *in vivo*: astrocyte endfeet adjacent to endothelial cells express the glucose transporters GLUT1 that enables astrocytes to take up glucose from blood (**Fig. 5a**). Astrocytes express the lactate dehydrogenase 5 (LDH$_5$) preferentially converting pyruvate into lactate, whereas neurons express the isoform LDH$_1$ preferentially converting lactate into pyruvate (Pellerin et al., 1998). The expression of monocarboxylate transporters 1 (MCT1) in astrocytes of the cerebral cortex (Pierre et al., 2000) and MCT4 in Bergmann glia (**Fig. 5b**, Bergersen, 2007) indicate that astroglia is able to export intracellular lactate. Neurons express MCT2 indicating that they are able to take up extracelllular lactate (**Fig. 5c**, Pierre and Pellerin, 2005). Finally, astrocytes express glutamine synthetase whereas neurons express glutaminase, and both express the transporters of the glutamine-glutamate cycle (Chaudhry et al., 2002).
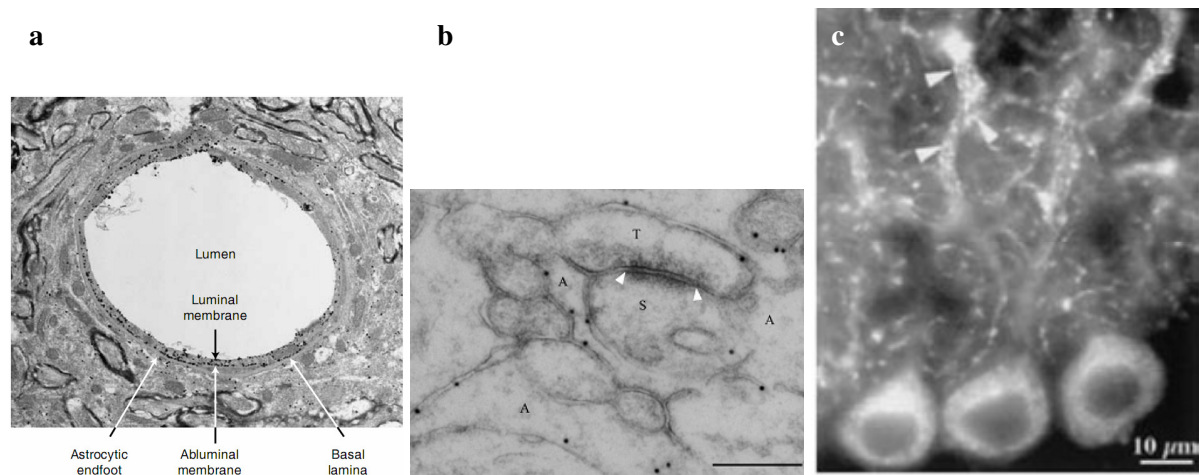
Fig. 5: *In vivo* **immunohistochemical pieces of evidence for the expression of the nutrient transporters involved in the astrocyte-neuron lactate shuttle** (a) Representative distribution of immunogold labelling of glucose transporter GLUT1 in endothelial cells and astrocytes endfeet. No scale bar was indicated. From Simpson et al., 2007. (b) Membranes of Bergmann glia facing the parallel fiber terminal and Purkinje cells spines and labelled with antibody to MCT4 (10 nm gold particles). Scale bar: 280nm. From Bergersen, 2007. (c) Immunoreactivity for MCT2 in Purkinje neurons of cerebellum. Arrowheads: punctiform staining for MCT2. From Pierre et al., 2002.

In vitro, glutamatergic stimulation of astrocytes was found to enhance lactate release through a signalling involving enhancement of Na$^+$/K$^+$ ATPase associated with intracellular Na$^+$ increase (Pellerin and Magistretti, 1994). Both the inhibition of Na$^+$/K$^+$ ATPase using ouabain (Pellerin and Magistretti, 1994) or replacement of cellular Na$^+$ by Li$^+$ (Voutsinos-Porche et al., 2003), a cation that is not transportable by the Na$^+$/K$^+$ ATPase, abolished the increase in glycolysis in cultured astrocytes stimulated with glutamate. In addition, glial glutamate transporters have been shown to play a pivotal role in neurometabolic coupling *in vivo* (Voutsinos-Porche et al., 2003). This study showed for instance that knockout mice for either the glutamate transporters GLAST or GLT-1 did not exhibit metabolic response to whisker stimulation, highlighting the pivotal role of glutamate uptake by astrocytes in the neurometabolic coupling.

C. Astrocyte metabolism

Although the key elements involved in the astrocyte-neuron lactate shuttle have been shown *in vivo*, the nature of the glucose metabolism within astrocytes remains a debated issue (Hertz et al., 2007). In particular, this model admittedly did not integrate the possibility of a mitochondrial contribution in the metabolic response induced by glutamate uptake (Pellerin and Magistretti, 2003). As in most cells, two major pathways of energetic metabolism for ATP synthesis co-exist in astrocytes, i.e. glycolysis and mitochondrial oxidative metabolism. The oxidative metabolism is the most efficient way to produce ATP and is confined in mitochondria. On the other hand, glycolysis is a less efficient pathway to produce ATP leading to high glucose consumption and lactate production.

1. Glycogen, the storage form of glucose

Glycogen is the largest energy reserve of the brain and is almost exclusively localized in the cytosol of astrocytes. The extremely rapid turnover of glycogen was found to be correlated with synaptic activity. After glycogen breakdown, the monomers of glucose-1-phosphate are converted into glucose-6-phosphate. However, glucose-6-phosphate cannot be dephosphorylated into glucose because of the lack of glucose-6-phosphatase expression in astrocytes. Therefore, the fate of glycogenolysis-derived glucose-6-phosphate is to be processed by glycolysis to produce energy.

2. Cytosolic glycolysis

Glycolysis is a 10-step sequence of enzymatic reactions taking place in the cytosol. The conversion of glucose in energy follows the stoichiometry:

$$\text{Glucose} + 2NAD^+ + 2ADP + 2Pi \rightarrow 2 \text{ pyruvate} + 2ATP + 2H_2O + 2NADH + 2H^+$$

The net glycolytic product is 2 molecules of pyruvate and 2 molecules of ATP from a single molecule of glucose. Pyruvate can further be used by mitochondria, entering the tricarboxylic acid cycle or can be converted to lactate by the lactate dehydrogenase using NADH as a co-factor.

According to the energy needs of the cell, three main glycolytic enzymes play a significant regulatory role in the glycolysis pathway. Most forms of hexokinases that phosphorylate glucose in glucose-6-phosphate are inhibited by high concentrations of its reaction product. Phosphofructokinase phosphorylating the fructose-6-phosphate is influenced by a wide range of inhibitors (mainly cytosolic ATP) and activators (ADP, AMP, Pi, Fructose bisphosphate). Finally, pyruvate kinase dephosphorylating phosphoenolpyruvate are inhibited by high concentrations of ATP or acetyl coenzyme A. These endogenous glycolysis inhibitors signal adequate levels of ATP to preserve the fuel stores within the cell, whereas activators promote the breakdown of glucose (Stavrianeas and Silverstein, 2005).

3. Mitochondrial physiology

a) Mechanisms of mitochondrial ATP synthesis

Under aerobic conditions, mitochondria are able to use pyruvate by a sequence of ten enzymatic reactions called tricarboxylic acid cycle to produce reduced cofactors. The reduced cofactors are then used by the mitochondrial respiratory chain to build up a proton electrochemical gradient across mitochondrial inner membrane.

First, pyruvate enters mitochondrial matrix through H^+-coupled mitochondrial monocarboxylate transporters expressed at mitochondrial inner membrane. Pyruvate is then converted into acetyl coenzyme A by the pyruvate dehydrogenase. Acetyl coenzyme A enters the tricarboxylic acid cycle, a chain of ten enzymatic reactions leading to production of coenzyme A, GTP and several cofactors following the stoichiometry:

Acetyl coenzyme A + $3NAD^+$ + FAD + GDP + Pi + $2H_2O$ →

$2 CO_2$ + 3NADH + $FADH_2$ + GTP + $2H^+$ + coenzyme A
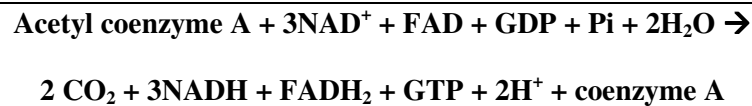
Then, the energy of electron transfer from NADH and $FADH_2$ to the final acceptor oxygen is dissipated by extrusion of protons by the mitochondrial respiratory chain (**Fig. 6**). The electron transport across mitochondrial inner membrane is accompanied by generation of reactive oxygen species (ROS) at sites I and III of the mitochondrial respiratory chain (Balaban et al., 2005). Finally, the free energy produced by the electrochemical proton gradient is used to drive the phosphorylation of ADP to ATP by the F_0F_1 ATP synthase.
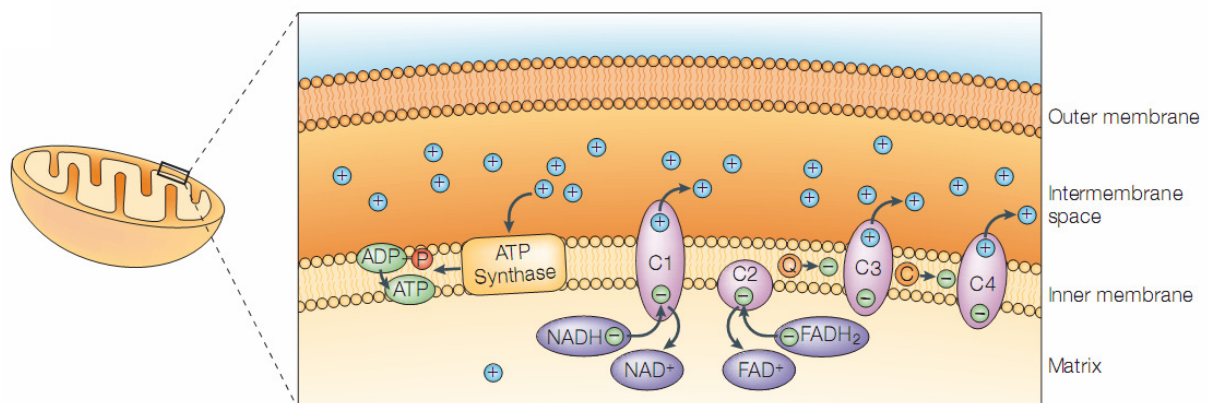
Fig. 6: Scheme of the oxidative phosphorylation in mitochondria. The energy embedded in the cofactors reduced by the tricarboxylic acid cycle is dissipated by complexes of the mitochondrial respiratory chain to maintain an electrochemical gradient across the mitochondrial inner membrane. The electrochemical proton gradient across mitochondrial inner membrane can be used by the F_0F_1 ATPase to phosphorylate ADP in ATP. From Andrews et al., 2005.

Importantly, according to the basic postulates of chemiosmotic coupling formulated by Peter Mitchell, the mitochondrial inner membrane should be poorly permeable to ions:

Fig. 7: Original representation and fourth basic postulate of the chemiosmotic coupling hypothesis. From Mitchell, 1979.

"System 1 to 3 [*mitochondrial ATP synthase, mitochondrial respiratory chain and metabolite transporters*] are plugged through a topologically closed insulating membrane, that has a nonaquaeous osmotic barrier phase of low permeability to solutes in general and to hydrogen ions and hydroxyl ions in particular. This is the cristae of mitochondria, the thylakoid membrane of chloroplasts, and the plasma membrane of bacteria." (*dixit* Mitchell, 1979).
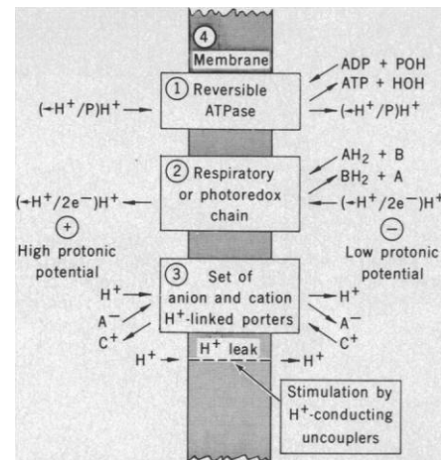
Therefore, according to the chemiosmotic coupling the electrochemical gradient ($\Delta\bar{\mu}_H$) used for ATP synthesis is calculated according to the following equation:

$$\Delta\bar{\mu}_{H^+} = zF\Delta\Psi_{mit} + RT \ln [H^+]_{matrix}/[H^+]_{mims}$$

Where $\Delta\Psi_{mit}$ is the membrane electrical potential difference ($\Psi_{in} - \Psi_{out}$) in millivolts, z is the number of electrons transferred in the reaction or half-reaction, F is the Faraday constant (coulombs per mole of electrons: F = 96 485 C.mol^{-1}), R is the universal gas constant (R = 8.31447 J.K^{-1}.mol^{-1}), T is the absolute temperature, matrix: mitochondrial matrix, mims: mitochondrial intermembrane space.

If we assume a mitochondrial potential of -180mV, with a mitochondrial matrix pH of 7.8 and a cytosolic pH of 7.1, the chemical gradient of H$^+$ accounts for 20% of the total proton motive force.

b) Regulation of mitochondrial ATP synthesis

Although mitochondria are able to produce ATP autonomously, the ATP production rate is tightly regulated by cytosolic molecules. In particular, calcium is the best described ion responsible for changes in mitochondrial metabolism (Nicholls and Budd, 2000), mainly because of activation of Ca^{2+}-dependent dehydrogenase (Hajnoczky et al., 1995).

The mitochondrial Na$^+$ concentration may also indirectly alter mitochondrial metabolism through the alteration of mitochondrial Ca^{2+} concentration by the activity of mitochondrial Na$^+$/Ca^{2+} exchanger (Jung et al., 1995). Na$^+$ also modulates the activity of mitochondrial enzymes such as oxoglutarate and pyruvate dehydrogenase by decreasing their sensitivity to Ca^{2+} (Denton et al., 1980). In addition, a pyruvate dehydrogenase may be activated by regulation of its conformation by the Na$^+$ concentration (Pawelczyk and Olson, 1995).

pH is known to influence the activity of many enzymes (Casey et al., 2010). In addition, the mitochondrial pH gradient across mitochondrial inner membrane influences the ability of ATP synthase to phosphorylate ADP in ATP. Little data exist about variations of mitochondrial potassium concentration during activity. In neurons, no significant change have been measured in mitochondrial K^+ concentration of stimulated dendrites (Pivovarova et al., 1999). As in neurons, it is likely that K^+ concentration do not vary significantly enough to alter mitochondrial ATP production rate in intact astrocytes stimulated with glutamate.

Glutamate stimulation has been shown to alter cytosolic pH and cytosolic concentrations of Na^+ and calcium in astrocytes *in vivo* (see below). However, the impact of glutamate on mitochondrial Na^+ concentration and pH remains poorly explored although mitochondria could have a potential significant contribution in the metabolic response induced by glutamate uptake.

c) Mitochondrial distribution in astrocytes

Although astrocytes are mainly glycolytic cells, they possess a substantial density of mitochondria. Accordingly, astrocytes account for about 25% of total oxidative metabolism as measured by nuclear magnetic resonance spectroscopy (Serres et al., 2008). Transcriptome analysis and the abundance of mitochondria all the way to fine astrocytic processes suggested that cortical astrocytes may have a high mitochondrial oxidative metabolism (Lovatt et al., 2007). A large proportion of the mitochondria is found in the soma and large processes of astrocytes (Maxwell and Kruger, 1965). In contrast to authors claiming that astrocyte processes are too thin for the presence of mitochondria (Hertz et al., 2007), mitochondria are also found in fine astrocytic processes (Lovatt et al., 2007) and also in close apposition to plasma membrane glutamate transporters (**Fig. 8**). Mitochondria are therefore close to the site of glutamate uptake associated with metabolic demand. Thus, the spatial distribution of mitochondria would be adequate to participate in the glutamate-induced metabolic response.
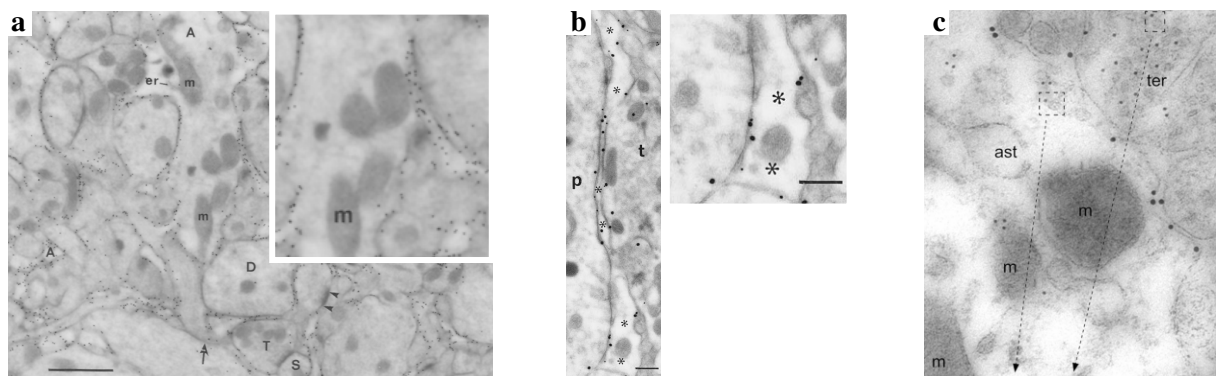
Fig. 8: Mitochondria in the vicinity of glutamate transporters GLT-1 revealed by post-embedding electron microscopy immunogold labelling. (**a**) Neuropil of hippocampus (CA1 striatum lacunosum-moleculare). The astrocyte is indicated by "A". Adapted from Chaudhry et al., 1995. (**b**) Hippocampus. The astrocyte is indicated by stars. From Haugeto et al., 1996. (**c**) Large gold particles revealed GLT-1 localization in astrocyte processes in the outer molecular layer of the hippocampal dentate gyrus. The astrocyte is indicated by "ast". Adapted from Bezzi et al., 2004.

d) Diseases linked to mitochondrial metabolism in astrocytes

Several pathological conditions have been shown to involve dysfunction of mitochondrial metabolism of astrocytes such as stroke (Ouyang et al., 2007) and epilepsia (Ito et al., 2009). In schizophrenia patients, a smaller proportion of mitochondria was found in the volume of astrocytes (Kolomeets and Uranova, 2009). Dysregulation of mitochondrial oxidative activity in astrocytes has been observed in Alzheimer disease (Zhu et al., 2006) and Down syndrome (Busciglio et al., 2002). On the contrary, a recent study showed that mitochondrial density is increased in astrocytes of active lesions associated with multiple sclerosis (Witte et al., 2009). Such cellular domains might be a source of cytotoxic production of ROS due to mitochondrial oxidative stress. No study has yet firmly identified dysfunction of astrocyte mitochondrial metabolism as the origin of brain disease. However, oxidative stress in astrocyte processes surrounding neurons might participate in the development of brain diseases by increasing the local concentration of free radicals.

D. Cellular ionic alterations in astrocytes due to glutamate stimulation

1. Ionic alterations induced by glutamatergic stimulation of astrocytes

a) Ionotropic glutamate receptors

Astrocytes express both *in vitro* and *in vivo*, sodium, calcium, potassium and proton conductive channels whose endogenous ligand is glutamate (Verkhratsky and Steinhauser, 2000). Alpha-amino-3-hydroxy-5-methyl-4-isoxazolepropionic acid (AMPA) receptors are permissive to Na^+ and protons. However, the open state duration of these channels is less than 1ms, even in the continuous presence of glutamate. Astrocytes do not express N-methyl-D-aspartate (NMDA) receptors *in vitro* but appear to express functional NMDA receptors *in vivo*. NMDA receptors are permissive to Na^+ and Ca^{2+} and may be involved in neuron-glia crosstalk (Lalo et al., 2006) but their physiological role is debated (Verkhratsky and Steinhauser, 2000). The contribution of ionotropic glutamate receptors appeared only minor in neurometabolic coupling, as most of the Na^+ concentration increase induced by glutamate is due to Na^+-dependent glutamate transporters (Chatton et al., 2000).

b) Metabotropic glutamate receptors

Among the eight different subtypes of metabotropic glutamate receptors (mGluR) grouped in three groups, astrocytes express mGluR5 (group I) and mGluR3 (group II). Group I of mGluR are specifically activated by (S)-3,5-dihydroxyphenylglycine (DHPG) and are coupled to the inositol-(1, 4, 5)-trisphosphate (IP_3)/Ca^{2+} signal transduction pathway via Gq G-proteins (D'Antoni et al., 2008). In astrocytes, the activation of IP_3 receptors inducing the release of Ca^{2+} from endoplasmic reticulum is the main contributor of Ca^{2+} signalling (Petravicz et al., 2008). The group II of mGluR is negatively coupled to adenylate cyclase through the Gi/o family of G proteins.

All subtypes of mGluR are activated by the non-specific mGluR agonist trans-1-aminocyclopentane-1,3-dicarboxylic acid (t-ACPD). Ca^{2+}-signaling through activation of mGluR may be involved in release of glutamate from astrocytes, as a mechanism for tuning of synaptic plasticity but this issue remains debated (Agulhon et al., 2010). The contribution of metabotropic glutamate receptors appeared only minor in neurometabolic coupling as a metabolic response can be stimulated in cultured astrocytes by superfusion of D-aspartate, a substrate of glutamate transporters that does not activate metabotropic glutamate receptors (Pellerin and Magistretti, 1994).

c) Glutamate transporters

Two types of glutamate transporters expressed in the rodent and human brain, GLAST (EEAT1 in human) and GLT1 (EAAT2 in human) are responsible for about 90% of the glutamate removed from the synaptic cleft during neurotransmission (Danbolt, 2001). Glutamate transporters are coupled to the sodium gradient with a stoichiometry of 3 Na^+ and 1 H^+ per molecule of glutamate with a countertransport of 1 K^+ (Levy et al., 1998). In knockout mice for either glial glutamate transporters, GLAST or GLT-1, the metabolic response to synaptic activation in the somatosensory barrel cortex was decreased following activation of whisker, indicating that glutamate transport is the main mechanism responsible for metabolic response in the brain (Voutsinos-Porche et al., 2003).

2. Transport systems involved in cellular ionic homeostasis

a) Plasma membrane transport systems

During glutamatergic stimulation, astrocytes experience significant changes in their ionic composition due to activation of metabotropic glutamate receptors, glutamate transport and opening of ionotropic glutamate receptors. The major pathways altering ionic concentration during glutamate stimulation of astrocytes are summarized in **Fig. 9**.
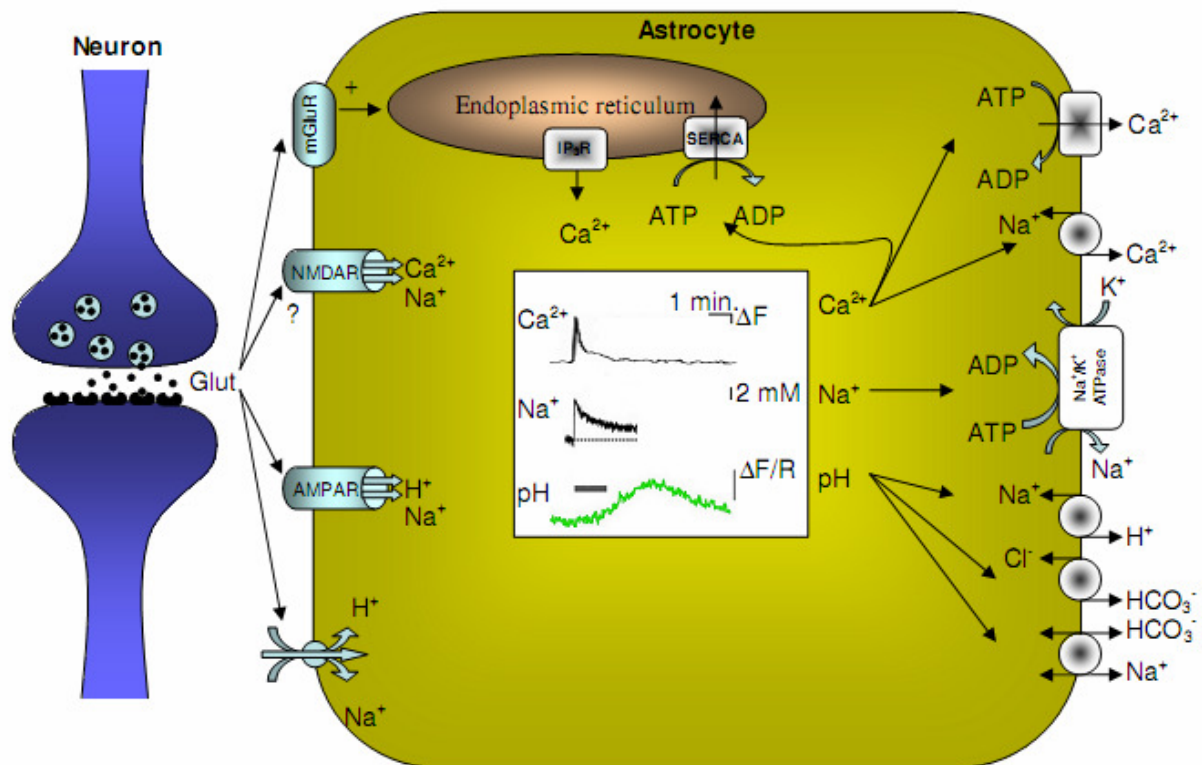
Fig. 9: Main ionic pathways involved during glutamatergic transmission. From Deitmer and Rose, 2009. Original traces of Ca^{2+}, Na^+ and pH alterations in response to neuronal stimulation from Rieger et al., 2007, Langer and Rose, 2009 and Zhou et al., 2010, respectively.

Cytosolic calcium increase is mainly due to release of Ca^{2+} from endoplasmic reticulum following activation of group I mGluR. Cytosolic calcium level is restored to basal level through ATP–dependent sarco/endoplasmic reticulum Ca^{2+}-ATPase (SERCA) and plasma membrane calcium ATPase (PMCA) and Na^+-dependent (Na^+/Ca^{2+} exchanger) mechanisms.

Sodium increase is mainly due to glutamate transporters (Chatton et al., 2000) and restored to basal levels by the Na^+/K^+ ATPase. The sodium increase has been identified as the main pathway responsible for metabolic demand during neurometabolic coupling (Magistretti et al., 1999).

Glutamate stimulation of astrocytes leads to entry of protons mainly due to glutamate transporters activity. The cellular pH is then restored by plasma membrane Na^+/H^+ exchanger, $Cl^-/HCO3^-$ anion exchanger, and $Na^+/HCO3^-$ cotransporter. Upon neuronal stimulation, it has been described that pH increases in the soma of astrocytes (Chesler and Kraig, 1989), mainly because of increase in extracelllular K^+ concentration accompanying neuronal activity. However, the pH in astrocyte processes surrounding neuronal glutamatergic synapses remains to be determined. On the contrary, it has been shown that glutamate stimulation of astrocytes leads to glutamate-transporter mediated cytosolic acidification *in vitro* (Rose and Ransom, 1996) and in slice (Amato et al., 1994).

b) Mitochondrial transport systems

Mitochondria are composed of two membranes, the outer mitochondrial membrane and inner mitochondrial membrane that delimit the intermembrane space (**Fig. 10**). The voltage dependent anion channel (VDAC) is permeable to small solutes and ions (Blachly-Dyson and Forte, 2001). Therefore, the concentrations of ions and small solutes are in equilibrium with those in the cytosol, at least in the immediate vicinity of the mitochondria. For instance, the mitochondrial intermembrane space Ca^{2+} concentration was found significantly higher than in the bulk cytosol when mitochondria were in the vicinity of Ca^{2+} microdomains created by local release of Ca^{2+} from the endoplasmic reticulum (Pinton et al., 1998). Interestingly, the pH in mitochondrial intermembrane space was found to be more acidic than cytosol in human ECV304 cells, suggesting that mitochondrial respiratory chain create an acidic microdomain in cell exhibiting a high oxidative metabolism (Porcelli et al., 2005). Nevertheless, the mitochondrial intermembrane space is generally considered as equal to cytosol because of rapid ionic equilibrium due to high VDAC permeability.
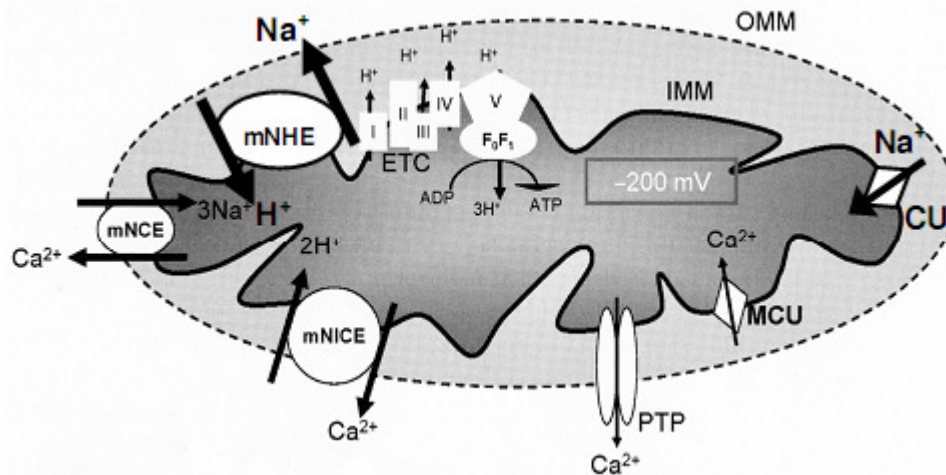
Fig. 10: Scheme of currently known pathways mediating flux of Na^+ and Ca^{2+} between intermembrane space and mitochondrial matrix. OMM: outer mitochondrial membrane, IMM: inner mitochondrial membrane, mNICE: mitochondrial Na^+-independent Ca^{2+} exchanger, mNCE: mitochondrial Na^+/Ca^{2+} exchanger, MCU mitochondrial cation uniporter, PTP: permeability transition pore, ETC: electron transport chain, F_0F_1: F_0F_1 ATP synthase, mNHE: mitochondrial Na^+/H^+ exchanger, CU: mitochondrial cation uniporter. Adapted from Pinton et al., 2007.

The mitochondrial inner membrane is equipped with a high density of ion channels and exchangers (Bernardi, 1999) that dynamically regulate the ionic concentrations of mitochondrial matrix. Importantly, the changes in cytosolic ionic concentrations alter the mitochondrial matrix ionic concentrations. Ca^{2+} is thought to enter the mitochondria through the electrogenic calcium uniporter (Kirichok et al., 2004), although the identity of this channel remains controversial (Demaurex et al., 2009). A new Ca^{2+}/H^+ exchanger has recently been identified as a pathway for Ca^{2+} entry into mitochondria (Jiang et al., 2009). Mitochondrial Ca^{2+} level is then restored by mitochondrial Ca^{2+}/H^+ and Na^+/Ca^{2+} exchangers. However, mitochondrial Na^+/Ca^{2+} exchanger can also work in reverse mode, leading to Na^+ influx and Ca^{2+} extrusion from the mitochondrial matrix (Poburko et al., 2007). In addition, mitochondrial Na^+ level is also restored by the mitochondrial Na^+/H^+ exchanger and the mitochondrial K^+/H^+ that also can transport Na^+ instead of K^+ (Bernardi, 1999). An electrogenic mitochondrial cation uniporter has been described in isolated mitochondria as permissive to Na^+ and whose open state probability is increased by decreasing Mg^{2+} concentration, increasing ATP concentration or increasing pH (Bernardi et al., 1990; Bernardi, 1999).

E. Spontaneous alterations of ionic concentration in mitochondria

1. Spontaneous mitochondrial depolarizations

The mitochondrial ionic concentration has always been thought to be tightly regulated and maintained stable by the transport systems described in the previous section. However, mitochondria have been shown in the last years to display transient alterations of their ionic content. Spontaneous individual mitochondrial transients have first been discovered using potential-sensitive mitochondrial dyes. Interestingly, mitochondrial transients occurs in several cell types including astrocytes (Jacobson and Duchen, 2002), neurons (Buckman and Reynolds, 2001), cardiomyocytes (Wang et al., 2008), smooth muscle cells (Chalmers and McCarron, 2008) and COS-7 cells (De Giorgi et al., 2000). An example of spontaneous individual transient depolarization of astrocyte mitochondria is shown in **Fig. 11**.

Time (milliseconds)
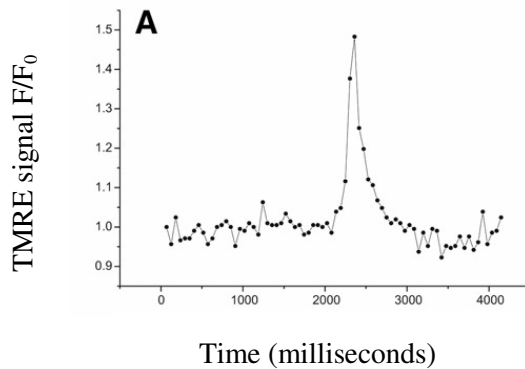
11: Spontaneous transient depolarization in individual mitochondrion of astrocytes. Mitochondrial electrical potential was measured using tetramethylrhodamine methyl and ethyl esters (TMRE) in quenched mode. From Jacobson and Duchen, 2002.

2. Spontaneous mitochondrial ROS transients

Recently Wang and colleagues reported that mitochondria exhibit transient increases of ROS concentration ("superoxide flashes") that are coincident with mitochondrial transient depolarizations. Superoxide flashes have been observed in cultured excitable cells (myocytes, neurons, neuroendocrine cells, and skeletal myotubes), non-excitable cells (fibroblasts and osteosarcoma cells) as well as in the myocardium of intact beating hearts (**Fig. 12**).
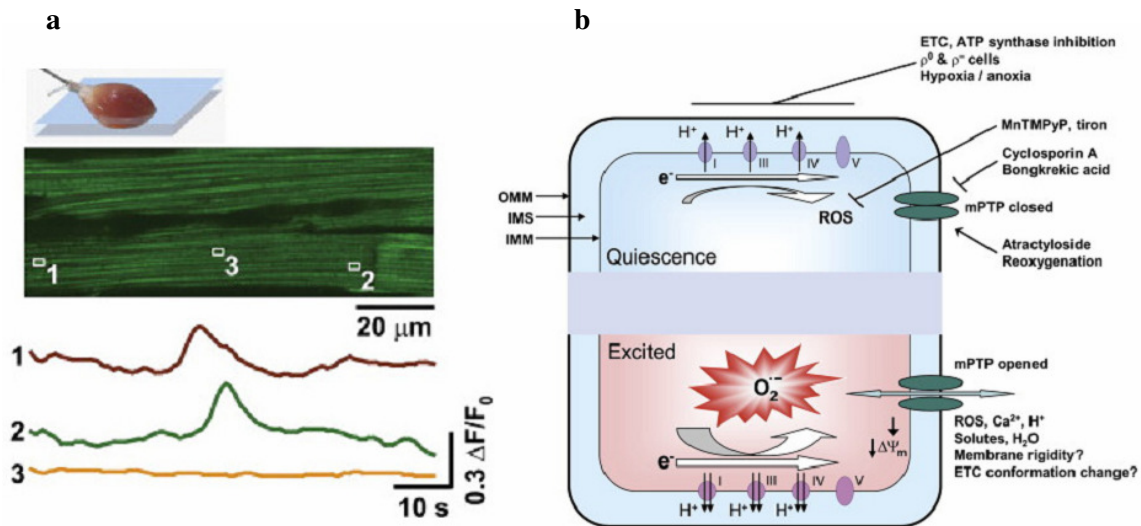
Fig. 12: Superoxide flashes in individual mitochondria. (a) Measurement of superoxide flashes in isolated heart. (b) Putative model for superoxide flash genesis. The transient opening of mitochondrial transition pore (mPTP) decrease mitochondrial electrical potential and transiently increase the mROS (O_2^-) production rate by the mitochondrial electron transport chain (ETC). From Wang et al., 2008.

According to the model of superoxide flashes, transient openings of the mitochondrial transition pore decrease mitochondrial potential. Therefore mitochondrial respiratory chain activity is facilitated explaining the origin of transient increase in mitochondrial ROS production. Consistently, the level of mROS in astrocytes was also found heterogeneous within individual mitochondria and was modulated by oxidative stress (Jou, 2008). An example of mROS heterogeneity is shown in **Fig. 13**.
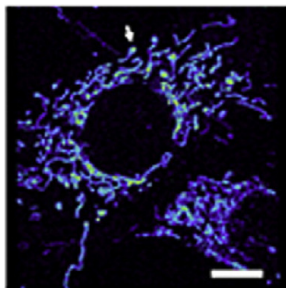
Fig. 13: Heterogeneity in mitochondrial ROS distribution in cultured astrocytes. 3-D reconstructed of an astrocyte labelled with the mROS sensitive dye dihydrorhodamine 123 targeted to mitochondria. Scale bar: 10µm. From Jou, 2008.

F. Methodological considerations

1. Experimental model

In biological research, it is crucial to select an experimental model that can be studied in optimal conditions, and whose experimental investigations provide relevant indications about the physiology and pathology of intact biological tissues. New generations of microscopes such as 2-photon and fast scanning confocal microscopes now enable to study biological tissues in their physiological environment. However, few tools compatible with these microscopes are currently available to adequately investigate the mitochondrial metabolism *in vivo*. To circumvent these technical problems, we used primary cultures of astrocytes and mixed cultures of neurons and astrocytes, two models that allow the use of low-light level high resolution imaging techniques to investigate mitochondrial metabolism.

a) Primary cultures of astrocytes

Primary cultures of astrocytes are relatively easy to prepare and maintain. Depending on the serum added to the culture medium, cell survival and proliferation are high compared with neuronal cultures and the proportion of astrocytes in culture is typically very high in the whole cell population. Another advantage of primary cultures of astrocytes is that they are easy to load with fluorescent dyes and can be transfected with DNA plasmids with acceptable yield.

However, the morphology of astrocytes in culture is dramatically different from the *in vivo* morphology. Thus, experimental results observed in the cultured astrocytes may only occur in specific cellular compartments of astrocytes *in vivo*. For instance, the cytosolic changes in cytosolic Na^+ concentration observed *in vitro* (Chatton et al., 2000) were only found in fine processes of astrocytes in slice (Langer and Rose, 2009). In addition, the transcriptome profile of astrocytes may also be different *in vivo* and *in vitro*. Although the gene expression in cultured astrocytes and *in vivo* astrocytes are similar, some genes expressed in cultured astroglia have not been found to be expressed *in vivo* (Cahoy et al., 2008). Another transcriptome analysis of freshly isolated astrocytes (Lovatt et al., 2007) and measurements of 1-^{11}C-acetate kinetics (Wyss et al., 2009) also indicated that astrocytes have a high mitochondrial oxidative metabolism *in vivo* whereas glycolysis is the major pathway of ATP synthesis in cultured astrocytes.

b) Primary cultures of neurons

The physiology of a network of neurons communicating to each other by action potentials can be studied in primary cultures of neurons. In such culture model, neurons typically grow in the presence of astrocytes that release neurotrophic factors. Data obtained by fluorescence imaging techniques with this culture model are sometimes difficult to interpret because of the difficulty to distinguish responses corresponding to astrocytes and neurons. This disadvantage can be avoided by specific labelling of neurons or astrocytes by microinjection, whole-cell patch-clamp, or as recently developed in our lab, by single-cell electroporation with soluble charged molecule (DNA, fluorescent probe in their free acid form). Although neurons are easy to electroporate, the risk of cell death during and following to electroporation is high. Astrocytes remain difficult to electroporate because of the very flat morphology and of the particular electrical properties of their plasma membrane.

c) Neuron-astrocyte mixed co-cultures

Several protocols are used for mixed neuron-astrocyte co-cultures. In order to ensure the astrocyte-specific origin of our measured fluorescence signals, we set up a culture model where mouse embryonic neurons were plated on astrocytes previously transfected with a plasmid encoding for a fluorescent biosensor. This model enabled the recording of astrocyte response to neuronal release of neurotransmitter. As a disadvantage of this procedure, neuronal release of neurotransmitter was only possible after about ten days of culture, the time needed for complete synaptogenesis. Therefore, depending on the toxicity of the protein expressed by transfection, astrocytes may not survive long enough or the expression of the transgene may decrease too much with time.

2. Fluorescence imaging of ion concentrations in cytosol and mitochondria of cultured astrocytes

a) Cytosolic probes

A large spectrum of fluorescent dyes is commercially available and enables monitoring the concentration of several ions in real time and with an excellent signal-to-noise ratio. The acetoxymethyl ester form of fluorescent probes enables the dye to the cross plasma membrane. After cleavage of the ester bound, the hydrophilic form of the indicator cannot cross the plasma membrane anymore and remains in the cytoplasm of the cells. Importantly, it is important to consider that the dye itself can chelate the ions to be monitored. For instance, 2',7'-bis-(2-carboxyethyl)-5-(and-6)-carboxyfluorescein (BCECF) is used to monitor the cytosolic pH but can also buffer pH (similar problems may also occur with Ca^{2+}-sensitive dyes). In addition, most of the fluorophores sensitive to monovalent cations do not have high specificity to ions but rather have a K_D corresponding to physiological ion concentration. For instance, sodium-binding benzofuran isophthalate (SBFI) is

commonly used to monitor cytosolic Na^+ concentration but is also sensitive to K^+. As K^+ concentration does not vary significantly during cellular activity, the changes in fluorescence excitation ratio can still be used as a specific dye for cytosolic Na^+ concentration. Magnesium Green is another fluorescent dye frequently used to indirectly monitor the cellular ATP concentration. However, Magnesium Green is also sensitive to Ca^{2+} and caution must be taken in the interpretation of experimental results.

b) Mitochondrial probes

There are three main types of mitochondrial probes for monitoring ion concentration in intact cells: genetically-encoded probes, mitochondrial membrane potential-independent dyes and liphophilic cationic mitochondrial dyes (De Vos and Sheetz, 2007).

- *Genetically-encoded fluorescent probes* include a mitochondrial-targeting sequence that contains all the information to target the protein to the correct submitochondrial domain. Some of them are made from the association of a truncated protein normally targeted to mitochondria with an ion-sensitive probe as shown in **Fig. 14**.
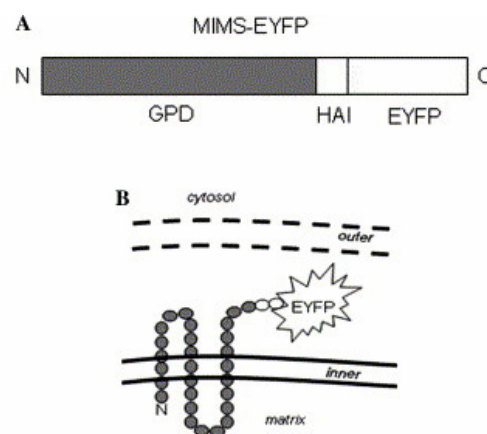
Fig. 14: Example of genetically-encoded fluorescent probe targeted to mitochondria: MIMS-EYFP, a pH-sensor targeted to the mitochondrial intermembrane space. (A) Schematic map of the MIMS-EYFP cDNA, where the aa 1–626 of encode for a truncated form of glycerol-phosphate dehydrogenase (GPD), a transmembrane protein of the mitochondrial inner membrane. The following regions encoding for HAI epitope (HAI) and EYFP (the pH-sensitive fluorescent biosensor) are shown. (B) Putative submitochondrial localization of MIMS-EYFP. Adapted from Porcelli et al., 2005.

- *Mitochondrial membrane independent dyes*, such as MitoTracker Green FM, stain mitochondria regardless of their electrical potential. The mechanism of targeting of this kind of dye is poorly understood but may be based on lipidic composition of the mitochondrial membrane (*Invitrogen manufacturer information*). These dyes have the advantage to stain all mitochondria, including non respiring mitochondria but may be not appropriate to evaluate mitochondrial dynamics in living cells (De Vos and Sheetz, 2007).

- *Lipophilic cationic mitochondrial dyes* exploit the large negative mitochondrial membrane potential (negative inside of ~-180-220mV). This kind of dye only stains mitochondria with respiratory activity, which precludes their use for cellular mechanisms involving mitochondrial depolarization such as cell death. Importantly, liphophilic cationic mitochondrial dyes generate ROS upon strong light illumination, which can induce artefacts such as mitochondrial depolarization. Therefore, liphophilic cationic mitochondrial dyes should be used at the minimal concentration and loading time to obtain a specific mitochondrial staining (cytosol and nuclei not stained) and correct signal-to-noise ratio. The use of a sensitive CCD camera is typically appropriate to study mitochondrial physiology. For technical reasons, the use of confocal laser microscope can be required (need of fluorescence emission wavelength splitting for instance). However, the excitation light intensity necessary for confocal image acquisition generally leads to significant phototoxicity. Several new generations of confocal microscopes are equipped with fast scanner possibility (confocal microscope with resonant scanner, spinning disk confocal microscope) that reduce phototoxicity. The phototoxic damages to mitochondria can be minimized by setting to the minimum the following parameters: frequency of image recording, power of light illumination and duration of illumination. In the course of our studies, great care was taken to work with the lowest possible light delivery to our samples, both for widefield and confocal imaging.

II. Results

A. Aims of the studies

These studies were designed to characterize the mitochondrial ionic homeostasis of intact living astrocytes. The first part of results is focussed on spontaneous transient alterations of ionic concentrations in individual mitochondria of living astrocytes. We discovered that astrocytic mitochondria exhibit spontaneous increases of their Na^+ concentration (Azarias et al., 2008). A section of unpublished data further characterizing spontaneous mitochondrial transients has been added.

The second part of results presents two studies focused on the impact of glutamatergic stimulation on the mitochondrial metabolism in astrocytes. Previous works at the origin of the astrocyte-neuron lactate shuttle provided a link between glutamate uptake and enhancement of glycolysis. In these studies, we investigated the possibility of a link between cellular glutamate uptake and decrease of mitochondrial oxidative metabolism (Bernardinelli et al, 2006, Azarias et al, *submitted*).

B. Spontaneous transients in individual mitochondria of astrocytes

In resting cells, cytosolic Na^+ and pH levels are kept stable thanks to regulatory systems expressed at the plasma membrane, whereas localized cytosolic domains of Ca^{2+} regulate specific cellular processes of the cell. In contrast to the cytosol, we found that mitochondria exhibit spontaneous transients of their Na^+ concentration and pH that were not directly related with Ca^{2+} changes.

1. Spontaneous Na^+ transients in individual mitochondria of intact astrocytes

This article shows by using fluorescence microscopy, that individual mitochondria exhibit spontaneous increases of their Na^+ concentration in primary cultures of astrocytes. Using a pharmacological approach and a novel image analysis algorithm developed to quantify mitochondrial transient frequency, we investigated the modulation and pathways of Na^+ trafficking in mitochondria exhibiting spontaneous transients. We presented a body of evidence suggesting that Na^+ entry is mediated by an electrogenic mitochondrial cation uniporter. The mitochondrial Na^+/H^+ exchanger contributed to restore mitochondrial Na^+ concentration to basal concentration. Finally, our findings suggest that the cellular ATP level modulates the frequency of mitochondrial Na^+ transient activity.

I performed the experiments presented in Fig. 1B-D, 3, Table 1 (partly), 4A-B;E-F, 5 and 6. I designed the experiments, analyzed the results, prepared the figures and wrote the manuscript with Jean-Yves Chatton.

Spontaneous Na$^+$ Transients in Individual Mitochondria of Intact Astrocytes

GUILLAUME AZARIAS,[1] **DIMITRI VAN DE VILLE,**[2] **MICHAEL UNSER,**[2] AND **JEAN-YVES CHATTON**[1,3,4]*
[1]*Department of Physiology, University of Lausanne, Switzerland*
[2]*Biomedical Imaging Group, Swiss Institute of Technology, Lausanne, Switzerland*
[3]*Department of Cell Biology and Morphology, University of Lausanne, Switzerland*
[4]*Cellular Imaging Facility, University of Lausanne, Switzerland*

ABSTRACT
Mitochondria in intact cells maintain low Na$^+$ levels despite the large electrochemical gradient favoring cation influx into the matrix. In addition, they display individual spontaneous transient depolarizations. We report here that individual mitochondria in living astrocytes exhibit spontaneous increases in their Na$^+$ concentration (Na$^+_{mit}$ spiking), as measured using the mitochondrial probe CoroNa Red. In a field of view with ~30 astrocytes, up to 1,400 transients per minute were typically detected under resting conditions. Na$^+_{mit}$ spiking was also observed in neurons, but was scarce in two nonneural cell types tested. Astrocytic Na$^+_{mit}$ spikes averaged 12.2 ± 0.8 s in duration and 35.5 ± 3.2 mM in amplitude and coincided with brief mitochondrial depolarizations; they were impaired by mitochondrial depolarization and ruthenium red pointing to the involvement of a cation uniporter. Na$^+_{mit}$ spiking activity was significantly inhibited by mitochondrial Na$^+$/H$^+$ exchanger inhibition and sensitive to cellular pH and Na$^+$ concentration. Ca^{2+} played a permissive role on Na$^+_{mit}$ spiking activity. Finally, we present evidence suggesting that Na$^+_{mit}$ spiking frequency was correlated with cellular ATP levels. This study shows that, under physiological conditions, individual mitochondria in living astrocytes exhibit fast Na$^+$ exchange across their inner membrane, which reveals a new form of highly dynamic and localized functional regulation. © 2007 Wiley-Liss, Inc.

INTRODUCTION

Mitochondria have the crucial function of producing ATP via oxidative phosphorylation (Mitchell, 1979). They are also known to be important regulators of cellular functions such as Ca^{2+} homeostasis and death pathways (Demaurex and Distelhorst, 2003; Nicholls and Budd, 2000). They can be addressed to specialized cellular domains (Reynolds and Rintoul, 2004) and have been shown to be in close interaction with subcellular organelles such as the endoplasmic reticulum and sub-plasmalemal compartments (Montero et al., 2000; Rizzuto et al., 1998; Walter and Hajnoczky, 2005). Even though the basic postulates of the chemiosmotic coupling hypothesis include an inner mitochondrial membrane with low permeability to cations (Mitchell, 1979), it is now admitted that the inner membrane contains channels and transporters with diverse selectivity for K$^+$ and Na$^+$ (Bernardi, 1999). Indeed regulatory mechanisms enable mitochondria to maintain both volume and cation content under control despite the extreme electronegativity of mitochondrial matrix would be sufficient to bring the concentration of monovalent cations such as Na$^+$ to molar range (Bernardi, 1999).

The isolated mitochondria model has provided a vast amount of information on mitochondrial transport of cations using kinetics measurements of the matching volume changes assessed with optical methods. More recently, with the availability of fluorescent probes selective for mitochondria and of sensitive imaging methods, the study of mitochondria in their native cellular environment has become possible. It includes the monitoring of mitochondrial electrical potential, pH and calcium concentration (e.g., Pinton et al., 2007). Such tools have permitted to establish that Ca^{2+} plays critical roles in mitochondrial physiology through the control of key mitochondrial enzymes such as Ca^{2+}-sensitive dehydrogenases, linking cellular Ca^{2+} homeostasis with metabolism (Hajnoczky et al., 1995). In addition, several studies report that mitochondria under physiological conditions exhibit spontaneous changes in their electrical membrane potential in neural (Buckman and Reynolds, 2001) and nonneural cells (Duchen et al., 1998).

Until recently, the dynamics of mitochondrial Na$^+$ (Na$^+_{mit}$) content has remained unexplored because of the lack of adequate methods. However, Na$^+_{mit}$ is likely to play both direct and indirect roles in mitochondrial physiology. Its most recognized function is to drive the mitochondrial Na$^+$/Ca^{2+} antiporters that extrude Ca^{2+} ions from the mitochondrial matrix (Jung et al., 1992,

1995). Na^+ has also been reported to modulate the activity of mitochondrial enzymes such as oxoglutarate and pyruvate dehydrogenase by decreasing their sensitivity to Ca^{2+} (Denton et al., 1980). Evidence also exists for a direct action of Na^+ on the activity of the pyruvate dehydrogenase complex by conformational changes (Pawelczyk and Olson, 1995). In addition, Na^+_{mit} has been reported to exhibit significant changes during cellular responses. For instance, afferent synaptic stimulation was shown to increase Na^+_{mit} concentration in hippocampal neurons (Pivovarova et al., 2002). We recently showed that in living astrocytes, Na^+_{mit} concentration displays rapid increase as a result of plasma membrane Na^+-dependent glutamate uptake, one of the most prominent functions of astrocytes in the brain (Bernardinelli et al., 2006). Thus, it is of critical importance to determine whether Na^+ could significantly influence mitochondrial functions such as ATP production. Indeed, it is expected that selective change in Na^+_{mit} concentration could alter the homeostasis of Ca^{2+} and proton through its respective Na^+-coupled exchangers expressed at inner mitochondrial membrane.

In the present study, we demonstrate for the first time that individual mitochondria in resting cells display spontaneous and rapid transients of their Na^+ concentration. Using a dedicated image analysis strategy, we characterized this Na^+_{mit} spiking activity at the level of single mitochondria using the Na^+-sensitive fluorescent probe CoroNa Red (CR) and investigated the underlying mechanisms of generation and regulation. We identified mitochondrial cation uniporters and mitochondrial Na^+/H^+ exchanger as critically involved in Na^+ entry and recovery, respectively. Ca^{2+} was found to play a permissive role in the regulation of the activity. We also found evidence for a modulation of spiking activity by the cellular energy metabolic status, which could point to the functional significance of these highly localized subcellular ion movements.

MATERIALS AND METHODS
Cell Culture and Solutions

Cortical astrocytes in primary culture were prepared from 1 to 3-days-old C57 Bl 6 mice as described elsewhere (Sorg and Magistretti, 1992). Astrocytes were cultured for 3–4 weeks in DME medium (Sigma) plus 10% FCS before experiments. Mouse cortical neurons were prepared as described before (Morgenthaler et al., 2006). All cell types, including MIN-6 and MCF-7 cells, were plated on glass coverslips for imaging. Experimental solutions contained (mM) NaCl, 135; KCl, 5.4; $NaHCO_3$ 25; $CaCl_2$, 1.3; $MgSO_4$, 0.8; and NaH_2PO_4, 0.78. Ca^{2+}-free solution contained NaCl, 135; KCl, 5.4; $NaHCO_3$, 25; $MgSO_4$, 0.8; NaH_2PO_4, 0.78; and EGTA, 0.1; both were bubbled with 5% CO_2/95% air. Na^+-free solutions contained N-methyl-D-glucamine chloride, 160; KCl, 5.4; $CaCl_2$, 1.3; $MgSO_4$, 0.8; K_3PO_4, 0.78; and HEPES, 20 (pH 7.4) and were compared with corresponding Na^+-containing control solutions buffered with HEPES, both

bubbled with air. The solution used to deliver BAPTA-AM (50 μM) to cells contained in addition 1 g % bovine serum albumin and was also buffered with HEPES. Unless otherwise indicated, experimental solutions contained 5 mM glucose as metabolic substrate. Solutions for dye-loading contained (mM) NaCl, 160; KCl, 5.4; HEPES, 20; $CaCl_2$, 1.3; $MgSO_4$, 0.8; NaH_2PO_4, 0.78; glucose, 20 and was supplemented with 0.1% Pluronic F-127 (Molecular Probes, Eugene, OR).

Fluorescence Imaging

Mitochondrial Na^+ concentration was investigated and calibrated as described by Bernardinelli et al. (2006). Briefly, astrocytes were loaded at 37°C for 18 min with 1 μM CR in a HEPES-buffered balanced solution and then placed in a thermostated chamber designed for rapid exchange of perfusion solutions (Chatton et al., 2000) and superfused at 35°C. Low-light level fluorescence imaging was performed on an inverted epifluorescence microscope (Axiovert 100M, Carl Zeiss) using a 40 × 1.3 N.A. oil-immersion objective lens. Fluorescence excitation wavelengths were selected using a monochromator (Till Photonics, Planegg, Germany) and fluorescence was detected using a 12-bit cooled CCD camera (Princeton Instruments). CR fluorescence was excited at 560 nm and detected at >580 nm. To avoid phototoxicity, excitation intensity was reduced to 10 μW (as measured at the entrance pupil of the objective) by means of neutral density filters. Image acquisition and time series were computer-controlled using the software Metafluor (Universal Imaging, Reading, PA) running on a Pentium computer. Two-minute sequences of images were recorded at 1.0 Hz during control and experimental conditions; images were also acquired at lower rate between experimental conditions. Simultaneous monitoring of Na^+_{mit} and mitochondrial electrical potential were performed using CR (1 μM) and JC-1 (1–2 μM), loaded together for 17 min and imaged by confocal microscopy (SP5 Resonant scanner, Leica Microsystems) using excitation light at 561 and 488 nm, respectively. Dye emissions were observed at 580–620 nm (CR and JC-1 aggregates) and 500–560 nm (JC-1 monomers). Intracellular pH measurement was performed using the pH-sensitive dye BCECF-AM as described previously (Chatton et al., 2001), in some cases co-loaded with CR. ATP levels were assessed indirectly by measuring intracellular free Mg^{2+} using Magnesium Green AM as described previously (Chatton and Magistretti, 2005).

Image Analysis

To quantify the CR signal transients in a reliable and efficient way, we developed a dedicated image analysis procedure. The complete algorithm is implemented in Java as a plug-in for the ImageJ software (W. Rasban, http://rsb.info.nih.gov/ij/). In what follows, we outline the important processing steps of the algorithm.

First, we make use of the wavelet transform (Mallat, 1989), which is a popular tool in many areas of signal and image processing (Unser and Aldroubi, 1996). The third degree Battle-Lemarié wavelet transform (Battle, 1987; Unser and Blu, 2000) is applied to the 2D + T (two spatial dimensions plus time) stack of images in a separable way (i.e., along each dimension). Note that the wavelet decomposition is a linear, one-to-one transform that is orthogonal. It can be interpreted as a subband decomposition whereby the signal is split into details at different scales in space and time. In Fig. 2A, we illustrate one decomposition level of the spatiotemporal transform. The various subbands are typically designated by the combination of lowpass (L) or highpass (H) filters along horizontal, vertical, and temporal dimensions; i.e., LLL, LLH, up to HHH. In the full transform, the low-pass subband (LLL) is then further decomposed. This multi-resolution decomposition of the stack of images allows us to separate features of specific spatial size and temporal duration by selecting appropriate subbands. We empirically identified the CR transient as being spatially clustered over at least 4 pixels in horizontal and vertical directions, and with a strong temporal correlation over at least four images. Once the corresponding subbands are selected, the inverse wavelet transform is computed. This operation can be interpreted as separating CR transient from the slowly varying background and the highly uncorrelated thermal noise from the CCD camera.

Secondly, the reconstructed 2D+T stack of images mainly containing CR transients is thresholded. The threshold value is computed as three times the standard deviation of the first highpass (spatial and temporal) subband of the wavelet decomposition. Note that this particular subband contains almost exclusively noise. Both the thresholded (intensity-preserved) and a binarized stacks of images are saved for further processing. The intensity-preserved stack is further summarized in a cumulative image (over time) to characterize the total signal intensity of the experimental condition (later named "Cumulative Intensity"). A paired stack that combines the untreated data and the detected transient is also generated and allows direct visual inspection of the performance of the algorithm. A high degree of correspondence of the extracted events and excellent sensitivity of detection was observed in routine.[1]

CR transients were analyzed in a square area of 160 μm × 160 μm of confluent astrocytes. Of the 120 images recorded at 1 Hz for each experimental condition, a stack of 64 consecutive images were extracted for analysis. The frequency of transients is presented in terms of "Spiking Frequency" as the total number of cluster counts detected in 64 consecutive images. For the analysis of Na^+_{mit} spiking mechanisms, as spiking frequencies varied among experiments, data are presented as percent ± SEM spiking frequency measured in control con-

ditions. For each group of experiments, a Student's t test was performed to assess the statistical significance against respective controls and *, **, and *** refer to P values <0.05, 0.01, and 0.001, respectively.

Materials

All used dyes were from Invitrogen-Molecular Probes. p-Trifluoromethoxy carbonyl cyanide phenyl hydrazone (FCCP), cyclosporin A, ouabain, BAPTA-AM, and rotenone were from Fluka (Buchs, Switzerland). Bongkrekic acid, CGP-37157 and U 37883A were from Biomol (ANAWA Trading, Zurich, Switzerland). CNQX and TBOA were from Tocris (ANAWA Trading). Ethyl-isopropyl amiloride was a gift from Dr. H. Lang (Aventis Pharma, Frankfurt, Germany). All other substances were from Sigma. S-nitroso-cysteine was freshly prepared according to Lei et al. (1992).

RESULTS
Individual Mitochondrial Na^+_{mit} Spiking

We previously showed that CR staining of living astrocytes was selective for mitochondria (Bernardinelli et al., 2006) as it was found for other cell types (Baron et al., 2005; Yang et al., 2004). CR can be safely used as a mitochondrial Na^+ sensitive fluorescent probe, as it was shown to be selective for Na^+ with no influence of pH, Ca^{2+}, or K^+ in their respective expected physiological ranges (Bernardinelli et al., 2006; Jayaraman et al., 2001a, b).

Mitochondria in cultured astrocytes appeared as morphologically heterogeneous organelles, with a perinuclear aggregation and a predominance of isolated mitochondria in the cell periphery as reported in other studies (Collins et al., 2002) (Fig. 1A). In primary culture, astrocytes exhibit a flat morphology making the resolution of individual mitochondria possible even with a nonconfocal optical system. In CR-labeled astrocytes, we have repeatedly observed the presence of spontaneous CR transients. Figure 1A depicts a dynamic image sequence and shows individual mitochondria spontaneously lighting up (see also Movie 1; provided in supplementary material). CR transients were invariably seen in all the performed experiments (total >150 exp) apparently randomly distributed in space and time throughout the cell. Initial controls indicated that transients could be observed during superfusion of experimental solutions and in stationary media; in bicarbonate/CO_2 and in HEPES-buffered saline (not shown). Long-term recordings indicated that virtually all mitochondria of a cell displayed at least one CR transient during a 20-min period, excluding that transients were restricted to a subpopulation of mitochondria (not shown). Individual mitochondria usually showed 1–2 transients in 2-min periods of recording (Fig. 1B). The analysis of fluorescence changes in individual mitochondria indicated that the duration of one transient was found to be 12.2 ± 0.8 s

---

[1]The algorithm developed for the wavelet-based extraction of mitochondrial spiking activity is available under the form of an ImageJ plug-in from the site http://bigwww.epfl.ch/jmitotransient/.
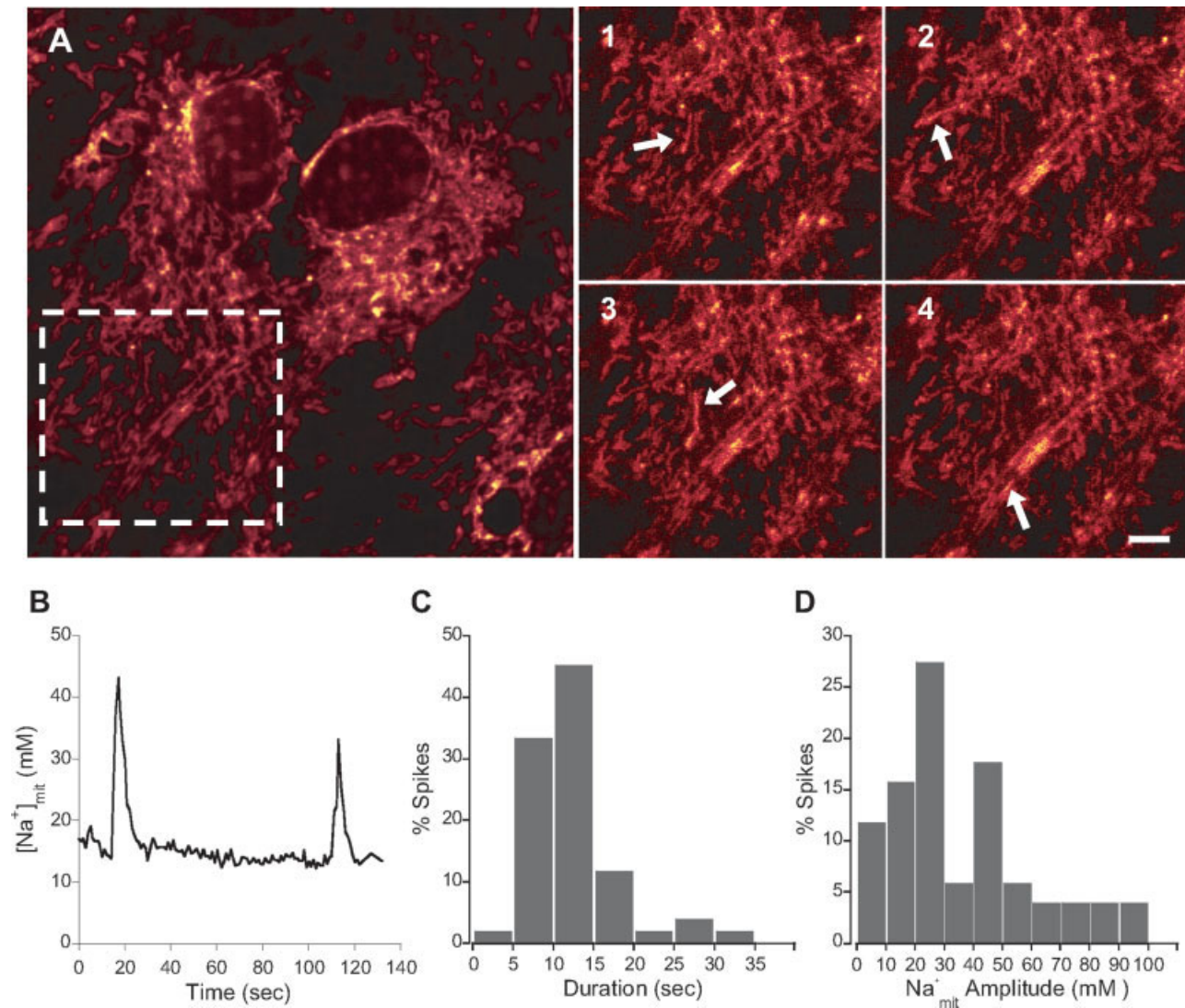
Fig. 1. Na_{mit}^+ spiking in individual mitochondria. (**A**) Confocal fluorescent images of CR-stained astrocytes showing typical mitochondrial loading pattern. Blown up views (1–4) show a sequence of images recorded at low light level showing CR fluorescence transients in individual mitochondria. Images were taken at $t = 0$, 7.0, 11.7, and 13.0 s. Several Na_{mit}^+ signal transients are indicated with arrows. Scale bar, 5 μm. (**B**) Trace of calibrated Na_{mit}^+ changes recorded in one single mito-chondrion which exhibited two Na_{mit}^+ spikes during the recording period. (**C**, **D**) Distribution of the duration and amplitude of Na_{mit}^+ spikes. Results from a total of 51 mitochondrial transients pooled from seven calibration experiments. Data are reported as percent of the total number of analyzed spikes. [Color figure can be viewed in the online issue, which is available at www. interscience.wiley.com.]

(median: 11.9 s; Fig. 1C). Calibration of mitochondrial Na^+ indicated that basal Na_{mit}^+ was 13 ± 0.6 mM and the amplitude of transients averaged 35.5 ± 3.2 mM (median: 27.3 mM; Fig. 1D). The rate of Na_{mit}^+ change during spiking was estimated at 12.3 ± 2.4 mM/s and 5.2 ± 0.7 mM/s for influx and efflux, respectively. In this report, we refer to CR transients in individual mitochondria as Na_{mit}^+ spiking.

Given the large number of Na_{mit}^+ spikes observable in an image sequence (>100 spikes/min in the field of view of 160 μm × 160 μm corresponding to about 30 confluent astrocytes), it rapidly became obvious that, to obtain a reliable and unbiased assessment of the Na_{mit}^+ spiking activity, we had to use a dedicated image analysis strategy. Therefore, they developed an image analysis algo-rithm based on the wavelet transform. From consecutive images recorded at 1 Hz, this algorithm produces a sparse representation of the data in the spatial and frequency domain (Fig. 2A and refer to the section Materials and Methods). The algorithm includes a spatio-temporal filter excluding an effect of mitochondrial small movements on the detection. As a result, we obtained for each image in the sequence the average number of events, later used for spiking frequency assessment. The cumulative intensity of the transients detected reflects a combined evaluation of frequency and strength of transients. Figure 2B shows an example of analysis for an individual image. In control conditions, the sum of detected spikes number increased linearly over time in a field of view ($R^2 > 0.995$ for seven calibration experi-
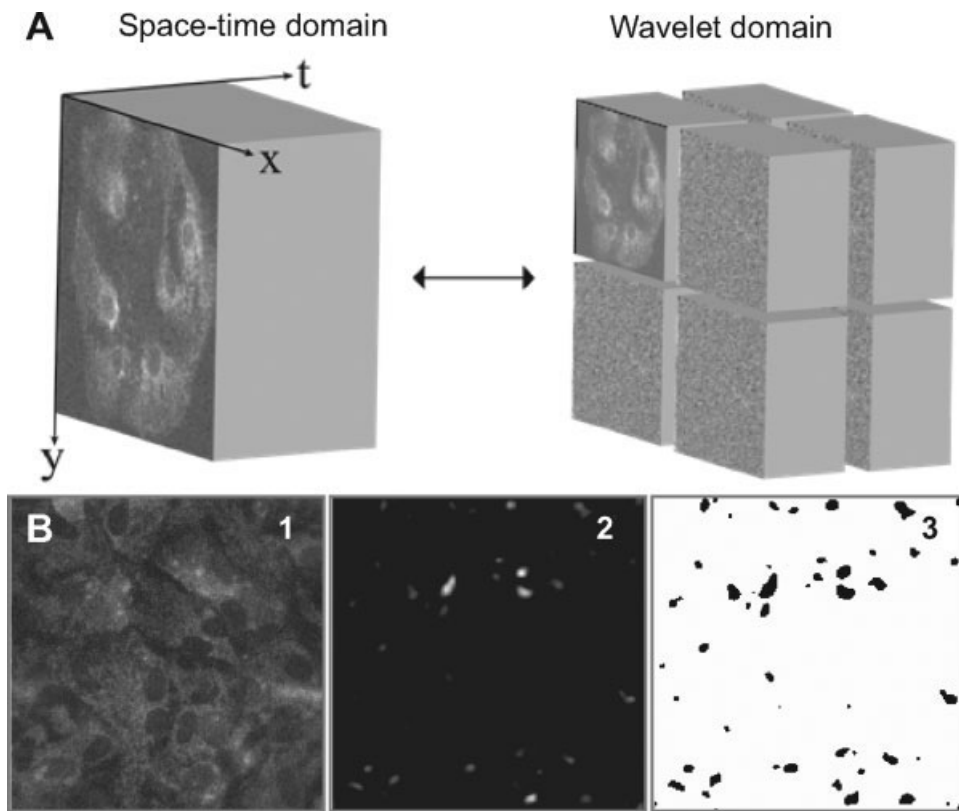
Fig. 2.   Quantification of Na$^{+}_{\mathrm{mit}}$ spiking. (**A**) Illustration of the spatiotemporal wavelet transform (one decomposition level) applied to the series of images on the left. The transform is linear, nonredundant, and orthogonal. The full transform further decomposes the lowpass subband. (**B**) The image analysis method for a single raw image of cells loaded with CR with several brighter spots indicative of a Na$^{+}_{\mathrm{mit}}$ spike (B1) isolates transients but preserves intensities (B2); these are used for cumulative intensity measurements of spiking activity on the whole image sequence. Cluster analysis of binarized results (B3) is then applied to the entire image sequence to assess the frequency of Na$^{+}_{\mathrm{mit}}$ spiking.
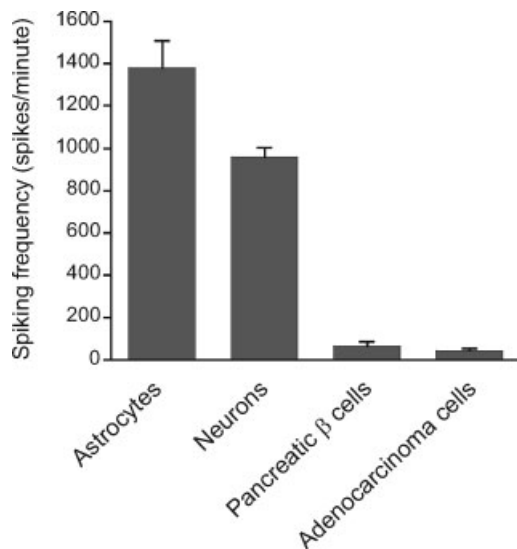
Fig. 3.   Comparison of Na$^{+}_{\mathrm{mit}}$ spiking in different cell types. Spiking activity was compared between astrocytes, cortical neurons, and nonneural cells, namely pancreatic β cells (MIN-6 cell line) and mammary adenocarcinoma cells (MCF-7 cell line). Data are mean number ($\pm$ SEM) of detected spikes per field per minute from $n = 156$ (astrocytes), 4 (neurons), 3 (MIN-6 cells), and 6 (MCF-7 cells) experiments.

ments, not shown). Spiking activity was thus rather steady and did not display bursting-like behavior.

Using this quantification tool, we then asked whether Na$^{+}_{\mathrm{mit}}$ spiking was a mitochondrial behavior found in all cell types. The presence of Na$^{+}_{\mathrm{mit}}$ spiking was investigated in mouse primary cortical neurons, in MIN-6 cells (mouse pancreatic β cell line), in MCF-7 cells (human mammary adenocarcinoma cell line), and compared with mouse cortical astrocytes under identical conditions. This analysis revealed that whereas both neural cell types exhibited robust Na$^{+}_{\mathrm{mit}}$ spiking, both MIN-6 cells and MCF-7 showed only marginal signs of Na$^{+}_{\mathrm{mit}}$ spiking (Fig. 3).

Collectively, this set of experiments indicated that the manifestation of Na$^{+}_{\mathrm{mit}}$ spiking is vastly different among cell types, which led us to consider Na$^{+}_{\mathrm{mit}}$ as a functional behavior of individual mitochondria. We therefore investigated the underlying pathways involved Na$^{+}_{\mathrm{mit}}$ spiking and focused our investigations in astrocytes.

Mechanisms Involved in the Generation of Na$^{+}_{\mathrm{mit}}$ Spiking

To determine which mechanisms and pathways are involved in Na$^{+}_{\mathrm{mit}}$ spiking, compounds described as

TABLE 1. Pathways Tested for Their Influence on Na^+_{mit} Spiking

Pathway	Drug	Cumulative mean intensity (% control)[a]	Spiking frequency (% control)[a]	n
NADH pathway—Complex I	Rotenone (1 μM)	100 ± 8	101 ± 3	7
Permeability transition pore	Bongkrekic acid (10 μM)	124 ± 30	116 ± 13	4
	Cyclosporin A (5 μM)	104 ± 24	114 ± 8	4
Adenine nucleotide transporter	Atractyloside (5 μM)	94 ± 36	107 ± 15	4
Mitochondrial K_{ATP} channel	U 37883A (100 μM)	113 ± 14	111 ± 1	2
	Diazoxide (100 μM)	146 ± 32	116 ± 12	15
Nitric oxide	S-nitroso-cysteine (200 μM)	102 ± 32	99 ± 5	2
Mitochondrial Na^+-Ca^{2+} exchanger	CGP-37157 (10 μM)	128 ± 44	120 ± 8	4
Mitochondrial H^+-K^+ exchanger	Quinine (100 μM)	125 ± 31	103 ± 13	6
Plasma membrane glutamate transporters	TBOA (500 μM)	103 ± 20	98 ± 6	6
AMPA/kainate receptors	CNQX (50 μM)	85 ± 17	91 ± 15	6

[a]Data are given as percent of control ±SEM; n, number of individual experiments. None of the listed compounds had a significant influence on Na^+_{mit} spiking activity ($P > 0.07$).

pharmacological blockers or modulators of mitochondrial conductances and transporters were tested. Those included CGP-37157, an inhibitor of mitochondrial Na^+/ Ca^{2+}; quinine, inhibitor of the nonselective Na^+/H^+ (K^+/H^+) antiporter; rotenone, inhibitor of complex I of the mitochondrial respiratory chain; cyclosporine A and bongkrekic acid, blockers of the mitochondrial permeability transition pore; atractyloside, a blocker of adenine nucleotide translocator; U 37883A and diazoxide, blocker and opener of mitochondrial K_{ATP} channels, respectively; S-nitrosocysteine, a nitric oxide donor. A possible link with tonic glutamate release and subsequent reuptake or receptor activation was also tested: Na^+-glutamate transporters were inhibited using the specific inhibitor TBOA and non-NMDA receptors were blocked using 6-cyano-7-nitroquinoxaline-2,3-dione (CNQX). None of these maneuvers was found to decrease or increase spiking activity in a reproducible manner (Table 1).

To test for the involvement of mitochondrial cation uniporters, we used the blocker ruthenium red, acting both at the level of mitochondrial Ca^{2+} (Kirichok et al., 2004) and Na^+ uniporters (Kapus et al., 1990). Ruthenium red strongly decreased the overall Na^+_{mit} spiking activity (Fig. 4A). This compound did not alter the overall Na^+_{mit} level during the experiment, but caused a slight decrease in mitochondrial Ca^{2+} level (not shown). As a Na^+ influx through cation uniporters should be electrogenic, we performed simultaneous monitoring of Na^+_{mit} and mitochondrial electrical potential ($\Delta\Psi_{mit}$) using CR and JC-1, respectively. Mitochondria with highly negative membrane potential promote the formation of JC-1 dye aggregates, which fluoresce red; mitochondria with low potential will contain monomeric JC-1 and fluoresce green. Therefore, mitochondrial depolarization should lead to reversible increased green and decreased red emission, respectively. When loaded alone in astrocytes, JC-1 signals displayed spontaneous transient increases in the green channel whose kinetic was consistent with Na^+_{mit} spikes. JC-1 green transients were accompanied by corresponding decreases in the red channel (aggregates) only in the less frequent cases of longer lasting transients (4 events out of 21). Therefore, Na^+_{mit} spikes detected with CR emitting in the red channel, should not be confounded with JC-1 signals. More-

over, when loaded alone, CR reported Na^+_{mit} spiking in the red channel as expected, but caused no change in the green channel (not shown). We found that ~90% of detected Na^+_{mit} spikes (181 out of 199 spikes) were accompanied by corresponding rapid $\Delta\Psi_{mit}$ depolarizations observed in the green JC-1 fluorescence channel (Fig. 4B). Nevertheless, Na^+_{mit} spikes with no or barely detectable changes in $\Delta\Psi_{mit}$ were observable in a low number of events (not shown). Analysis of coincident Na^+_{mit} and $\Delta\Psi_{mit}$ spikes indicated that the onset of depolarizations started 0.45 ± 0.06 s ($n = 177$ analyzed events, $P < 0.001$) after the onset of Na^+_{mit} spikes. The depolarization transient reached its maximum 2.17 ± 0.13 s ($P < 0.001$) after the Na^+_{mit} spike maximum. It is unclear whether the observed delays reflect a lag between changes of Na^+_{mit} and potential, or is caused by a differential reactivity of the two fluorescent probes. The existence of this delay is another indication that there is no crosstalk between the two fluorescent signals. Surprisingly, experiments performed under similar conditions using the mitochondrial potentiometric dye rhodamine 123 (1 μM) did not reveal simultaneous depolarizations (not shown). The discrepancy can probably be explained by a difference in the sensitivity of the two probes; the amplitude of depolarization could have been too small or fast to be detectable by rhodamine 123, or the resting $\Delta\Psi_{mit}$ was too negative to lead to significant transmembrane dye movement (Ubl et al., 1996). Alternatively, there are indications that rhodamine 123 induce photodamage that impede spontaneous mitochondrial depolarization in neurons (Buckman and Reynolds, 2001), which could explain the observed differences. Finally, applying the mitochondrial uncoupler FCCP at low concentrations (0.01 and 0.05 μM), thereby weakening the driving force of the mitochondrial cation uniporter, diminished the frequency of CR transients (Fig. 4C). Taken together, these data suggest that mitochondrial cation uniporters are the Na^+ entry pathway during spiking.

In a previous study, we showed that the selective mitochondrial Na^+/H^+ exchanger is the main mechanism enabling the regulation of Na^+_{mit} concentration in astrocytes (Bernardinelli et al., 2006). This exchanger uses the proton (pH) gradient across the inner membrane to drive Na^+ out of the matrix. Involvement of this anti-
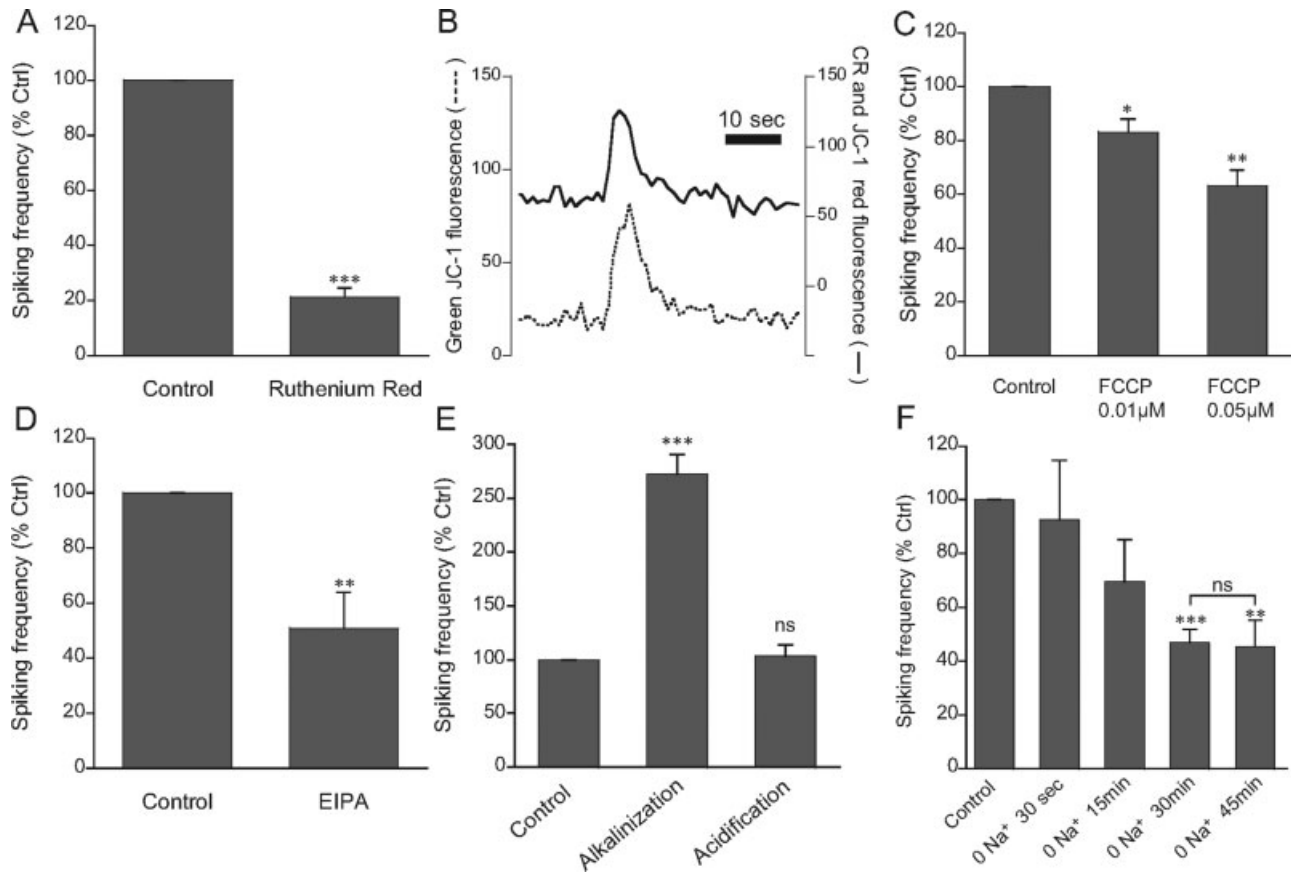
Fig. 4.   Involvement of mitochondrial cation uniporters and mitochondrial Na^+/H^+ exchanger in Na^+_{mit} spiking. (**A–C**) Involvement of the mitochondrial cation uniporter. (A) After a control period, application of the uniporter blocker ruthenium red (50 μM) for 15 min strongly decreased Na^+_{mit} frequency ($n = 5$). Data are shown as percent of control ± SEM (B) Simultaneous Na^+_{mit} and $\Delta\Psi_{mit}$ measurements in individual mitochondria. The graph shows an example of mitochondrion exhibiting a Na^+_{mit} spike measured using CR (plain line, right axis) that was accompanied by a depolarizing transient measured using JC-1 in the green channel (dotted line, left axis). Experimental procedure is detailed in supplementary information. (C) Weakening of $\Delta\Psi_{mit}$ using the mitochon-

drial uncoupler FCCP decreased Na^+_{mit} spiking frequency ($n = 5$). (**D, E**) Involvement of the mitochondrial Na^+/H^+ exchanger. (D) Cells were perfused with the inhibitor of Na^+/H^+ exchanger EIPA (50 μM, $n = 5$), which decreased the spiking frequency. (E) Cytosolic alkalinization using a CO_2-free buffer ($n = 6$) dramatically increased the spiking frequency whereas intracellular acidification induced by ammonium pulse (20 mM, $n = 5$) did not alter the spiking frequency. (**F**) After a measurement in control condition, cells were perfused in Na^+-free solution (0 Na^+) and spiking frequency was measured at indicated time points ($n = 6$–10). Data are percent of respective controls ± SEM; ns, nonsignificant; *$P < 0.05$; **$P < 0.01$; ***$P < 0.001$ using a paired t-test.

porter for Na^+_{mit} spiking was then investigated. Five minutes superfusion of the inhibitor of mitochondrial Na^+/H^+ exchanger ethyl-isopropyl amiloride (EIPA) markedly decreased the Na^+_{mit} spiking frequency (Fig. 4D) without altering cytosolic pH as measured using the pH-sensitive fluorescent probe 2′,7′-bis-(2-carboxyethyl)-5-(and-6)-carboxyfluorescein acetoxymethyl ester (BCECF-AM) (not shown). The dependency of Na^+_{mit} spiking on cellular pH was then tested. Cellular alkalinization was accomplished by perfusion of a CO_2-free bicarbonate buffer, which increased the cell pH by 0.78 ± 0.02 units ($n = 4$ exp). This treatment strongly increased Na^+_{mit} spiking frequency (Fig. 4E). Acidification was obtained by introduction of an intracellular proton load following rapid washout of ammonium chloride. In this situation, pH decreased by 0.83 ± 0.02 units (30 cells, from 5 exp). This maneuver did not significantly alter Na^+_{mit} spiking frequency (Fig. 4E). The same result was obtained by mild acidification (0.07 ± 0.004 pH units, $n = 4$ exp) caused by application of the or-

ganic anion propionate (20 mM) that enters cells by non-ionic diffusion (not shown). We then tested if the cellular Na^+ concentration could modulate the Na^+_{mit} spiking frequency. Astrocytes were first superfused with a Na^+-free solution. This treatment that lowers cellular Na^+ is expected to decrease Na^+_{mit} levels as well. As expected, under these conditions, both the overall Na^+_{mit} level and the amplitude of Na^+_{mit} spikes decreased gradually (not shown). However, the frequency of Na^+_{mit} spiking also declined significantly (Fig. 4F). Interestingly, the Na^+_{mit} spiking frequency reached a minimum at 30 min of Na^+ free solution perfusion and did not further decrease, whereas the cumulative mean intensity relative to spikes amplitude continued to drop. Conversely, we tested if Na^+_{mit} spiking frequency could be altered in increased Na^+_{mit} conditions. Induction of Na^+_{mit} increase by opening the K_{ATP} channel or by 5 min ouabain treatment (Bernardinelli et al., 2006) did not significantly enhance the Na^+_{mit} spiking activity (Table 1 and Fig. 6C). Thus, whereas Na^+_{mit} spiking activity was sensitive
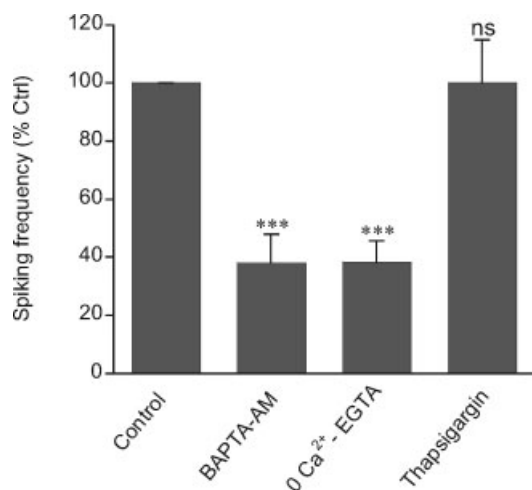
Fig. 5. Ca^{2+} plays a permissive role on Na^+_{mit} spiking activity. After a control period, BAPTA-AM (50 μM) was applied for 30 min after which Na^+_{mit} frequency was measured and showed a decrease in frequency ($n = 5$). Cell perfusion for 30 min with a Ca^{2+}-free solution (see Materials and Methods) decreased Na^+_{mit} spiking frequency by the same amount ($n = 5$). However, thapsigargin (1 μM) which induces an ER Ca^{2+} release did not alter spiking frequency ($n = 3$). Data are shown as percent of control ± SEM. (ns, nonsignificant; ***$P < 0.001$ using a paired t-test, compared with the control condition).

to lowered Na^+_{mit}, the spiking frequency was not correlated with cellular Na^+ level above basal level. Taken together, this set of experiments emphasizes the involvement of mitochondrial Na^+/H^+ exchangers as efflux pathways during Na^+_{mit} spiking.

Modulation of Na^+_{mit} Spiking Activity

We then looked into factors that could modulate Na^+_{mit} spiking activity. We first tested a role of intracellular Ca^{2+}, which was found to be involved in the glutamate-mediated increase of Na^+_{mit} level in astrocytes (Bernardinelli et al., 2006). In a first phase, cells were loaded with 1,2 bis(o-aminophenoxy)ethane-N,N,N',N'-tetraacetic acid acetoxymethyl ester (BAPTA-AM) to chelate intracellular free $Ca.^{2+}$ Figure 5 shows that the frequency of Na^+_{mit} spiking was strongly diminished by chelating Ca^{2+}. In addition, decreasing cellular Ca^{2+} by superfusing astrocytes in a Ca^{2+}-free solution led to the same inhibition of Na^+_{mit} spiking activity (Fig. 5). However, acutely increasing cytosolic Ca^{2+} by endoplasmic reticulum (ER) Ca^{2+} release using thapsigargin did not cause an increase in Na^+_{mit} frequency. This set of experiments indicated that Ca^{2+} is involved in the regulation of Na^+_{mit} spiking.

We then explored the possible link between Na^+_{mit} spiking and cellular bioenergetics. In particular, ATP levels can undergo significant variations during activity in astrocytes. In these experiments, we applied maneuvers to manipulate cellular ATP and assessed the relative ATP level changes indirectly by measuring free Mg^{2+} using the fluorescent probe Magnesium Green as previously described (Chatton and Magistretti, 2005). As

ATP hydrolysis releases bound Mg^{2+}, Magnesium Green fluorescence intensity is inversely related to cytosolic ATP concentration. To cause a severe ATP depletion, cells were treated with 2-deoxyglucose (2-DG) plus oligomycin, inhibitors of glycolysis and mitochondrial ATP synthase, respectively (Fig. 6A, left). To induce an intermediate ATP decrease, cells were superfused with the neurotransmitter glutamate (Fig. 6A, center). In astrocytes, the cellular uptake of glutamate significantly lowers ATP levels by strong stimulation of the Na,K-ATPase (Chatton and Magistretti, 2005; Chatton et al., 2000). Finally, to increase ATP levels, the Na,K-ATPase was inhibited using ouabain. The Na^+ pump being a major ATP consumer in astrocytes (Chatton and Magistretti, 2005), its inhibition led to a transient increase in cellular ATP levels (maximal at ~30 s) which decreased close to baseline after 5 min (Fig. 6A, right). The relative ATP level changes caused by these maneuvers are summarized in Fig. 6B. In a second phase, the same experimental maneuvers were repeated on cells and Na^+_{mit} spiking was recorded. Figure 6C shows that Na^+_{mit} spiking frequency was influenced by maneuvers altering ATP levels and followed a positive correlation with the relative ATP level. ATP synthesis blockers impaired Na^+_{mit} spiking activity by 29%. However, this treatment was found in separate experiments to cause a mild mitochondrial depolarization (not shown). Glutamate, which, by its stimulation of Na,K-ATPase activity, decreased ATP levels to a lesser extent, also decreased Na^+_{mit} spiking activity. It is worthy of note that glutamate application did not depolarize mitochondria, rather slightly hyperpolarized them (not shown). Ouabain, inducing a transient increase in ATP level, which was maximal at 30 s, induced an increase in Na^+_{mit} spiking frequency. Collectively, these data suggest that the cellular ATP level could provide a feedback regulation on Na^+_{mit} spiking activity.

DISCUSSION

The present study shows that individual mitochondria in resting astrocytes exhibit rapid spontaneous Na^+ concentration transients. This first demonstration of Na^+_{mit} activity has been made possible by the Na^+-sensitive probe CR that loads into the matrix of mitochondria in living cells. The calibrated resting Na^+_{mit} level in astrocytes (~12–20 mM) was found to be consistent with values estimated for mitochondria of neurons (Pivovarova et al., 2002). Na^+_{mit} spikes of individual mitochondria have substantial amplitude and well-defined kinetics, with spike duration homogeneous among different mitochondria, cover-slips and cell cultures. Although Na^+_{mit} changes in certain mitochondria reached high values during spiking—often three times the basal concentration—Na^+_{mit} transients did not appear to be transmitted to neighboring mitochondria as a wave, which suggests that mitochondria of astrocytes do not form a lumenally continuous network but are morphological and functional distinct units as reported in other studies (Collins
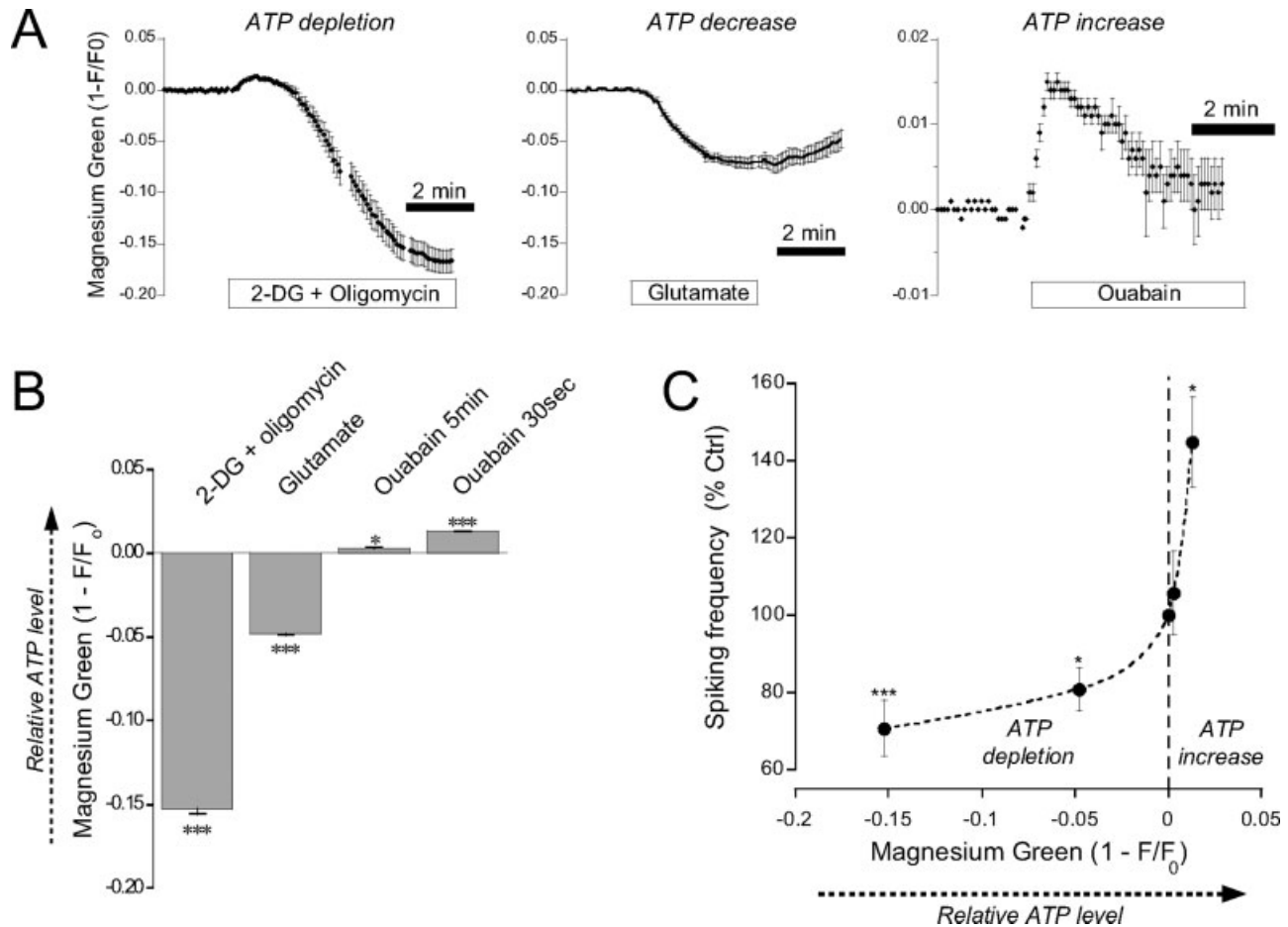
Fig. 6. Relationship between Na^+_{mit} spiking activity and cellular ATP levels. (**A**) Cellular ATP was depleted using 10 mM 2DG plus 1 μM oligomycin (left), or was decreased by glutamate (200 μM) application (center), or transiently increased by treatment of the cells with ouabain 1mM (right). The effectiveness of these maneuvers was assessed by monitoring relative ATP levels using Magnesium Green fluorescence changes. To make the data more legible, the fluorescence scale is shown as $1-F/F_0$, which is directly proportional with ATP levels.

(**B**) Relative ATP levels during corresponding protocol shown in (A). Data are means ± SEM of three to four experiments for each protocol. (**C**) Using identical protocols, Na^+_{mit} spiking frequency was measured. The resulting spiking frequency was then plotted against the relative ATP levels summarized in (B) and showed a monotonical relationship between the two parameters. Spiking frequencies are presented as percent of control ± SEM from five to seven experiments for each protocol.

et al., 2002). During the recording period, stained mitochondria displayed no detectable morphological signs of fission or fusion linked to CR transients. Fission or fusion should result in similar change in other mitochondrial labeling. However, CR transients occurred without coincident alteration of rhodamine 123 staining, a mitochondrial selective dye. In addition, it has been recently reported that thapsigargin induces rapid Ca^{2+}-dependent fragmentation of mitochondria (Hom et al., 2007). Such treatment did not modify Na^+_{mit} spiking activity in our astrocyte preparation. Thus, it can be concluded that Na^+_{mit} spiking activity is a mitochondrial process distinct from fusion or fission. It is interesting to note that, whereas the nonneural cell types tested in our study (MIN-6 and MCF-7 cells) displayed a typical mitochondrial staining pattern, they exhibited a 21-fold and 31-fold lower Na^+_{mit} spiking activity, respectively, than astrocytes under identical experimental conditions. This observation could indicate that Na^+_{mit} spiking is preferentially expressed in cell types experiencing sub-

stantial intracellular Na^+ concentration changes during activity, such as neurons and astrocytes (Bernardinelli et al., 2004; Pivovarova et al., 2002).

To elucidate whether the driving force of Na^+ influx into mitochondria during spiking derives from the strongly negative potential across the inner membrane, we set up an experimental protocol to simultaneously record both Na^+_{mit} and $\Delta\Psi_{mit}$ and found that the vast majority of Na^+_{mit} spikes were accompanied with depolarizations of similar aspect. However both the onset and the peak of depolarization appeared to follow Na^+_{mit} changes with a certain lag. This lag is most probably due to differences in response kinetics of the two probes. Nevertheless, the coincidence and similar timecourse of $\Delta\Psi_{mit}$ and Na^+_{mit} signals are consistent with the notion that the electrophoretic Na^+ entry induces mitochondrial depolarization (Bernardi et al., 1990). The fact that such coincident depolarizations could not be detected using rhodamine 123, a potential-sensitive dye based on a different principle, probably indicates that the magnitude

of transient depolarizations was limited. In addition, the complete reversibility of both $\Delta\Psi_{mit}$ and Na^+_{mit} signals after spiking speaks against a complete collapse of potential. Assuming that mitochondrial depolarization was caused by Na^+_{mit} influx and considering that the involvement of the electrogenic Na^+/Ca^{2+} exchanger was excluded on the basis of the lack of effect of the inhibitor CGP-37157, the identity of the pathway for electrophoretic Na^+ entry appears to be a cation uniporter. Indeed Na^+_{mit} spiking activity was severely impaired by ruthenium red, a blocker of the mitochondrial Ca^{2+} and Na^+ uniporters (Kapus et al., 1990; Kirichok et al., 2004). Conversely, weakening of the driving force of the mitochondrial cation uniporter using the uncoupler FCCP diminished Na^+_{mit} spiking activity. Finally, the flux through the mitochondrial Na^+ uniporter was reported to display an optimum at alkaline pH (7.5–8), which is consistent with our observations of increased spiking activity at higher intracellular pH (Bernardi, 1999; Bernardi et al., 1990). Taken together, mitochondrial cation uniporters are realistic candidates for mediating Na^+ entry pathway during spiking.

The Na^+/H^+ exchanger of the inner mitochondrial membrane is described as the mechanism responsible for maintaining or restoring low Na^+_{mit} levels. We have recently shown that this transport system is critically involved in the regulation of Na^+_{mit} in astrocytes subjected to global intracellular Na^+ increase (Bernardinelli et al., 2006). An integrated model of Ca^{2+}, Na^+ and H^+ fluxes occurring in mitochondria during cardiac myocyte pacing activity recently showed that the Na^+ flux mediated by the Na^+/H^+ exchanger can reach 20 mM/s during pacing at 1–2 Hz (Nguyen et al., 2007). This value is higher than what found in our experiments during Na^+_{mit} spiking (5.2 ± 0.7 mM/s), making the Na^+/H^+ exchanger a plausible pathway involved during Na^+_{mit} spiking. The present report shows that inhibition of mitochondrial Na^+/H^+ exchanger strongly diminished Na^+_{mit} spiking activity. Other pieces of evidence point to a key role of this mechanism, namely the relationship with Na^+ and pH changes. In particular, the frequency of Na^+_{mit} spiking was found to be diminished by cellular Na^+ depletion. However, Na^+_{mit} spiking frequency was not correlated with Na^+_{mit} above basal level. For instance, ouabain treatment, which increases cytosolic as well as mitochondrial Na^+_{mit} levels, had a more pronounced effect on spiking frequency at 30 s when Na^+ levels are only increased by a few milimolar than after 5 min of ouabain application, when Na^+_{mit} levels have considerably increased (Bernardinelli et al., 2006). The Na^+/H^+ exchanger isoform NHE1 at the plasma membrane has an affinity for extracellular Na^+ of 3–50 mM (Putney et al., 2002), which means that because extracellular Na^+ concentration greatly exceeds these values, most exchangers operate under condition of saturation with respect to external Na^+ and under the driving force of the transmembrane Na^+ concentration. It might be a different situation in mitochondria, as the mitochondrial matrix Na^+ concentration was estimated to be in the range 12–18 mM in astrocytes (Bernardinelli et al.,

2006) and where the driving force for Na^+/H^+ exchange is rather the transmembrane proton gradient. It is assumed that mitochondrial Na^+/H^+ exchangers display a Km of ~26 mM for Na^+ and are symmetrical in their interaction with Na^+ (Bers et al., 2003), with a consequence of being reversible. Another characteristic of the exchanger could also explain the observation that Na^+_{mit} spiking was strongly enhanced by cellular alkalinization. The corresponding exchanger at the plasma membrane is known to contain proton modifier sites, distinct from the proton transport site that critically controls the activity of transport (Wakabayashi et al., 2003). This was shown to be the case for three isoforms of the exchanger (NHE1, NHE2, and NHE3), and is likely to be also found in the mitochondrial isoform. Thus, in addition to cation uniporters (see above), the Na^+/H^+ exchanger could also underlie the observed effects of alkalinization both by a modulation of transporter turnover rate and by the alteration of pH gradients.

We found that Na^+_{mit} spiking activity was strongly affected by a decrease in calcium concentration, which indicated that Ca^{2+} appears to have a permissive role on spiking, although not through direct involvement of mitochondrial Na^+/Ca^{2+} exchangers. As mitochondria are in close interaction with ER (Rizzuto et al., 1998), we tested if Na^+_{mit} could be induced by spontaneous ER Ca^{2+} release as it was reported in cardiomyocytes (Duchen et al., 1998). Emptying the Ca^{2+} stores with thapsigargin had no effect on Na^+_{mit} spiking. In addition, astrocytes are known to display spontaneous cytosolic Ca^{2+} oscillations both in culture and in situ (Parri et al., 2001). However, these oscillations involve generalized cellular Ca^{2+} movements, very different from the localized Na^+_{mit} spikes observed here. Moreover, Ca^{2+} transients have threefold to fivefold longer duration than Na^+_{mit} spikes. Thus, it can be concluded that Na^+_{mit} spiking activity was not correlated with cellular Ca^{2+} oscillation, without excluding a potential long-term regulatory effect of Ca^{2+} oscillations.

As discussed earlier, several observations led us to conclude that increased cytosolic or mitochondrial Na^+ levels were not directly influencing Na^+_{mit} spiking frequency. For instance, glutamate application rapidly and substantially increases cytosolic and mitochondrial Na^+ concentrations in astrocytes, yet it decreased spiking frequency. These considerations led us to look into another element that could link these observations, namely ATP levels. Na^+-coupled glutamate uptake causes a substantial energy burden to astrocytes. The influx of Na^+ causes the Na^+ pump to more than double its activity, with corresponding increase in ATP hydrolysis (Chatton and Magistretti, 2005). Conversely, blocking the Na^+ pump, which accounts for about half of the total cellular ATP consumption in these cells, causes a sizable decreased ATP hydrolysis. Therefore we investigated to what extent cellular ATP levels, could be considered a factor influencing mitochondrial Na^+ spiking. Using a set of experimental maneuvers aimed at either decreasing or increasing ATP levels, we found indications that spiking was positively correlated with ATP

levels, which might indicate that ATP plays a modulatory or feedback role on Na^+_{mit} spiking. Several cellular elements could mediate such a modulation. For instance, a mitochondrial Na^+ permeable uniporter was described to be opened in low divalent cation containing medium and its open-state could be induced by ATP (Bernardi et al., 1990). Also, the activity of the Na^+/H^+ exchanger at the plasma membrane is known to be modulated by ATP (Demaurex et al., 1997; Wakabayashi et al., 2003).

Spontaneous mitochondrial depolarizations have been observed in neurons using the same mitochondrial potentiometric dye JC-1 used in our studies with astrocytes (Buckman and Reynolds, 2001). It is conceivable that a similar situation occurs in neurons and that Na^+_{mit} spikes could be at the origin of the observed mitochondrial depolarization. Taking the results of the present study together, we could speculate that mitochondrial depolarizations are driven by the opening of a mitochondrial cation uniporter in microdomains containing a high levels of ATP, inducing a substantial increase in Na^+_{mit} subsequently extruded by the mitochondrial Na^+/H^+ exchanger powered by the proton motive force. However, the experiments performed in this study do not allow discriminating between intra- and extramitochondrial ATP. As the existence of cytosolic ATP domains has been recently proposed to be unlikely (Barros and Martinez, 2007), mitochondrial ATP could be the triggering factor. Conversely, the activity of the mitochondrial Na^+/H^+ exchanger during Na^+_{mit} spiking, is expected to substantially alter pH in the mitochondrial matrix and intermembrane space, which could impact on the proton electrochemical gradient used by the ATP synthase. Thus, Na^+_{mit} spiking could have a modulatory role on mitochondrial energy production.

Finally, this first demonstration of spontaneous Na^+_{mit} spiking activity might reveal of critical importance for the understanding of astrocyte metabolism. First, intracellular Na^+ is a pivotal element in the bioenergetics of astrocytes enabling the coupling of neuronal activity and astrocyte metabolic response (Magistretti et al., 1999). In astrocytes, intracellular Na^+ is increasingly recognized as a factor critically involved in the regulation of energy metabolism, at the level of both intercellular and sub-cellular communication (Bernardinelli et al., 2004, 2006). Although astrocytes are electrically nonexcitable, they are subject to substantial variations in their cytosolic Na^+ concentration, as they are responsible for actively maintaining low extracellular levels of glutamate in the brain using the Na^+-coupled glutamate uptake (Danbolt, 2001). Astrocytes are known to favor aerobic glycolysis over oxidative phosphorylation as a response to enhanced glutamate uptake (Magistretti et al., 1999). Further work is needed to determine whether the decrease in Na^+_{mit} spiking frequency coincident with glutamate application is involved in the pattern of metabolic response of astrocytes, and whether spiking represents a form of frequency encoding of sub-cellular metabolic information, as proposed for Ca^{2+} oscillations in hepatocytes (Hajnoczky et al., 1995).

In conclusion, the present study shows that individual mitochondria in intact astrocytes display spontaneous transients of their Na^+ content. The underlying mechanisms of this spiking activity involve the activity of mitochondrial cation uniporters and mitochondrial Na^+/H^+ exchangers. Ca^{2+} was found to play a permissive role, whereas cellular ATP level a positive influence on Na^+_{mit} spiking activity.

ACKNOWLEDGMENTS

REFERENCES

Baron S, Caplanusi A, van de Ven M, Radu M, Despa S, Lambrichts I, Ameloot M, Steels P, Smets I. 2005. Role of mitochondrial Na^+ concentration, measured by CoroNa Red, in the protection of metabolically inhibited MDCK cells. J Am Soc Nephrol 16:3490–3497.

Barros LF, Martinez C. 2007. An enquiry into metabolite domains. Biophys J 92:3878–3884.

Battle G. 1987. A block spin construction of ondelettes. I. Lemarie functions. Commun Math Phys 110:601–615.

Bernardi P. 1999. Mitochondrial transport of cations: Channels, exchangers, and permeability transition. Physiol Rev 79:1127–1155.

Bernardi P, Angrilli A, Azzone GF. 1990. A gated pathway for electrophoretic Na^+ fluxes in rat liver mitochondria. Regulation by surface Mg^{2+}. Eur J Biochem 188:91–97.

Bernardinelli Y, Azarias G, Chatton J-Y. 2006. In situ fluorescence imaging of glutamate-evoked mitochondrial Na^+ responses in astrocytes. Glia 54:460–470.

Bernardinelli Y, Magistretti PJ, Chatton J-Y. 2004. Astrocytes generate Na^+-mediated metabolic waves. Proc Natl Acad Sci USA 101:14937–14942.

Bers DM, Barry WH, Despa S. 2003. Intracellular Na^+ regulation in cardiac myocytes. Cardiovasc Res 57:897–912.

Buckman JF, Reynolds IJ. 2001. Spontaneous changes in mitochondrial membrane potential in cultured neurons. J Neurosci 21:5054–5065.

Chatton J-Y, Idle JR, Vågbø CB, Magistretti PJ. 2001. Insights into the mechanisms of ifosfamide encephalopathy: Drug metabolites have agonistic effects on a-amino-3-hydroxy- 5-methyl-4-isoxazolepropionic acid (AMPA)/kainate receptors and induce cellular acidification in mouse cortical neurons. J Pharmacol Exp Ther 299:1161–1168.

Chatton J-Y, Magistretti PJ. 2005. Relationship between L-glutamate-regulated intracellular Na^+ dynamics and ATP hydrolysis in astrocytes. J Neural Transm 112:77–85.

Chatton J-Y, Marquet P, Magistretti PJ. 2000. A quantitative analysis of L-glutamate-regulated Na^+ dynamics in mouse cortical astrocytes: Implications for cellular bioenergetics. Eur J Neurosci 12:3843–3853.

Collins TJ, Berridge MJ, Lipp P, Bootman MD. 2002. Mitochondria are morphologically and functionally heterogeneous within cells. EMBO J 21:1616–1627.

Danbolt NC. 2001. Glutamate uptake. Prog Neurobiol 65:1–105.

Demaurex N, Distelhorst C. 2003. Cell biology. Apoptosis—The calcium connection. Science 300:65–67.

Demaurex N, Romanek RR, Orlowski J, Grinstein S. 1997. ATP dependence of Na^+/H^+ exchange. Nucleotide specificity and assessment of the role of phospholipids. J Gen Physiol 109:117–128.

Denton RM, McCormack JG, Edgell NJ. 1980. Role of calcium ions in the regulation of intramitochondrial metabolism. Effects of Na^+, Mg2$^+$ and ruthenium red on the Ca2$^+$-stimulated oxidation of oxoglutarate and on pyruvate dehydrogenase activity in intact rat heart mitochondria. Biochem J 190:107–117.

Duchen MR, Leyssens A, Crompton M. 1998. Transient mitochondrial depolarizations reflect focal sarcoplasmic reticular calcium release in single rat cardiomyocytes. J Cell Biol 142:975–988.

Hajnoczky G, Robbgaspers LD, Seitz MB, Thomas AP. 1995. Decoding of cytosolic calcium oscillations in the mitochondria. Cell 82:415–424.

Hom JR, Gewandter JS, Michael L, Sheu SS, Yoon Y. 2007. Thapsigargin induces biphasic fragmentation of mitochondria through calcium-mediated mitochondrial fission and apoptosis. J Cell Physiol 212:498–508.

Jayaraman S, Joo NS, Reitz B, Wine JJ, Verkman AS. 2001a. Submucosal gland secretions in airways from cystic fibrosis patients have normal [Na^+] and pH but elevated viscosity. Proc Natl Acad Sci USA 98:8119–8123.

Jayaraman S, Song Y, Vetrivel L, Shankar L, Verkman AS. 2001b. Noninvasive in vivo fluorescence measurement of airway-surface liquid depth, salt concentration, and pH. J Clin Invest 107:317–324.

Jung DW, Apel LM, Brierley GP. 1992. Transmembrane gradients of free Na^+ in isolated heart mitochondria estimated using a fluorescent probe. Am J Physiol 262:C1047–C1055.

Jung DW, Baysal K, Brierley GP. 1995. The sodium-calcium antiport of heart mitochondria is not electroneutral. J Biol Chem 270:672–678.

Kapus A, Szaszi K, Kaldi K, Ligeti E, Fonyo A. 1990. Ruthenium red inhibits mitochondrial Na^+ and K^+ uniports induced by magnesium removal. J Biol Chem 265:18063–18066.

Kirichok Y, Krapivinsky G, Clapham DE. 2004. The mitochondrial calcium uniporter is a highly selective ion channel. Nature 427:360–364.

Lei SZ, Pan ZH, Aggarwal SK, Chen HS, Hartman J, Sucher NJ, Lipton SA. 1992. Effect of nitric oxide production on the redox modulatory site of the NMDA receptor-channel complex. Neuron 8:1087–1099.

Magistretti PJ, Pellerin L, Rothman DL, Shulman RG. 1999. Energy on demand. Science 283:496–497.

Mallat S. 1989. A theory for multiresolution signal decomposition: The wavelet decomposition. IEEE Trans Pattern Anal Mach Intell 11:674–693.

Mitchell P. 1979. Keilin's respiratory chain concept and its chemiosmotic consequences. Science 206:1148–1159.

Montero M, Alonso MT, Carnicero E, Cuchillo-Ibanez I, Albillos A, Garcia AG, Garcia-Sancho J, Alvarez J. 2000. Chromaffin-cell stimulation triggers fast millimolar mitochondrial Ca^{2+} transients that modulate secretion. Nat Cell Biol 2:57–61.

Morgenthaler FD, Kraftsik R, Catsicas S, Magistretti PJ, Chatton J-Y. 2006. Glucose and lactate are equally effective in energizing activity-dependent synaptic vesicle turnover in purified cortical neurons. Neuroscience 141:157–165.

Nguyen MH, Dudycha SJ, Jafri MS. 2007. The effects of Ca^{2+} on cardiac mitochondrial energy production is modulated by Na^+ and H^+ dynamics. Am J Physiol Cell Physiol 292:C2004–C2020.

Nicholls DG, Budd SL. 2000. Mitochondria and neuronal survival. Physiol Rev 80:315–360.

Parri HR, Gould TM, Crunelli V. 2001. Spontaneous astrocytic Ca^{2+} oscillations in situ drive NMDAR-mediated neuronal excitation. Nat Neurosci 4:803–812.

Pawelczyk T, Olson MS. 1995. Changes in the structure of pyruvate dehydrogenase complex induced by mono- and divalent ions. Int J Biochem Cell Biol 27:513–521.

Pinton P, Rimessi A, Romagnoli A, Prandini A, Rizzuto R. 2007. Biosensors for the detection of calcium and pH. Methods Cell Biol 80:297–325.

Pivovarova NB, Pozzo-Miller LD, Hongpaisan J, Andrews SB. 2002. Correlated calcium uptake and release by mitochondria and endoplasmic reticulum of CA3 hippocampal dendrites after afferent synaptic stimulation. J Neurosci 22:10653–10661.

Putney LK, Denker SP, Barber DL. 2002. The changing face of the Na^+/H^+ exchanger, NHE1: structure, regulation, and cellular actions. Annu Rev Pharmacol Toxicol 42:527–552.

Reynolds IJ, Rintoul GL. 2004. Mitochondrial stop and go: Signals that regulate organelle movement. Sci STKE 2004:PE46.

Rizzuto R, Pinton P, Carrington W, Fay FS, Fogarty KE, Lifshitz LM, Tuft RA, Pozzan T. 1998. Close contacts with the endoplasmic reticulum as determinants of mitochondrial Ca^{2+} response. Science 280:1763–1766.

Sorg O, Magistretti PJ. 1992. Vasoactive intestinal peptide and noradrenaline exert long-term control on glycogen levels in astrocytes: Blockade by protein synthesis inhibition. J Neurosci 12:4923–4931.

Ubl JJ, Chatton J-Y, Chen S, Stucki JW. 1996. A critical evaluation of in situ measurement of mitochondrial electrical potentials in single hepatocytes. Biochim Biophys Acta 1276:124–132.

Unser M, Aldroubi A. 1996. A review of wavelets in biomedical applications. Proc IEEE 84:626–638.

Unser M, Blu T. 2000. Fractional splines and wavelets. SIAM Rev 42:43–67.

Wakabayashi S, Hisamitsu T, Pang T, Shigekawa M. 2003. Kinetic dissection of two distinct proton binding sites in Na^+/H^+ exchangers by measurement of reverse mode reaction. J Biol Chem 278:43580–43585.

Walter L, Hajnoczky G. 2005. Mitochondria and endoplasmic reticulum: The lethal interorganelle cross-talk. J Bioenerg Biomembr 37:191–206.

Yang KT, Pan SF, Chien CL, Hsu SM, Tseng YZ, Wang SM, Wu ML. 2004. Mitochondrial Na^+ overload is caused by oxidative stress and leads to activation of the caspase 3-dependent apoptotic machinery. FASEB J 18:1442–1444.

2. Specificity of ionic alterations during spontaneous mitochondrial Na⁺ transient

The detailed mechanisms mediating Na^+ entry into mitochondria as well as events triggering mitochondrial Na^+ transients remain to be clarified. In particular, mitochondrial Na^+ transients involve a ruthenium red-sensitive pathway, compatible with cation uniporter, whose identity is still unclear. In this part of the project, we have investigated the specificity of ionic alterations during mitochondrial Na^+ transients. I performed the experiments. I analyzed the results and prepared the figures with Jean-Yves Chatton. Part of this work was presented on a poster presented at the 6th FENS forum of European Neurosciences (Geneva, 2008).

In the previous section, we showed that individual mitochondria of astrocytes exhibit spontaneous transient increases of Na^+ concentration, simultaneously with transient mitochondrial depolarization (Azarias et al., 2008). In myocytes, spontaneous individual mitochondrial depolarizations have been linked to an increase of the activity of the mitochondrial inner membrane chain (Wang et al., 2008). As mitochondrial Na^+ transients are also coincident with transient mitochondrial depolarizations, we hypothesized that mitochondrial Na^+ transients may be coincident with alterations of the mitochondrial matrix pH potentially due to increase of the mitochondrial respiratory chain activity. We addressed this issue by using transfected astrocytes expressing MitoSypHer, a genetically-encoded fluorescent probe targeted to mitochondrial matrix and sensitive to pH (Azarias et al., *submitted*; Demaurex and Poburko, 2009). We observed that individual mitochondria of resting astrocytes exhibited transient increases of their MitoSypHer fluorescence intensity corresponding to mitochondrial alkaline transients (**Fig. 15**).
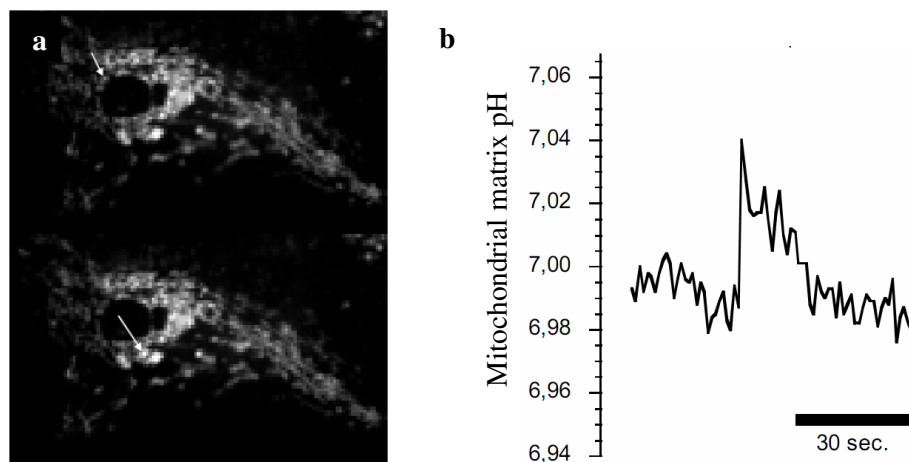
Fig. 15: Astrocyte mitochondria exhibit individual spontaneous transient alkalinizations of mitochondrial matrix as revealed with the mitochondrially-targeted pH-sensitive probe MitoSypHer. (**a**) Fluorescence images depicting MitoSypHer fluorescence pattern. A mitochondrion exhibiting a mitochondrial alkaline transient is indicated with an arrow in the bottom image. (**b**) Example trace of calibrated mitochondrial alkaline transient in single mitochondrion of resting astrocytes.

Similar to mitochondrial Na^+ transients, mitochondrial alkaline transients occurred spontaneously in individual mitochondria and with durations comparable with mitochondrial Na^+ transients. Therefore, we tested if spontaneous mitochondrial Na^+ transients were coincident with mitochondrial alkaline transients by labelling MitoSypHer transfected astrocytes with CoroNa Red to monitor both Na^+_{mit} and pH_{mit} in the same mitochondrion (**Fig. 16**).
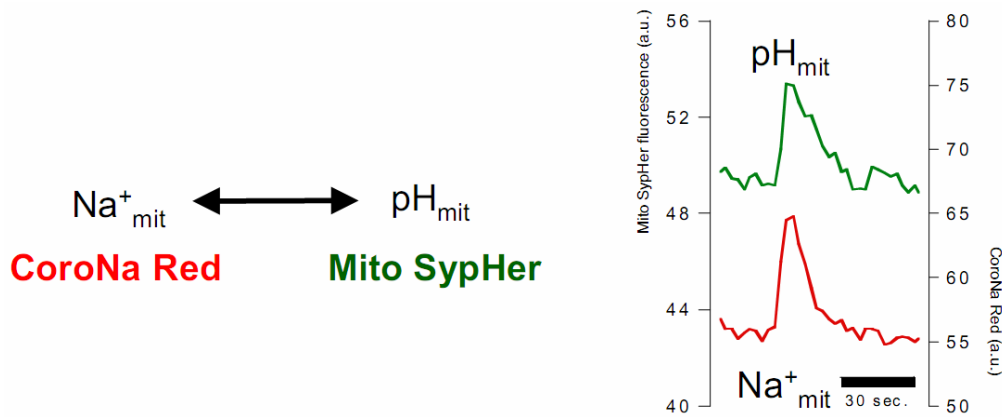
Fig. 16: Mitochondrial Na^+ transients are coincident with mitochondrial alkaline transients. MitoSypHer transfected astrocytes loaded with CoroNa Red.

As seen in **Fig. 16**, we observed that spontaneous mitochondrial Na^+ transients are coincident with mitochondrial alkaline transients. As we reported that mitochondrial Na^+ transients were also coincident with mitochondrial depolarizations, we verified that mitochondrial alkaline transients were coincident with mitochondrial depolarization. We addressed this issue by labelling MitoSypHer transfected astrocytes with the mitochondrial dye TMRE, sensitive to electrical potential. As could be expected from our previous results, we observed that spontaneous pH transients coincided with transient mitochondrial depolarizations (**Fig. 17**).
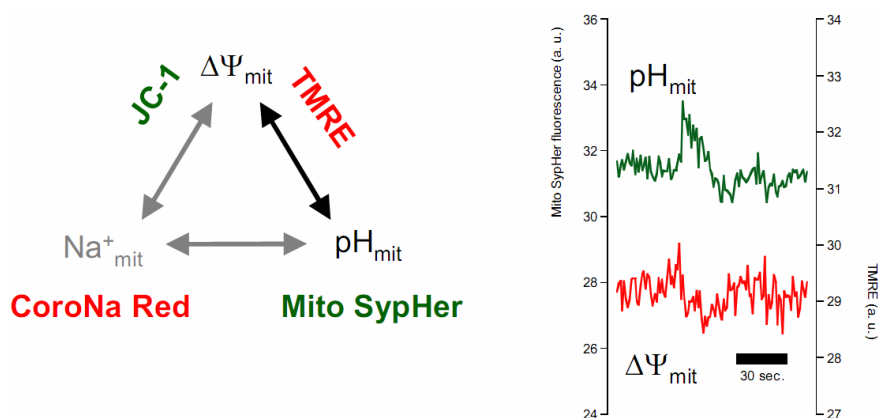
Fig. 17. Mitochondrial alkaline transients are coincident with mitochondrial depolarization. MitoSypHer transfected astrocytes loaded with the mitochondrial electrical potential-sensitive probe TMRE in unquenched mode.

Finally, we asked whether mitochondrial transients involved other ions such as Ca^{2+}. We tested this hypothesis by monitoring mitochondrial alkaline transients and mitochondrial Ca^{2+} concentration in the same astrocytes. We found that mitochondrial alkaline transients were not coincident with detectable alteration of mitochondrial Ca^{2+} level (**Fig. 18**). In several experiments, the mitochondrial Ca^{2+} level spontaneously oscillated at a stable frequency. These mitochondrial Ca^{2+} oscillations, certainly reflecting the cytosolic Ca^{2+} oscillations, were without temporal or spatial coincidence with mitochondrial alkaline transients. We found that mitochondrial alkaline transients occurred at any moment during and between mitochondrial Ca^{2+} oscillations (*not shown*).
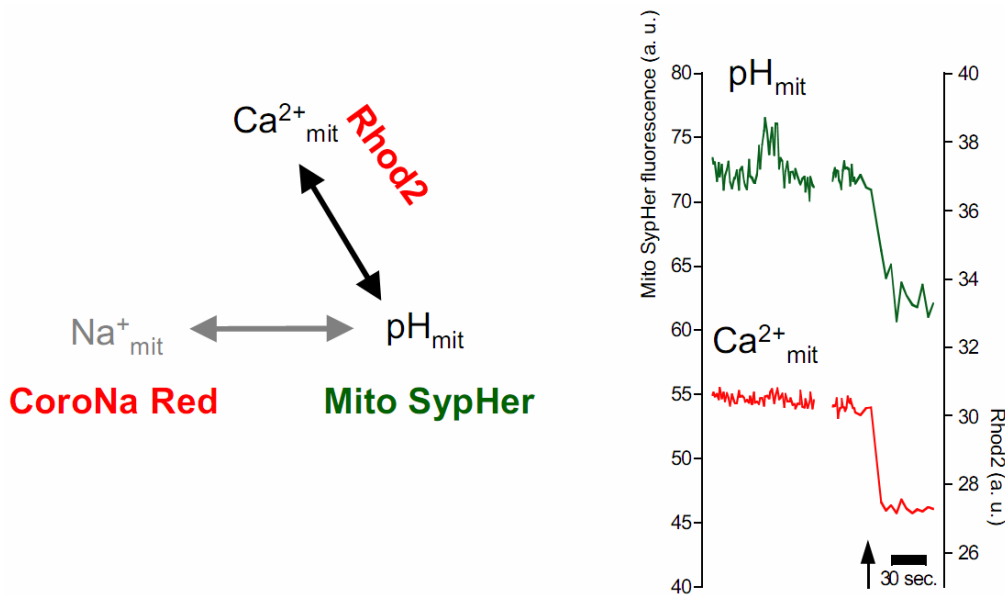
Fig. 18: Mitochondrial alkaline transients are not coincident with detectable changes in mitochondrial Ca^{2+} concentration. MitoSypHer transfected astrocytes labelled with the mitochondrial specific Ca^{2+} sensor Rhod2. Application of p-Trifluoromethoxy carbonyl cyanide phenyl hydrazone (FCCP 1μM, represented by a black arrow) was used as control of mitochondrial specificity of MitoSypHer and Rhod2 (n=7, 16 mitochondria).

Taken together, our results indicated that mitochondrial transients correspond to selective changes in ionic concentrations within the same mitochondria. Spontaneous mitochondrial transients were characterized by an entry of Na^+ and increase of mitochondrial matrix pH without coincident change in mitochondrial Ca^{2+} level.

However, the mechanisms leading to the initiation of a mitochondrial transient remained unexplored. As we showed that the frequency of mitochondrial Na^+ transients was sensitive to the cellular ATP level, we investigated the possibility of a link between mitochondrial Na^+ transients and ATP levels in the local mitochondrial environment. To address this issue, we performed a simultaneous labelling of astrocytes with CoroNa Red (mitochondrial Na^+ concentration) and Magnesium Green (free magnesium concentration). The Magnesium Green method provides an indirect assessment of intracellular ATP concentration, as ATP displays a ~10 fold higher affinity for Mg^{2+} than ADP and

binds a large proportion of Mg^{2+}. Therefore, a decrease in Magnesium Green fluorescence indicates an increase in ATP concentration. Mitochondrial Na^+ transients were coincident with transient decrease of free magnesium concentration suggesting a brief increase of ATP availability in the immediate vicinity of mitochondria exhibiting a transient (**Fig. 19**).
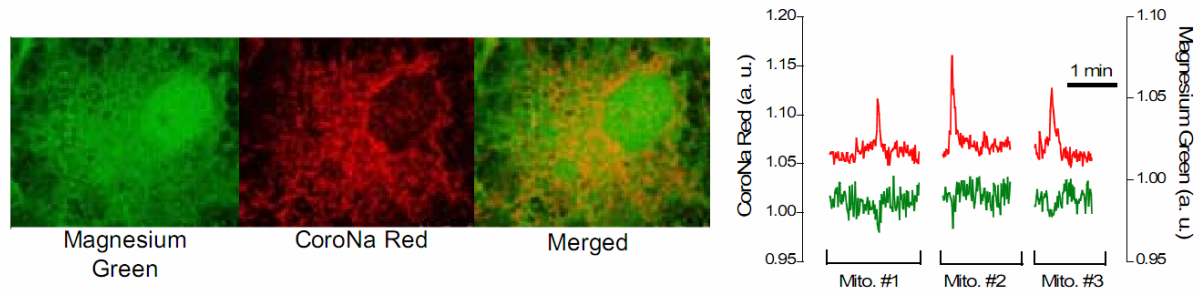
Fig. 19: Simultaneous monitoring of ATP level using Magnesium Green and mitochondrial Na^+ transients in resting astrocytes. (n=6, 24 mitochondria).

Taken together, these experiments provide a more complete picture of spontaneous mitochondrial transients in resting astrocytes. We found that mitochondria exhibiting a mitochondrial transient experienced opposite changes in Na^+ and H^+ concentrations whereas Ca^{2+} level remained stable. In addition we showed evidence suggesting that a microdomain of low free Mg^{2+} concentration, potentially associated with increase of ATP concentration, was coincident with mitochondrial Na^+ transient.

C. Effect of glutamatergic stimulation on mitochondrial ionic homeostasis

Astrocytes exhibit a substantial density of mitochondria able to transform glucose in energy in a highly efficient manner. However, according to the astrocyte-neuron lactate hypothesis, the metabolic response of astrocytes is predominantly glycolytic. This biocellular paradox raises the following question: why does excitatory neurotransmission evoke a metabolic response in astrocytes with a prevalence of glycolysis instead of mitochondrial oxidative phosphorylation?

To tackle this issue, we used fluorescence imaging techniques in cultured cortical astrocytes to investigate the impact of neuronal activity on mitochondrial metabolism. We showed that astrocyte mitochondria are sensitive to the alterations of cytosolic ion concentrations induced by glutamate-uptake. Glutamate uptake increased mitochondrial Na^+ concentration in parallel with cytosolic Na^+ (Bernardinelli et al., 2006). Similarly, we found that glutamate uptake led to mitochondrial acidification. We provided several pieces of evidence suggesting that glutamate mediates a pH-mediated tuning of mitochondrial metabolism in astrocytes (Azarias et al., *submitted*).

1. *In situ* fluorescence imaging of glutamate-evoked mitochondrial Na^+ responses in astrocytes

This study shows that mitochondrial Na^+ concentration increases in astrocytes as a result of plasma membrane glutamate transporter activity. We investigated the dynamics of mitochondrial Na^+ concentration in astrocytes using fluorescence microscopy. Several pieces of evidence pointed to the involvement of the mitochondrial Na^+/Ca^{2+} exchanger in the entry of Na^+ into mitochondria and of the mitochondrial Na^+/H^+ exchanger as a mechanism to restore mitochondrial Na^+ concentration to basal level.

I performed the experiments shown in Fig. 4 and I participated in writing the manuscript with Jean-Yves Chatton and Yann Bernardinelli.

In Situ Fluorescence Imaging of Glutamate-Evoked Mitochondrial Na$^+$ Responses in Astrocytes

YANN BERNARDINELLI,[1] GUILLAUME AZARIAS,[1] AND JEAN-YVES CHATTON[1–3]*
[1]Department of Physiology, University of Lausanne, Switzerland
[2]Department of Cell Biology and Morphology, University of Lausanne, Switzerland
[3]Cellular Imaging Facility, University of Lausanne, Switzerland

ABSTRACT
Astrocytes can experience large intracellular Na$^+$ changes following the activation of the Na$^+$-coupled glutamate transport. The present study investigated whether cytosolic Na$^+$ changes are transmitted to mitochondria, which could therefore influence their function and contribute to the overall intracellular Na$^+$ regulation. Mitochondrial Na$^+$ (Na$^+_{mit}$) changes were monitored using the Na$^+$-sensitive fluorescent probe CoroNa Red (CR) in intact primary cortical astrocytes, as opposed to the classical isolated mitochondria preparation. The mitochondrial localization and Na$^+$ sensitivity of the dye were first verified and indicated that it can be safely used as a selective Na$^+_{mit}$ indicator. We found by simultaneously monitoring cytosolic and mitochondrial Na$^+$ using sodium-binding benzofuran isophthalate and CR, respectively, that glutamate-evoked cytosolic Na$^+$ elevations are transmitted to mitochondria. The resting Na$^+_{mit}$ concentration was estimated at 19.0 ± 0.8 mM, reaching 30.1 ± 1.2 mM during 200 µM glutamate application. Blockers of conductances potentially mediating Na$^+$ entry (calcium uniporter, monovalent cation conductances, K$^+_{ATP}$ channels) were not able to prevent the Na$^+_{mit}$ response to glutamate. However, Ca^{2+} and its exchange with Na$^+$ appear to play an important role in mediating mitochondrial Na$^+$ entry as chelating intracellular Ca^{2+} with BAPTA or inhibiting Na$^+$/Ca^{2+} exchanger with CGP-37157 diminished the Na$^+_{mit}$ response. Moreover, intracellular Ca^{2+} increase achieved by photoactivation of caged Ca^{2+} also induced a Na$^+_{mit}$ elevation. Inhibition of mitochondrial Na/H antiporter using ethylisopropyl-amiloride caused a steady increase in Na$^+_{mit}$ without increasing cytosolic Na$^+$, indicating that Na$^+$ extrusion from mitochondria is mediated by these exchangers. Thus, mitochondria in intact astrocytes are equipped to efficiently sense cellular Na$^+$ signals and to dynamically regulate their Na$^+$ content.   ©2006 Wiley-Liss, Inc.

INTRODUCTION

After its synaptic release, glutamate is rapidly taken up by surrounding astrocytes, thus preventing the excitotoxic buildup of extracellular glutamate. This extremely efficient transport system of astrocytes utilizes the steep electrochemical gradient of Na$^+$ across the cell membrane as the driving force (Danbolt, 2001). As a consequence of this transport activity, the astrocytes are among the few cell types that can experience large variations in their cytosolic Na$^+$ concentration (Na$^+_{cyt}$), which can increase by 20–30 mM in a few seconds (Bernardinelli et al., 2004; Chatton et al., 2000; Rose and Ransom, 1996).

The Na$^+_{cyt}$ increases lead to a >2-fold enhancement of Na$^+$/K$^+$-ATPase activity for extracellular glutamate concentrations expected to be seen by astrocytes during neuronal activity (Chatton et al., 2000, 2003), thus causing an energy burden sufficient to lead to a drop in cellular ATP levels (Chatton and Magistretti, 2005). This increased energy need is believed to stimulate the astrocyte energy metabolism and glucose uptake. These processes appear to be spatially and temporally coordinated by an elaborate dynamic intercellular signaling (Bernardinelli et al., 2004).

Mitochondria play a central role in cellular ATP production as they host the citric acid cycle and oxidative phosphorylation. Despite the highly efficient mitochondrial energy production, it appears that the glutamate-evoked metabolic response of astrocytes is primarily glycolytic (Pellerin and Magistretti, 1994).

If glutamate-evoked variations of Na$^+_{cyt}$ were transmitted to mitochondria, they could participate to the modulation of the overall Na$^+$ and metabolic responses of astrocytes. Mitochondria are thought to express a complex repertoire of cation conductances and transporters (Bernardi, 1999; Brierley et al., 1994) that could mediate a significant Na$^+$ flux across mitochondrial membranes. Because electrophysiological approaches are extremely difficult to apply on mitochondria due to the small size of these organelles, these conductances have been unveiled mostly using pharmacological approaches on isolated mitochondria. Studying mitochondrial function in situ in intact living cells is complicated by the presence of the cell membrane. Nevertheless, these types of studies become accessible owing to the development of fluorescent indicators of mitochondrial functions and imaging tools. In particular, Ca^{2+} is known to be

exchanged across the inner mitochondrial membrane in a dynamic way (Malli et al., 2003) in register with cytosolic Ca^{2+} changes. As other cations, Na^+ is expected to be strongly attracted into mitochondria because of the highly negative electrical potential inside the mitochondrial matrix. Recently, a Na^+ fluorescent indicator CoroNa Red (CR) was described (Jayaraman et al., 2001a,b), and shown to localize in mitochondria of different cell types (Baron et al., 2005; Yang et al., 2004), opening to new perspectives for the study of mitochondrial Na^+ homeostasis and its potential link to energy metabolism in astrocytes. Here, we investigated the Na^+ dynamics in mitochondria in their native cellular environment and, more specifically, assessed whether Na^+_{cyt} changes observed in response to glutamate transport activation are transmitted to mitochondria. We show that mitochondria in intact astrocytes possess mechanisms for efficiently sensing cytosolic Na^+ changes and dynamically regulating their Na^+ content.

MATERIALS AND METHODS
Cell Culture

Cortical astrocytes in primary culture were obtained from 1- to 3-day-old OF1 and C57BL/6 mice as described previously (Sorg and Magistretti, 1992). Cells were grown at confluency for 3 weeks on glass coverslips in DME medium supplemented with 10% FCS.

Fluorimetric Characterization

The Na^+ sensitivity and selectivity of CoroNa Red (CR; Molecular Probes, Eugene, OR) was tested in vitro on a spectrofluorimeter (Perkin–Elmer, Wellesley, MA) in the absence of cells or mitochondria. Fluorescence was excited at 530 nm and measured at 580 nm. CR was dissolved at 0.1 μM in intracellular-like saline containing (mM) the following: K^+-gluconate, 138, NaCl 8; $MgCl_2$, 5; EGTA, 1; $CaCl_2$, 0.5; HEPES, 10, pH 7.2. For Na^+ titration, NaCl concentration was varied from 0 to 400 mM. Solutions with various pH values were titrated using KOH. Sensitivity of the CR to K^+ was tested by adding known amounts of K^+-gluconate. CR sensitivity to Ca^{2+} was tested using solutions of defined free Ca^{2+} concentration in the presence of 1 mM EGTA as calculated using the Maxchelator software (Chris Patton, Stanford University, http://www.stanford.edu/~cpatton/maxc.html).

Fluorescence Imaging

Cells were loaded at 37°C for 18 min with 1 μM CR in a HEPES-buffered balanced solution (see below) and then superfused at 37°C in a thermostated chamber (Chatton et al., 2000). MitoTracker Green FM (5 μM, Molecular Probes) was loaded using the same procedure. For simultaneous cytosolic and mitochondrial Na^+ imaging, cells were loaded for 75 min with 15 μM of the acetoxymethyl ester derivative of sodium-binding benzofuran isophthalate (SBFI-AM, Teflabs, Austin, TX) at 37°C, and with CR (1 μM) for the last 18 min of incubation.

Dynamic intracellular ion imaging was performed on an inverted epifluorescence microscope (Axiovert 100M, Carl Zeiss, Germany) using a 40 × 1.3 N.A. oil-immersion objective lens. Fluorescence excitation wavelengths were selected using a monochromator (Till Photonics, Planegg, Germany) and fluorescence was detected using a 12-bit cooled CCD camera (Princeton Instruments, Trenton, NJ). CR fluorescence was excited at 560 nm and detected at >580 nm. For dual CR and SBFI imaging, a double band dichroic mirror (~420 and ~575 nm) and emission filter (~510 and ~600 nm) were used (Chroma Technology Rockingham, VT), and fluorescence was sequentially excited at 340, 380, and 550 nm. Image acquisition was computer-controlled using the software Metafluor (Universal Imaging, Reading, PA) running on a Pentium computer. Regions of interest with high density of mitochondria and excluding nuclei were selected in individual cells, and the average fluorescence signal inside these regions was analyzed over time.

Flash Photolysis

Ca^{2+} photorelease was performed using a high power UV LED (365 nm/100 mW) system as previously described (Bernardinelli et al., 2005). The UV light was delivered to the specimen by means of a multimode fused silica 50-μm core optical fiber positioned 20 μm above the cell surface to illuminate a spot of about 30×60 μm^2 corresponding to 3–4 cells of the confluent monolayer. For these experiments, we used the caged Ca^{2+} compound o-nitrophenyl EGTA (NP-EGTA) that gets fragmented by UV light in two parts having negligible Ca^{2+} affinities, resulting in fast Ca^{2+} release (Ellis-Davies et al., 1996). NP-EGTA was loaded into astrocytes using its membrane-permeant derivative NP-EGTA-AM (30 min, 8 μM; Molecular Probes). Cells were then placed back in the incubator for 3–4 h to allow the compound to become gradually saturated with Ca^{2+} before loading the Ca^{2+}-probe Fluo-4 AM (6 μM, 30 min; Teflabs) or CR as described earlier. For these experiments, we used an inverted epifluorescence microscope (Diaphot 300, Nikon, Tokyo, Japan) equipped with a 40 × 1.3 N.A. oil-immersion objective lens (Nikon), a fast filter wheel for selection of excitation wavelengths (Sutter Instruments, Novato, CA), and a Gen III$^+$ intensified CCD Camera (VideoScope International, Washington DC).

Confocal Imaging

Confocal imaging of CR and MitoTracker Green FM was performed on living cells on a LSM 510 Meta confocal microscope with a 63 × 1.4 N.A. oil immersion objective (Carl Zeiss), with sequential excitation at 543 and 488 nm, respectively. For dual staining experiments, a double band primary dichroic mirror was used (488/543 nm), and the fluorescence emission was detected on two channels (496–529 nm and 561–636 nm, respectively)
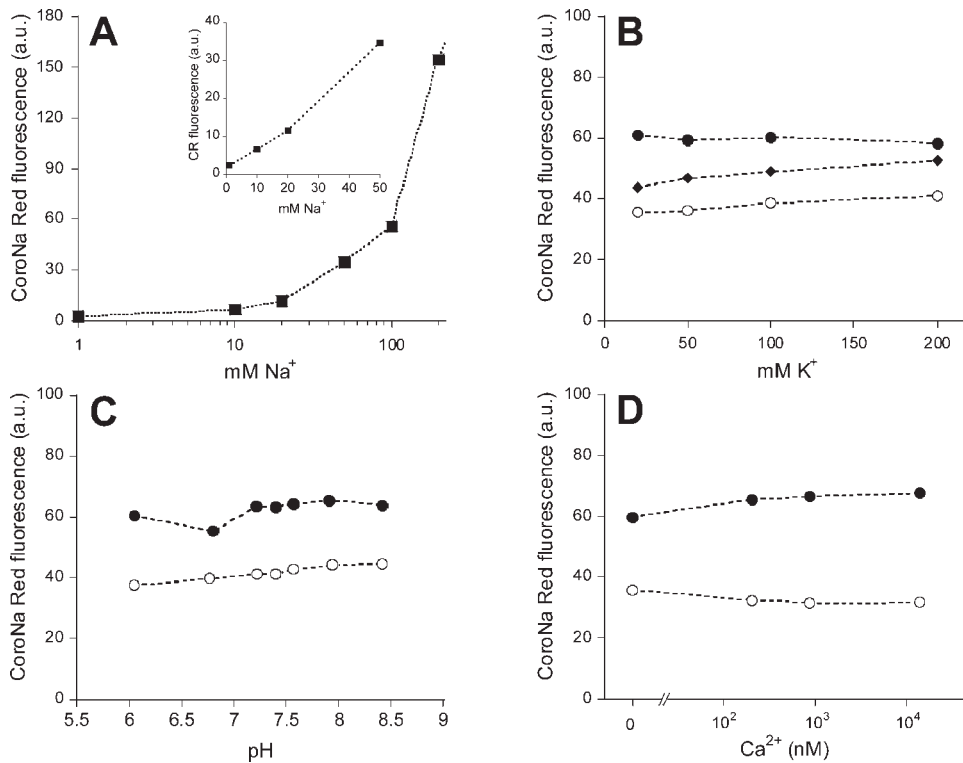
Fig. 1. Fluorometric characterization of CR cation sensitivity. CR dissolved at 0.1 μM in intracellular-like solution (see Methods) was excited at 530 nm and emission was recorded at 580 nm in the absence of cells or mitochondria. (**A**) Sensitivity to increasing medium Na^+ concentration in the range 0–400 mM. For graphical clarity only values up to 200 mM are shown, although higher concentrations display monotonic fluorescence increase. The inset shows the fluorescence change in the range 0–50 mM Na^+. Sensitivity to ambient K^+ (**B**), pH (**C**), and Ca^{2+} (**D**) measured at constant Na^+ concentration of 8 mM (○), 20 mM (◆), or 50 mM (●).

selected on the photomultiplier array spectral detector (Meta detector). The spectral detector was also used to record dye emission spectra from single mitochondria.

Experimental Solutions

Solutions contained (mM) the following: NaCl, 135; KCl, 5.4; NaHCO₃, 25; CaCl₂, 1.3; MgSO₄, 0.8; NaH₂PO₄, 0.78; glucose, 5, bubbled with 5% CO₂/95% air. The solution used to deliver BAPTA-AM (50 μM) to cells contained in addition 1 g% bovine serum albumin and 10 mM HEPES (pH 7.4). The solution for cellular dye loading contained (mM) the following: NaCl, 135; KCl, 5.4; HEPES, 20; CaCl₂, 1.3; MgSO₄, 0.8; NaH₂PO₄, 0.78; glucose, 20 (pH 7.4), and was supplemented with 0.1% Pluronic F-127 (Molecular Probes). For experiments involving La^{3+}, because of the poor solubility of this ion in salines containing bicarbonate and phosphate, we used the following solutions (mM): NaCl, 160.8; KCl, 5.4; CaCl₂, 1.3; MgSO₄, 0.8; HEPES, 20; glucose, 5, bubbled with air and adjusted to pH 7.4.

In situ calibration of CR signal was attempted using a protocol previously used for mitochondrial (Yang et al., 2004) and cytosolic Na^+ calibration (Chatton et al., 2000, 2003). Cells were permeabilized for monovalent cations using 6 μg/ml gramicidin and 10 μM monensin with simultaneous inhibition the Na^+/K^+-ATPase using 1 mM ouabain. Cells were then sequentially perfused with solutions buffered at pH 7.2 with 20 mM HEPES and containing 0, 10, 20, and 50 mM Na^+, respectively, and 30 mM Cl^- and 136 mM gluconate with a constant total concentration of Na^+ and K^+ of 165 mM. Individual four-point calibration curves were computed for cells in the field of view and used to convert CR fluorescence ratio values into Na^+ concentrations. During the entire procedure, the mitochondrial staining pattern was not altered.

Materials

Ouabain was from Fluka (Buchs, Switzerland). CGP-37157, U37883A, and glibenclamide were from Biomol-Anawa Trading (Zurich, Switzerland). RU-360 was from Calbiochem. Ethyl-isopropyl amiloride (EIPA) was gift from Dr. H. Lang (Aventis Pharma, Frankfurt, Germany). BAPTA-AM was from Molecular Probes. All other compounds were from Sigma.

RESULTS
Corona Red Characterization

The ability of CR to monitor Na^+ was first assessed in vitro by spectrofluorimetry using experimental solutions mimicking the cellular ionic environment. CR fluorescence increased monotonically as a function of Na^+ concentration in the range 0–400 mM, consistent with the K_D of ~200 mM reported by the manufacturer. Figure 1A depicts the fluorescence response of CR in the range 0–200 mM Na^+ that has physiological relevance, and indicates that the probe displays significant fluorescence change in this range. We then tested the ability of the probe to discriminate against other cations. Figure 1B shows that K^+ in the range 20–200 mM has only minor influence on CR fluorescence. Neither pH in the range 6–
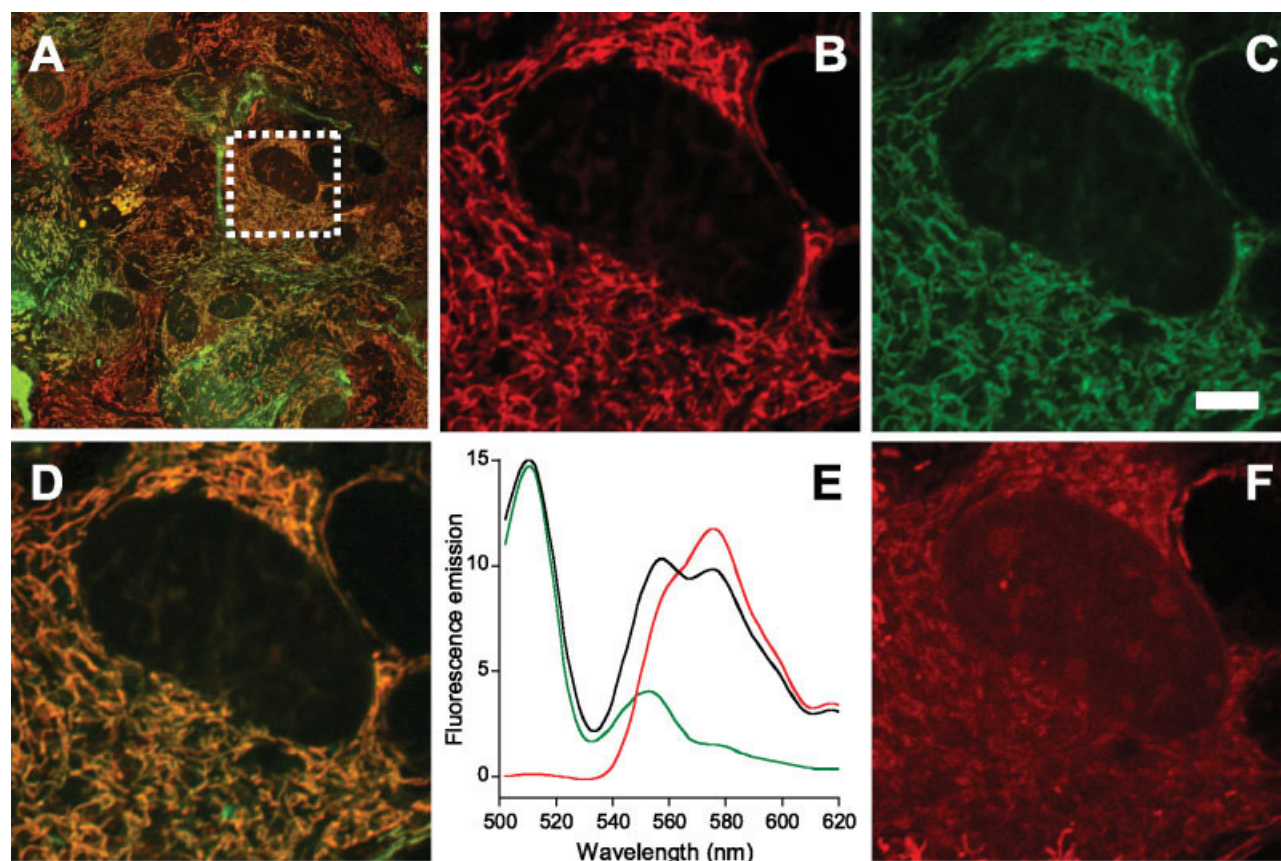
Fig. 2. Mitochondrial localization of CR signal. Confocal images of living astrocytes loaded with MitoTracker Green (MTG) and CR (**A**). Images of CR (**B**), MTG (**C**), and the overlay of both (**D**) at higher magnification for the region depicted in A (dotted box). Scale bar, 5 μM. (**E**) Emission spectra recorded in individual mitochondria from cells loaded with MTG (green), with CR (red), and with both (black) show that mitochondria contain the spectral signature of both dyes. (**F**) Longer incubations or higher concentrations of CR results in a diffuse staining, where cytosolic and nuclear distribution becomes more prominent.

8.5 (Fig. 1C) nor Ca^{2+} in the range 0–10 μM (Fig. 1D) markedly influenced CR fluorescence in the presence of 8 or 50 mM Na^+. One can conclude from this in vitro characterization that CR can be safely used as a Na^+-sensitive probe, which is consistent with previous reports (Jayaraman et al., 2001a,b).

We then tested whether CR staining of living astrocytes was specific to mitochondria. After a 18 min loading time, 0.7-μm thick confocal optical sections of CR-loaded cells displayed the typical pattern of mitochondrial loading, with dark nuclei and punctated staining of rod-like structures (Figs. 2A–D). Close-up view shows that CR stain matched almost perfectly the mitochondrial stain Mitotracker Green FM loaded in the same cells. To ascertain that MitoTracker dye and CR localized within the same organelles, fluorescence emission spectra were recorded using the confocal spectral detector in structures of living cells with typical mitochondrial appearance and showed the spectral signature of both dyes (Fig. 2E), with an emission peak at ∼600 nm for CR and at ∼520 nm for MitoTracker Green FM. These results indicated that CR indeed localizes into mitochondria of living astrocytes. However, as observed by others (Yang et al., 2004), when longer loading time or higher CR concentrations are used, CR stained not only mitochondria but also the rest of the cell, as shown by the diffuse staining in Fig. 2F. For the entire study, we optimized the loading conditions to maximize mitochondrial loading and systematically discarded any experiment where cytosolic fluorescent staining was observed at the beginning or during the course of an experiment.

Cytosolic Na^+ Changes are Transmitted to Mitochondria

Glutamate is known to induce robust Na^+_{cyt} increases in astrocytes mediated almost entirely by an avid Na^+-coupled uptake mechanism (Chatton et al., 2000). To test whether these Na^+ increases are transmitted to mitochondria, astrocytes were loaded with CR and fluorescence changes were monitored by dynamic fluorescence microscopy. Glutamate superfusion induced a clear-cut Na^+_{mit} signal increase that returned to baseline after glutamate washout (Fig. 3A). Because glutamate interacts with several classes of receptors and is a metabolic substrate of mitochondria, we assessed whether the ob-
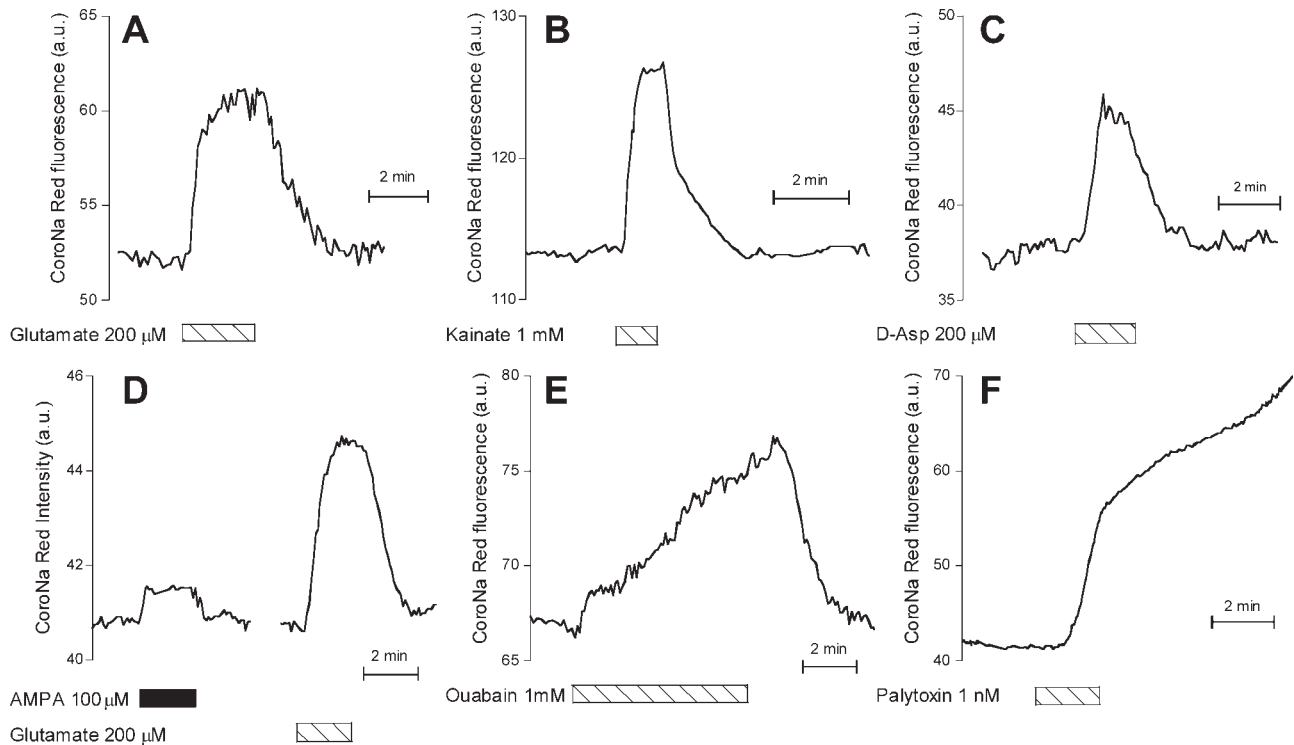
Fig. 3. Agents known to increase cytosolic Na^+ in astrocytes lead to Na^+_{mit} increase. Representative traces of Na^+_{mit} changes in single cells are shown for bath application of (**A**) glutamate (200 μM; $n = 48$ cells from 7 experiments), (**B**) kainate (1 mM, $n = 68$ cells from 9 experiments), (**C**) D-aspartate (200 μM; $n = 72$ cells from 8 experiments), (**D**) AMPA (100 μM) compared to glutamate (200 μM) on the same cell ($n = 38$ cells from 5 experiments), (**E**) ouabain (1 mM; $n = 12$ cells from 2 experiments), and (**F**) palytoxin (1 nM; $n = 24$ cells from 3 experiments). The paradigm of drug applications is indicated in the bottom of each graph by dashed rectangles.

served Na^+_{mit} increase could be induced by other means. Activation of non-NMDA receptors using kainate that is known to induce Na^+_{cyt} responses (Chatton et al., 2000) also produced robust Na^+_{mit} responses (Fig. 3B), as well a the glutamate transporter substrate D-aspartate (Fig. 3C). Maximal activation of AMPA receptors using AMPA was found to cause a weak cytosolic Na^+ response with an amplitude of 23% of the response to glutamate (Chatton et al., 2000). This was found to be also the case on the Na^+_{mit} response (Fig. 3D). Application of ouabain, which increases Na^+_{cyt} by specifically inhibiting the cellular Na^+ extrusion by the Na^+/K^+-ATPase, led to a steady increase in Na^+_{mit} (Fig. 3E). Finally, application of palytoxin, a 2,700 kDa polypeptide toxin, which binds to the Na^+/K^+-ATPase on its extracellular side and transforms it into a nonselective cation channel (Horisberger et al., 2004), induced a massive and irreversible increase in Na^+_{mit} (Fig. 3F).

Estimation of Na^+_{mit} Concentration in Intact Astrocytes

To obtain estimates of the resting Na^+_{mit} concentration as well as the amplitude of the observed Na^+_{mit} response, attempts were made to calibrate CR fluorescence in situ. The approaches described by others in Madin Darby ca-

nine kidney (MDCK) cells (Baron et al., 2005) used permabilization of plasma membrane with ionophore in addition to mitochondrial depolarization using p-trifluoromethoxy carbonyl cyanide phenyl hydrazone (FCCP). In our hands, FCCP could not be used as it resulted in a rapid loss of mitochondrial staining and widespread cellular dye redistribution. We used instead the approach proposed in another study in cardiomyocytes (Yang et al., 2004), in which the plasma membrane Na^+/K^+-ATPase was inhibited using ouabain, and the ionophores monensin and gramicidin were added to permeabilize both plasma and intracellular membranes for monovalent cations. Four solutions with Na^+ concentrations ranging from 0 to 50 mM were then applied to cells and the CR fluorescence signal measured. Under these conditions, CR remained associated to mitochondria throughout the entire procedure. Figure 4A shows an experiment during which a first 200 μM glutamate application was performed and evoked the CR response described above, after which a zero Na^+ bath application rapidly decreased the signal. Subsequent addition of permeabilization cocktail further reduced the signal. Bath Na^+ concentration was then stepwise increased and resulted in proportionate CR fluorescence increase. Plateau values of CR fluorescence for each applied Na^+ concentration and each cell under study were measured and show a monotonic increase with respect to Na^+

A

B
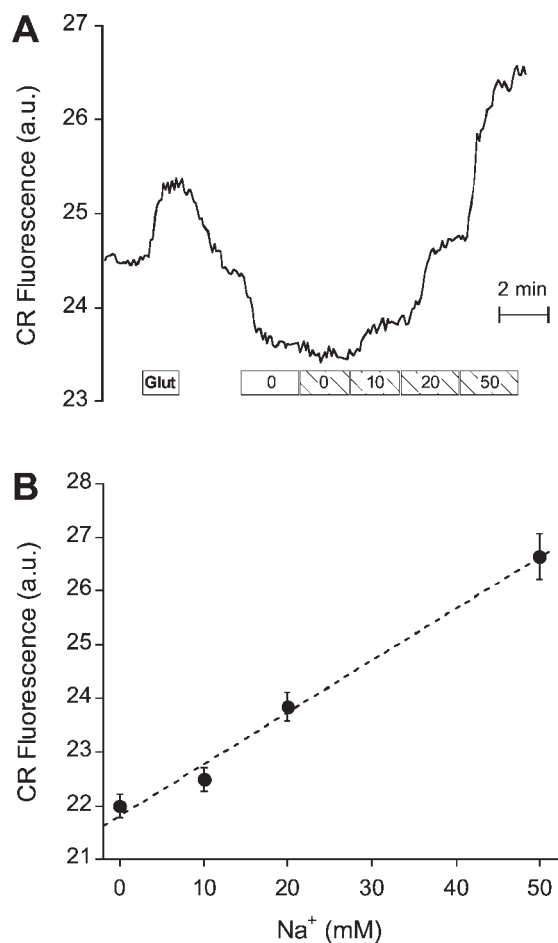
Fig. 4. Estimation of Na^+_{mit} concentration. (**A**) Example trace of CR fluorescence (arbitrary fluorescence units) measured in individual intact astrocytes showing the response to a first 200 μM glutamate application and the CR fluorescence change caused by a switch to zero Na^+ perfusion solution and the subsequent adjunction of ouabain and the ionophores monensin and gramicidin (hatched bars). The Na^+ concentration in the perfusion solution was then varied as depicted in the graph (see solution composition under material and methods). (**B**) Dependency of in situ CR fluorescence and applied bath Na^+ concentration. The raw CR plateau fluorescence values were measured for each applied Na^+ solution and for each individual cell of this series of experiments. The mean values ± SEM of a total of 57 cells from 8 independent experiments were plotted as a function of bath Na^+ concentration, and show a monotonic relationship between the two variables with a linear correlation $R = 0.995$ (dotted line).

(Fig. 4B). When applying each individual titration curve to its corresponding cell, the average resting Na^+_{mit} concentration was found to be 19.0 ± 0.8 mM, reaching 30.1 ± 1.2 mM during 200 μM glutamate application ($n = 57$ cells from 8 independent experiments). In comparison, calibration of Na^+_{cyt} changes measured with SBFI as described previously (Chatton et al., 2000) yielded a resting Na^+_{cyt} concentration of 13.2 ± 0.1 mM ($n = 12$ cells from 2 experiments) in the same batch of cells. It is difficult to evaluate how well Na^+_{mit} was clamped under these conditions; however, these values fall in the range of estimated Na^+_{mit} values reported in the literature (see Discussion).

Potential Pathways for Mitochondrial Na⁺ Entry

The inner mitochondrial membrane, capable of sustaining a large transmembrane electrical gradient, is considered as the main barrier to the diffusion of ions, but nevertheless contains several potential pathways that could mediate the Na^+_{mit} response, including mitochondrial transporters, conductances, or permeability transition pore (Bernardi, 1999; Brierley et al., 1994).

We first tested whether activating mitochondrial cation conductances would indeed cause a Na^+_{mit} increase and developed a methodological approach to simultaneously monitor Na^+_{cyt} and Na^+_{mit} using SBFI and CR, respectively. Figure 5A shows that SBFI displays the typical staining of cytosol and nuclei observed in several cell types including astrocytes (Borin et al., 1993; Chatton et al., 2003), and CR staining is punctated and excluded from nuclei. The proper controls were performed to ensure the independency of the two fluorescent signals that show no spectral overlap (not shown).

A first 200 μM glutamate application led to an increase in Na^+ in the cytosolic and mitochondrial compartments with similar kinetics and without delay detectable given the temporal resolution of the measurement. We then used diazoxide, a compound known to open mitochondrial K_{ATP} channels that are found in the brain (Bajgar et al., 2001). Figure 5B shows that although diazoxide did not influence on Na^+_{cyt}, it induced a measurable Na^+_{mit} increase, indicating that even in absence of Na^+_{cyt} rise, opening of mitochondrial K_{ATP} channels could indeed cause an increase in Na^+_{mit}.

We then attempted to identify the pathway responsible for the glutamate-evoked Na^+_{mit} response. We first tested compounds described as pharmacological blockers of several mitochondrial conductances. The compounds were preincubated for up to 30 min before glutamate application to take into account their potential delayed access to mitochondrial membranes. However, none of them was found to be alone effective at preventing Na^+_{mit} increase induced by 200 μM glutamate. The compounds tested were RU-360 (10 μM, $n = 7$) a blocker of the mitochondrial Ca^{2+} uniporter; La^{3+} (200 μM, $n = 5$) a broad spectrum cation conductance blocker; cyclosporine A (5 μM, $n = 5$) and bongkrekic acid (10 μM, $n = 3$) two compounds known to block the mitochondrial permeability transition pore; glibenclamide (1, 10, 50 μM, $n = 12$), U37883A (100 μM, $n = 6$) and 5-hydroxydecanoate (500 μM, $n = 8$) blockers of mitochondrial K_{ATP} channels; and carbenoxolone (20 μM, $n = 4$) blockers of connexins, recently identified in mitochondrial membranes (Boengler et al., 2005) (not shown).

The possible involvement of mitochondrial Na^+/Ca^{2+} exchanger was tested by applying its inhibitor CGP-37157 (30 μM), which caused a ~20% inhibition of the glutamate-evoked Na^+_{mit} response (Fig. 5C). To directly probe for a role of intracellular Ca^{2+}, BAPTA-AM (50 μM, 30 min) was loaded into the cells in order to chelate intracellular free Ca^{2+}. We first verified that this maneuver efficiently prevented subsequent glutamate-evoked Ca^{2+}
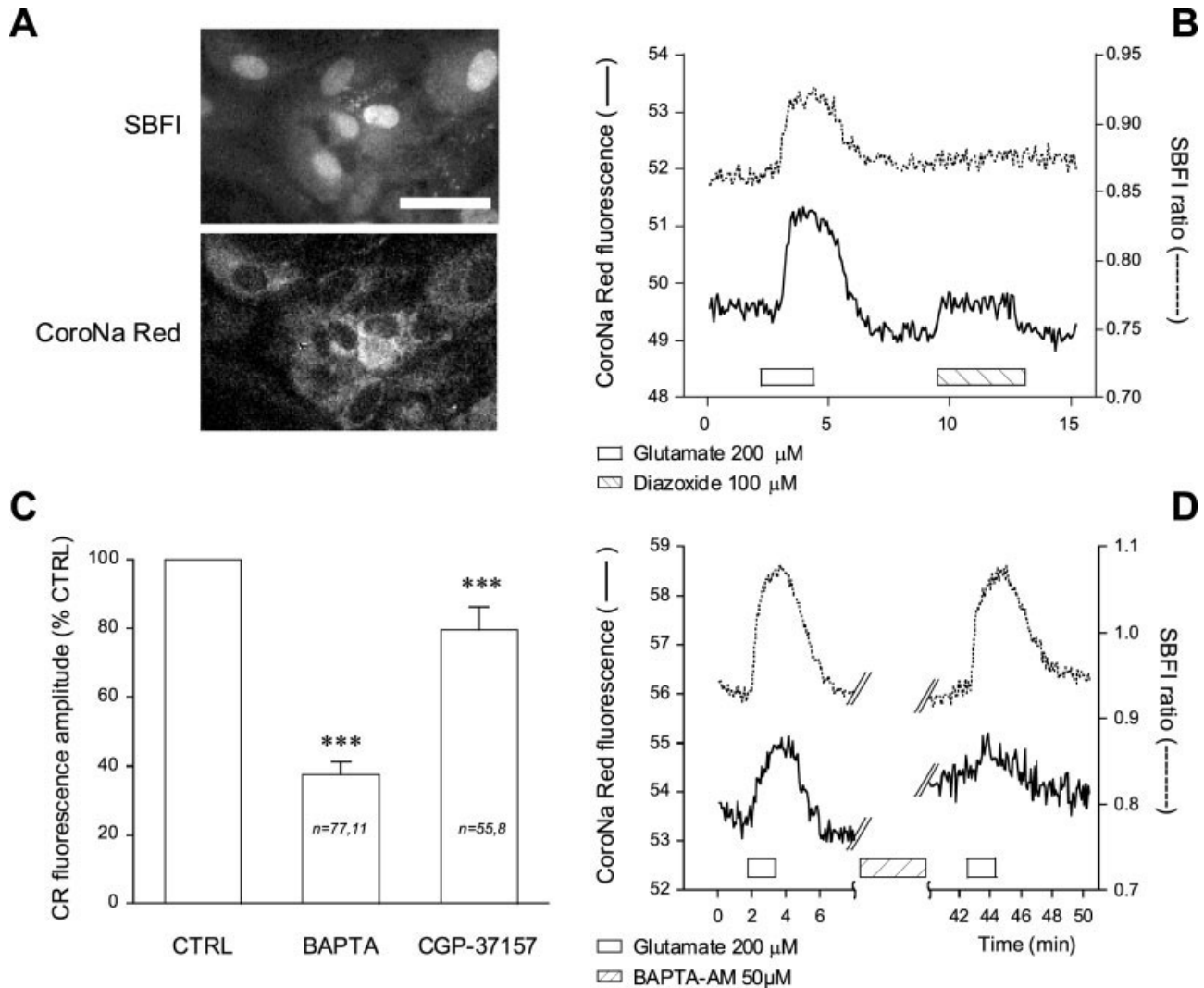
Fig. 5. Pathways for Na^+ entry in mitochondria. (**A**) Na^+_{mit} and Na^+_{cyt} were measured simultaneously by loading astrocytes with CR and SBFI, respectively. Scale bar, 20 μm. (**B**) A first glutamate (200 μM) application leads to a Na^+ response both in the cytosol (dotted line) and mitochondria (plain line). The responses appear to occur in the two compartments with a similar kinetics and without measurable delay. Application of the K_{ATP} channel opener diazoxide led to an increase in Na^+_{mit} without altering Na^+_{cyt}. Representative responses of one cell out of 56 from 7 experiments. (**C**) Bar graph of glutamate-evoked Na^+_{mit} response comparing the control condition with responses after BAPTA-AM treatment and CGP-37157 (30 μM) application. Data are mean amplitude of CR fluorescence increase measured in 77 cells from 11 experiments (BAPTA) and 55 cells from 8 experiments (CGP-37175). ***$P < 0.0001$ using paired t-test. (**D**) After a first glutamate pulse leading to a Na^+ response in the cytosol and mitochondria, BAPTA-AM (50 μM) was applied for 30 min and caused a strong (62%, see panel C) inhibition of the Na^+_{mit} response to glutamate, without decreasing the Na^+_{cyt} response (representative curve).

elevation (not shown). After a control glutamate application that led to Na^+ response in the cytosol and mitochondria, chelating Ca^{2+} strongly inhibited the Na^+_{mit} response without influencing Na^+_{cyt} response on the same cells as shown in the traces in Fig. 5D. It should be mentioned that the drift in the baseline CR signal after BAPTA application in this figure was not observed in all experiments and was less marked in cells loaded with CR alone. Overall, BAPTA inhibited the glutamate-evoked Na^+_{mit} response by 62.5% ± 3.7% (Fig. 5C).

We finally tested whether elevating Ca^{2+} would cause an increase in Na^+_{mit} by locally releasing Ca^{2+} using UV flash photolysis. Figure 6A shows that photoactivation of caged Ca^{2+} indeed caused a rapid rise in intracellular free

Ca^{2+} measured using the Ca^{2+} probe Fluo-4 returning to the baseline in ~2 min. Interestingly, photoactivation of NP-EGTA also caused a Na^+_{mit} response (Fig. 6B) with a clearly distinct kinetics, but which also recovered within ~2 min. UV flashes applied on cells that had not been loaded with NP-EGTA evoked no Na^+_{mit} response (Fig. 6C). Taken together, these experiments show the prominent role of Ca^{2+} in the observed Na^+_{mit} increase, which is likely to involve mitochondrial Ca^{2+} exchangers.

Na^+_{mit} Regulation

The mitochondrial Na^+/H^+ exchanger was proposed to be the main mechanism preventing Na^+_{mit} concentration
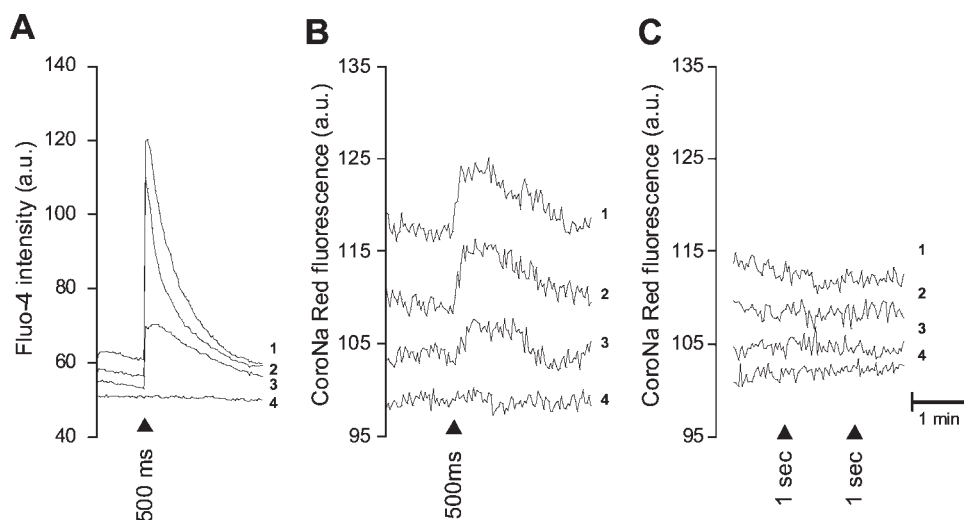
Fig. 6. Intracellular Ca^{2+} photorelease cause Na^+_{mit} responses. The caged Ca^{2+} compound NP-EGTA loaded in astrocytes was photoactivated in a group of 3–4 cells. (**A**) Effect of a 500-ms flash on cells loaded with Fluo-4 showing the rapid cellular Ca^{2+} rise and its recovery. (**B**) On cells loaded with CR, a 500-ms flash evoked a Na^+_{mit} response, whereas no response was seen for flashes as long as 1 s in cells contain-ing no caged Ca^{2+} (**C**). For all panels, Cells 1–3 were located within the illuminated spot, whereas Cell 4 was outside the photoactivated spot (internal control). The protocols were repeated on 2–4 different cover-lips and with up to 10 fields. The time scale for all plots is indicated in the graph C.
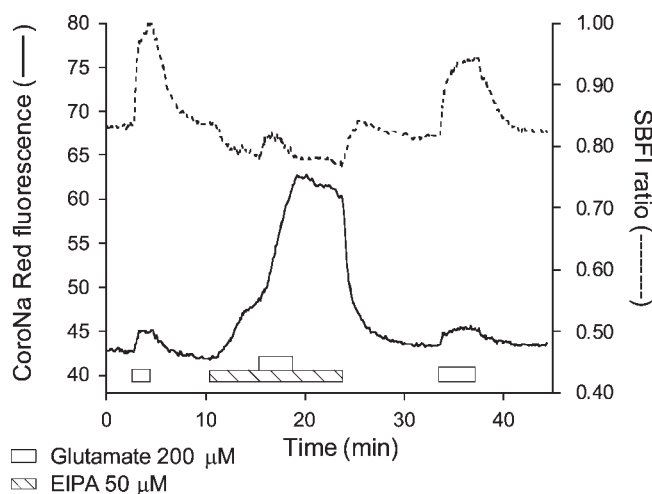
Fig. 7. Regulation of Na^+_{mit} by the mitochondrial Na^+/H^+ exchanger. A first 200 μM glutamate application evoked a Na^+ increase in both cytosolic and mitochondrial compartments. Application of EIPA, an in-hibitor of cell membrane, and mitochondrial Na^+/H^+ exchangers had strikingly different effects on Na^+_{cyt} and Na^+_{mit}. In the presence of EIPA, Na^+_{mit} steadily increased and additional application of glutamate accelerated its rise, whereas Na^+_{cyt} rapidly stabilized to a lower level from which glutamate evoked a modest response. Upon glutamate washout, Na^+_{mit} rise ceased but it went back to baseline only after EIPA washout. A final control application of glutamate showed that the effects of EIPA were reversible. Representative responses of one cell out of 86 from 13 experiments.

buildup favored by the large electrochemical gradient. To test whether this is the case in situ we used the EIPA, an inhibitor of both plasma membrane and mito-chondrial Na^+/H^+ exchangers (Sastrasinh et al., 1995). In this series of experiments, a first glutamate applica-tion led to the Na^+_{cyt} response described in detail pre-viously (Chatton et al., 2000) and to a simultaneous Na^+_{mit} response (Fig. 7). When the Na^+/H^+ exchanger in-hibitor EIPA was applied, Na^+_{cyt} rapidly decreased to a lower steady-state, compatible with the cessation of a cell membrane transport system using the transmem-brane Na^+ gradient. On the contrary, at the same time Na^+_{mit} started to steadily increase, consistent with the in-hibition of a transport system responsible of maintaining a low Na^+_{mit} level against the large electrochemical gradi-ent favoring influx of Na^+ into mitochondria. When glu-tamate was applied, the slope of this Na^+_{mit} increase was abruptly accelerated by a factor of ~3 that only ceased when glutamate was washed out, whereas a cytosolic Na^+ response of low amplitude but regular kinetics was evoked. It is conceivable that with their Na^+ extrusion mechanism inhibited, mitochondria become a significant sink for cellular Na^+, explaining both the initial Na^+_{cyt} decline and the low amplitude response to glutamate. Both Na^+_{mit} and Na^+_{cyt} recovered to their respective basal levels after EIPA washout and a final control glutamate application led to a similar response as the first one, demonstrating the reversibility of effects of EIPA. Na^+_{mit} is therefore dynamically regulated in living astrocytes by the continuous activity of mitochondrial Na^+/H^+ exchangers.

DISCUSSION

Astrocytes express a high density of Na^+-coupled glu-tamate transporters, enabling them to play the essential role of clearing up synaptically released glutamate from the extracellular space (Danbolt, 2001). This extremely efficient transporter system endow them with the prop-erty of experiencing large amplitude intracellular Na^+ variations, rising to up to 30–40 mM from a resting
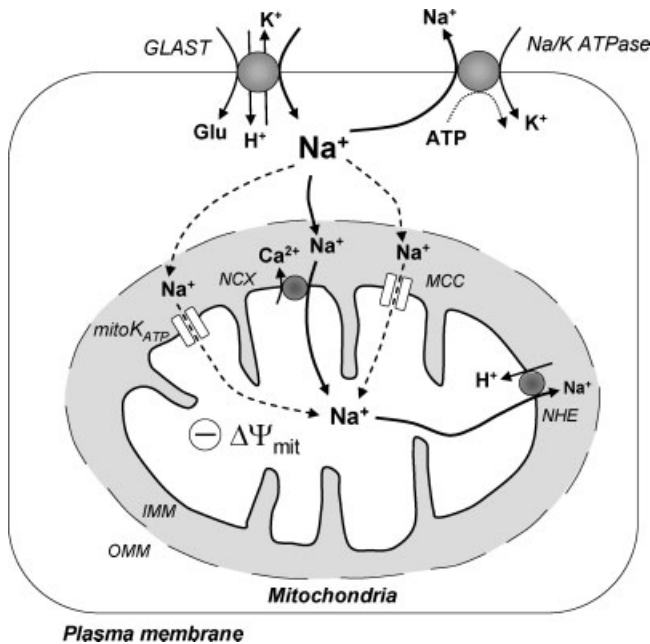
Fig. 8. Glutamate-induced Na$^+$ elevations in astrocytes. Schematic model of astrocytic Na$^+$ regulation in response to glutamate (Glu). The major cellular Na$^+$ influx pathways in response to glutamate application are due to Na$^+$-dependent glutamate transporters (GLAST). Glutamate also activates non-NMDA receptors that induce only minor Na$^+$ entry as compared to transporters (not shown). Cytosolic Na$^+_{cyt}$ is mainly regulated by the Na$^+$/K$^+$-ATPase. Na$^+$ also enters mitochondria after crossing the highly permeable outer mitochondrial membrane (OMM) and the inner mitochondrial membrane (IMM), driven by the highly negative electrical potential ($\Delta\psi_{mit}$). The mitochondrial entry of Na$^+$ involves its exchange with Ca^{2+} by the mitochondrial Na$^+$/Ca^{2+} exchangers (NCX). In addition, other entry pathways, including several mitochondrial cation conductances (MCC), or mitochondrial K$_{ATP}$ channels (mitoK$_{ATP}$) may be involved. The mitochondrial Na$^+$/H$^+$ exchangers (NHE) is the main mechanism of Na$^+$ extrusion from mitochondria.

value of $\sim$10 mM in the presence of physiological concentrations of glutamate (Chatton et al., 2000). The present study demonstrates that these robust Na$^+$ changes occurring in the cytosol of astrocytes propagate to the mitochondrial matrix with very similar kinetics. This was observed for glutamate concentrations compatible with values expected in the extrasynaptic space during activity (Dzubay and Jahr, 1999).

The study of Na$^+_{mit}$ has been so far hampered by the lack of Na$^+$-sensitive probe with mitochondrial specificity. We show in the present study that the newly released fluorescent probe CR is selective for Na$^+$ and specifically localizes in mitochondria of astrocytes. Resting Na$^+_{mit}$ concentration was estimated to be $\sim$19 mM, i.e. moderately higher than the 13 mM cytosolic Na$^+$ concentration found in the present study, which falls in the range of values (10–15 mM) that we previously reported for astrocytes (Chatton et al., 2000, 2003). In response to glutamate application, Na$^+_{mit}$ increased to $\sim$30 mM, a value similar to the one observed in the cytosol. To our knowledge, Na$^+_{mit}$ concentrations had not been reported before for astrocytes. However, studies using electron probe X-ray microanalysis of freeze-dried cryosections of CA3 hippocampal dendrites (Pivovarova

et al., 2002) have reported resting mitochondrial Na$^+$ levels of 25 mmol/kg dry weight. When adjusted to the units used in the present study (i.e. $\sim$11–12 mmol/L), these values are in a similar range as what we found for astrocyte mitochondria. In comparison, resting Na$^+_{mit}$ was recently estimated to be $\sim$50 mM in MDCK cells (Baron et al., 2005). Lower Na$^+_{mit}$ values of 9.8 mM were estimated in intact cardiomyocytes (Yang et al., 2004) and even lower resting Na$^+_{mit}$ concentration ($\sim$5 mM) were reported from experiments using SBFI in permeabilized ventricular cardiomyocytes (Donoso et al., 1992).

To enter the mitochondrial matrix, Na$^+$ has to cross two membranes in series (Fig. 8), the outer and the inner mitochondrial membranes. In resting conditions, the outer mitochondrial membrane is thought to present a high permeability to small molecules and ions, because of the presence of voltage-dependent anion channel (VDAC) also called mitochondrial porin (Shoshan-Barmatz and Gincel, 2003). Several mitochondrial transporters and conductances could mediate the Na$^+$ influx across the inner mitochondrial membrane that contains several cation conductances such as mitochondrial K$^+$ channels or Ca^{2+} channels with broad ion selectivity (Bernardi, 1999; Brierley et al., 1994). However, none of the pharmacological blockers of these cation conductances could convincingly prevent the Na$^+_{mit}$ response to glutamate. One cannot exclude that some of the compounds used here on intact cells had a poor, if any, access to their mitochondrial target or that this Na$^+$ influx is simultaneously mediated by several entry pathways.

Another potential pathway for mitochondrial Na$^+$ entry is the mitochondrial Na$^+$/Ca^{2+} exchanger (Bernardi, 1999). Indeed, Na$^+_{mit}$ has been so far attributed a main role in the regulation of intramitochondrial Ca^{2+}, through the activity of the mitochondrial Na$^+$/Ca^{2+} exchanger (Bers et al., 2003; Brierley et al., 1994). For this reason, Na$^+_{mit}$ has attracted the attention of cardiac myocyte research because these cells experience large cytosolic Ca^{2+} changes that are transmitted to their mitochondria (Bers et al., 2003). In these cells, Na$^+_{mit}$ overload has been reported following H$_2$O$_2$-induced oxidative stress (Yang et al., 2004). In axon terminals, it has been shown that mitochondria could act either as Ca^{2+} sinks (Scotti et al., 1998) or as Ca^{2+} reservoirs mobilized by cellular Na$^+$ influx using mitochondrial Na$^+$/Ca^{2+} as the route for mitochondrial Ca^{2+} efflux (Yang et al., 2003). We show in the present study that Ca^{2+}, probably by exchange with Na$^+$, is implicated in the Na$^+$ entry across the inner mitochondrial membrane. Indeed, the described inhibitor of this exchanger (CGP-37157) significantly diminished the Na$^+_{mit}$ response to glutamate and chelating intracellular Ca^{2+} inhibited the Na$^+_{mit}$ response by $\sim$62%, without affecting the Na$^+_{cyt}$ response to glutamate. The fact that CGP-37157 had a modest inhibitory effect of $\sim$20% could indicate a limited access of the compound to the mitochondria in situ or could support the notion that more than one pathway contributes to the

influx of Na^+ into mitochondria. Another evidence that supports the involvement of Ca^{2+} is that rapid intracellular Ca^{2+} photorelease in astrocytes caused a Na_{mit}^+ response.

With an electrical potential as negative as -150 to -180 mV, mitochondria tend to attract cations such as Na^+, which could accumulate to concentrations higher than 1 M (Bernardi, 1999) if no regulatory mechanisms were present. It has been proposed that resting cardiac myocytes maintain a low Na_{mit}^+ (Donoso et al., 1992; Jung et al., 1992) that allow them to extrude Ca^{2+} ions from the mitochondrial matrix using the mitochondrial Na^+/Ca^{2+} exchanger activity. The mitochondrial Na^+/H^+ antiporter is the likely mechanism responsible for maintaining the Na^+ electrochemical gradient across the inner mitochondrial membrane (Bers et al., 2003; Brierley et al., 1994) by using the proton gradient actively generated by the respiratory chain (Mitchell, 1979). The mitochondrial Na^+/H^+ exchanger probably belongs to the NHE family of transporters, but presents different functional properties from its corresponding antiport in the plasma membrane (Brierley et al., 1994). In particular, it does not appear to be inhibited by the plasma membrane NHE inhibitor amiloride but is strongly inhibited by its analogue EIPA (Brierley et al., 1994; Sastrasinh et al., 1995). The present study provides evidence that in intact astrocytes, mitochondrial Na^+/H^+ dynamically prevents the excessive increase in Na_{mit}^+ and maintains it in a dynamic steady-state with a resting level close to the Na_{cyt}^+ concentration.

Astrocytes can generate massive Na_{cyt}^+ increases caused by Na^+/glutamate uptake, one of the most prominent astrocytic functions (Danbolt, 2001). Besides preventing the excitotoxic buildup of interstitial glutamate during activity, this transport plays a pivotal role in coupling excitatory neuronal activity with energy metabolism (Magistretti et al., 1999). The increased Na_{cyt}^+ activates the plasma membrane Na^+/K^+ ATPase, which more than doubles its activity (Chatton et al., 2000), along with its associated ATP consumption, leading to a substantial decrease in ATP levels (Chatton and Magistretti, 2005). The purpose of this ability of mitochondria to sense Na_{cyt}^+ increases is yet to be clarified and could be different from that of regulating mitochondrial Ca^{2+} levels as proposed for other cell types. In particular, although astrocytes possess a substantial density of mitochondria, glutamate uptake enhances the formation of lactate from aerobic glycolysis (Pellerin and Magistretti, 1994). Evidence also supports this conclusion in acute hippocampal slices (Kasischke et al., 2004). One can speculate whether the increased Na^+ influx into mitochondria plays a role in modulating the metabolic response of astrocytes, as the associated activation of mitochondrial Na^+/H^+ antiporters, which occurs to the expense of the H^+ gradient generated by the respiratory chain, could weaken mitochondrial production of ATP. In contrast, Ca^{2+} that is shown in the present study to be intimately linked to the Na_{mit}^+ response is known to stimulate mitochondrial oxidative phosphorylation (Gunter et al., 2004). Thus, the impact of Na_{mit}^+ increases on the overall cellular energy metabolism and its relevance for the metabolic responses in the context of neurometabolic coupling has to be evaluated.

Little, if anything, was known on astrocytic Na_{mit}^+ and on the contribution of mitochondria to the overall intracellular Na^+ homeostasis. By simultaneous in situ fluorescence imaging of mitochondrial and cytosolic Na^+, the present study identifies Na^+ as a signal dynamically transmitted to mitochondria and describes the mechanisms involved in its regulation.

ACKNOWLEDGMENTS

REFERENCES

Bajgar R, Seetharaman S, Kowaltowski AJ, Garlid KD, Paucek P. 2001. Identification and properties of a novel intracellular (mitochondrial) ATP-sensitive potassium channel in brain. J Biol Chem 276:33369–33374.

Baron S, Caplanusi A, van de Ven M, Radu M, Despa S, Lambrichts I, Ameloot M, Steels P, Smets I. 2005. Role of mitochondrial Na^+ concentration, measured by CoroNa Red, in the protection of metabolically inhibited MDCK cells. J Am Soc Nephrol 16:3490–3497.

Bernardi P. 1999. Mitochondrial transport of cations: Channels, exchangers, and permeability transition. Physiol Rev 79:1127–1155.

Bernardinelli Y, Haeberli C, Chatton J-Y. 2005. Flash photolysis using a light emitting diode: An efficient, compact, and affordable solution. Cell Calcium 37:565–572.

Bernardinelli Y, Magistretti PJ, Chatton J-Y. 2004. Astrocytes generate Na^+-mediated metabolic waves. Proc Natl Acad Sci USA 101:14937–14942.

Bers DM, Barry WH, Despa S. 2003. Intracellular Na^+ regulation in cardiac myocytes. Cardiovasc Res 57:897–912.

Boengler K, Dodoni G, Rodriguez-Sinovas A, Cabestrero A, Ruiz-Meana M, Gres P, Konietzka I, Lopez-Iglesias C, Garcia-Dorado D, Di Lisa F, Heusch G, Schulz R. 2005. Connexin 43 in cardiomyocyte mitochondria and its increase by ischemic preconditioning. Cardiovasc Res 67:234–244.

Borin ML, Goldman WF, Blaustein MP. 1993. Intracellular free Na^+ in resting and activated A7r5 vascular smooth muscle cells. Am J Physiol 264:C1513–C1524.

Brierley GP, Baysal K, Jung DW. 1994. Cation transport systems in mitochondria: Na^+ and K^+ uniports and exchangers. J Bioenerg Biomembr 26:519–526.

Chatton J-Y, Magistretti PJ. 2005. Relationship between L-glutamate-regulated intracellular Na^+ dynamics and ATP hydrolysis in astrocytes. J Neural Transm 112:77–85.

Chatton J-Y, Marquet P, Magistretti PJ. 2000. A quantitative analysis of L-glutamate-regulated Na^+ dynamics in mouse cortical astrocytes: Implications for cellular bioenergetics. Eur J Neurosci 12:3843–3853.

Chatton J-Y, Pellerin L, Magistretti PJ. 2003. GABA uptake into astrocytes is not associated with significant metabolic cost: Implications for brain imaging of inhibitory transmission. Proc Natl Acad Sci USA 100:12456–12461.

Danbolt NC. 2001. Glutamate uptake. Prog Neurobiol 65:1–105.

Donoso P, Mill JG, O'Neill SC, Eisner DA. 1992. Fluorescence measurements of cytoplasmic and mitochondrial sodium concentration in rat ventricular myocytes. J Physiol (London) 448:493–509.

Dzubay JA, Jahr CE. 1999. The concentration of synaptically released glutamate outside of the climbing fiber-Purkinje cell synaptic cleft. J Neurosci 19:5265–5274.

Ellis-Davies GCR, Kaplan JH, Barsotti RJ. 1996. Laser photolysis of caged calcium: Rates of calcium release by nitrophenyl-EGTA and DM-nitrophen. Biophys J 70:1006–1016.

Gunter TE, Yule DI, Gunter KK, Eliseev RA, Salter JD. 2004. Calcium and mitochondria. FEBS Lett 567:96–102.

Horisberger JD, Kharoubi-Hess S, Guennoun S, Michielin O. 2004. The fourth transmembrane segment of the Na, K-ATPase α subunit: A systematic mutagenesis study. J Biol Chem 279:29542–29550.

Jayaraman S, Joo NS, Reitz B, Wine JJ, Verkman AS. 2001a. Submucosal gland secretions in airways from cystic fibrosis patients have nor-

mal [Na$^+$] and pH but elevated viscosity. Proc Natl Acad Sci USA 98:8119–8123.

Jayaraman S, Song Y, Vetrivel L, Shankar L, Verkman AS. 2001b. Non-invasive in vivo fluorescence measurement of airway-surface liquid depth, salt concentration, and pH. J Clin Invest 107:317–324.

Jung DW, Apel LM, Brierley GP. 1992. Transmembrane gradients of free Na$^+$ in isolated heart mitochondria estimated using a fluorescent probe. Am J Physiol 262:C1047–1055.

Kasischke KA, Vishwasrao HD, Fisher PJ, Zipfel WR, Webb WW. 2004. Neural activity triggers neuronal oxidative metabolism followed by astrocytic glycolysis. Science 305:99–103.

Magistretti PJ, Pellerin L, Rothman DL, Shulman RG. 1999. Energy on demand. Science 283:496, 497.

Malli R, Frieden M, Osibow K, Zoratti C, Mayer M, Demaurex N, Graier WF. 2003. Sustained Ca^{2+} transfer across mitochondria is essential for mitochondrial Ca^{2+} buffering, store-operated Ca^{2+} entry, and Ca^{2+} store refilling. J Biol Chem 278:44769–44779.

Mitchell P. 1979. Keilin's respiratory chain concept and its chemiosmotic consequences. Science 206:1148–1159.

Pellerin L, Magistretti PJ. 1994. Glutamate uptake into astrocytes stimulates aerobic glycolysis: A mechanism coupling neuronal activity to glucose utilization. Proc Natl Acad Sci USA 91:10625–10629.

Pivovarova NB, Pozzo-Miller LD, Hongpaisan J, Andrews SB. 2002. Correlated calcium uptake and release by mitochondria and endo-plasmic reticulum of CA3 hippocampal dendrites after afferent synaptic stimulation. J Neurosci 22:10653–10661.

Rose CR, Ransom BR. 1996. Mechanisms of H$^+$ and Na$^+$ changes induced by glutamate, kainate, and D-aspartate in rat hippocampal astrocytes. J Neurosci 16:5393–5404.

Sastrasinh M, Young P, Cragoe EJ Jr, Sastrasinh S. 1995. The Na$^+$/H$^+$ antiport in renal mitochondria. Am J Physiol 268:C1227–C1234.

Scotti AL, Chatton J-Y, Reuter H. 1998. Roles of Na$^+$/Ca^{2+} exchange and of mitochondria in the regulation of presynaptic Ca^{2+} and spontaneous glutamate release. Philos Trans R Soc Lond B 354:357–364.

Shoshan-Barmatz V, Gincel D. 2003. The voltage-dependent anion channel: characterization, modulation, and role in mitochondrial function in cell life and death. Cell Biochem Biophys 39:279–292.

Sorg O, Magistretti PJ. 1992. Vasoactive intestinal peptide and noradrenaline exert long-term control on glycogen levels in astrocytes: Blockade by protein synthesis inhibition. J Neurosci 12:4923–4931.

Yang F, He XP, Russell J, Lu B. 2003. Ca^{2+} influx-independent synaptic potentiation mediated by mitochondrial Na$^+$-Ca^{2+} exchanger and protein kinase C. J Cell Biol 163:511–523.

Yang KT, Pan SF, Chien CL, Hsu SM, Tseng YZ, Wang SM, Wu ML. 2004. Mitochondrial Na$^+$ overload is caused by oxidative stress and leads to activation of the caspase 3-dependent apoptotic machinery. FASEB J 18:1442–1444.

2. Tuning of the energy metabolic response in astrocytes by mitochondrial pH modulation

This study investigates the role of pH changes induced by glutamate uptake on mitochondria of astrocytes. Using a novel genetically-encoded fluorescent probe targeted to mitochondria and sensitive to pH, we showed that neuronally released glutamate acidifies mitochondrial matrix of astrocytes. We presented several pieces of evidence suggesting that glutamate transport at the plasma membrane is the main mechanism responsible for mitochondrial matrix acidification. We also presented several pieces of evidence indicating that intracellular acidification induced by glutamate uptake decreases mitochondrial metabolism. This study is currently submitted for publication.

I performed all the experiments except those presented in Fig. 5. I designed the experiments, analyzed the results, prepared the figures and wrote the manuscript with Jean-Yves Chatton.

Highlights

- Neuronally-released glutamate causes mitochondrial acidification in astrocytes

- Glutamate uptake induces mitochondrial matrix acidification in astrocytes

- Glutamate-induced acidification abrogates the mitochondrial pH gradient

- Glutamate-induced acidification decreases in mitochondrial oxidative metabolism
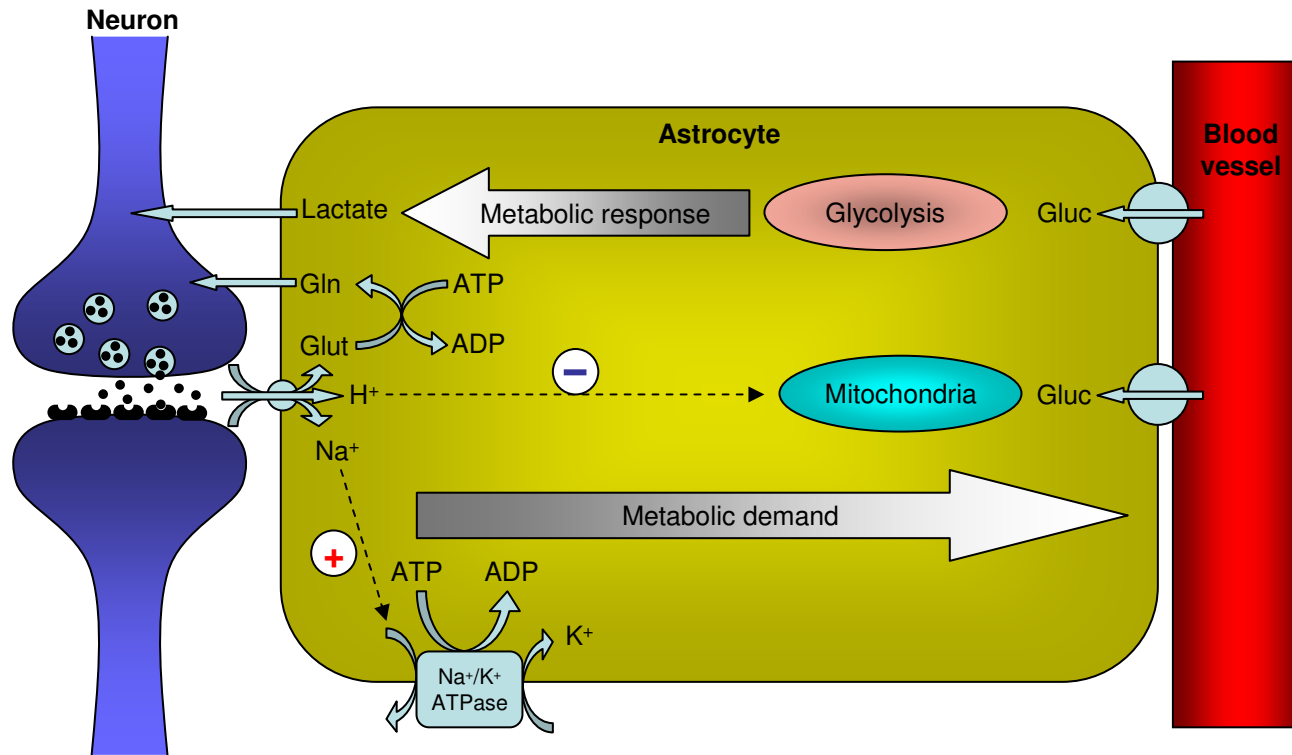
Tuning of the Energy Metabolic Response in Astrocytes by Mitochondrial pH Modulation

Guillaume Azarias[1], Hélène Perreten[2], Sylvain Lengacher[2], Damon Poburko[3], Nicolas Demaurex[3], Pierre J. Magistretti[2,4] and Jean-Yves Chatton[1,5]

[1] Department of Cell Biology and Morphology, University of Lausanne, Switzerland

[2] Laboratory of Neuroenergetics and Cellular Dynamics, Brain and Mind Institute, Ecole Polytechnique Fédérale de Lausanne, Lausanne, Switzerland.

[3] Department of Cell Physiology and Metabolism, University of Geneva, Switzerland

[4] Center for Psychiatric Neuroscience Lausanne, Switzerland

[5] Cellular Imaging Facility, University of Lausanne, Switzerland

Short Title : Astrocyte mitochondrial metabolism regulation

Corresponding author:

Jean-Yves Chatton
Dept. of Cell Biology and Morphology
University of Lausanne
Rue du Bugnon 9
CH-1005 Lausanne
Switzerland
Tel. +41-21-692-5106
Fax. +41-21-692-5105
E-mail: jean-yves.chatton@unil.ch

Summary

Clearance of neuronally released glutamate leads to an intracellular sodium concentration increase in astrocytes that is associated with significant metabolic cost. The proximity of mitochondria at glutamate uptake sites in astrocytes raises the question of the ability of mitochondria to respond to these energy demands. We used dynamic fluorescence imaging to investigate the impact of glutamatergic transmission on mitochondria in living astrocytes. Neuronal release of glutamate induced an intracellular acidification in astrocytes, via glutamate transporters, that spread over the mitochondrial matrix. Glutamate-induced mitochondrial matrix acidification exceeded cytosolic acidification and abrogated cytosol-to-mitochondrial matrix pH gradient. By decoupling glutamate uptake from cellular acidification, we found that glutamate induced a pH-mediated decrease in mitochondrial metabolism. These findings suggest a model where excitatory neurotransmission dynamically regulates astrocyte energy metabolism by limiting the contribution of mitochondria to the metabolic response, thereby preventing excessive mitochondrial reactive oxygen species production and increasing oxygen availability for neurons.

Introduction

Recent advances in neuroenergetics tend to indicate that the major energetic cost in brain cortex takes place at glutamatergic synapses (Alle et al., 2009; Sibson et al., 1998) and involves a tight metabolic coupling between neurons and perisynaptic astroglial processes surrounding glutamatergic synapses (Chatton et al., 2003; Magistretti, 2009; Voutsinos-Porche et al., 2003). It has been proposed that the activity of glutamate transporters expressed at the plasma membrane of astrocytes is associated with an intracellular Na^+ increase correlated with the mobilization of the plasma membrane Na,K-ATPase activity and an ensuing substantial increase in ATP consumption (Magistretti et al., 1999). Consistently, it has been recently shown that glutamatergic synaptic activity triggers an energetic demand in astrocytes that generates a diffusion gradient for glucose within a network of astrocytes, directly linked to the level of neuronal activity (Rouach et al., 2008). The nature and regulation of the glucose metabolism within astrocytes are of crucial importance for the interpretation of functional neuroimaging signals and remain a debated issue. *In vitro* experiments showed that glutamate uptake enhances lactate release suggesting that glycolysis is the dominant pathway involved (Pellerin and Magistretti, 1994). However, the contribution of mitochondria to the metabolic response remains elusive (Pellerin and Magistretti, 2003), even though direct and indirect evidence suggests a certain degree of oxidative activity in astrocytes (Lovatt et al., 2007; Wyss et al., 2009).

Ultrastructural analysis of astrocyte-neuron tripartite synapses have indicated that fine astrocytic processes ensheathing synapses contain a substantial density of mitochondria (Grosche et al., 1999; Lovatt et al., 2007; Oberheim et al., 2009). Accordingly, it was estimated that astrocytes account for about 25% of total brain oxidative metabolism as measured by nuclear magnetic resonance spectroscopy (Serres et al., 2008). The presence of mitochondria in the immediate vicinity of plasmalemmal glutamate transporters in astrocytes (Bezzi et al., 2004; Chaudhry et al., 1995; Haugeto et al., 1996) raises the question of whether factors such as ion concentration changes associated with glutamate uptake have an impact on mitochondrial metabolism.

To address this issue, we used cultured cortical astrocytes as a model of perisynaptic astroglial process. The thin morphology of astrocytes in culture enables studying mitochondria in the immediate proximity of plasma membrane glutamate transporters and in an intact cellular environment. We used real time fluorescence imaging to follow intracellular ionic alterations during glutamate superfusion and studied the impact of glutamate on the

metabolism of astrocyte mitochondria *in situ*. In previous studies, we have shown that the mitochondrial Na^+ concentration increases as a result of glutamate transporter activity (Bernardinelli et al., 2006). In the present study, using a fluorescent pH biosensor targeted to the mitochondrial matrix, we show that glutamate, released from neurons or applied by superfusion, induces a dose-dependent proton transfer into mitochondria that depends on glutamate transporter activity. We further show that this proton transfer weakens the cytosol-to-mitochondrial matrix pH gradient and decreases mitochondrial oxidative metabolism.

Results

Glutamate Induces Mitochondrial pH Changes in Astrocytes

Glutamate uptake was shown to decrease cytosolic pH in cultured astrocytes (Rose and Ransom, 1996) and in hippocampal slices (Amato et al., 1994) but the impact of cytosolic acidification on mitochondrial physiology is not known. To address this issue, we used the genetically-encoded pH-sensitive fluorescent biosensor MitoSypHer targeted to the mitochondrial matrix (Demaurex and Poburko, 2009). Two-week old cultured astrocytes transfected with MitoSypHer plasmid exhibited a fluorescent protein expression pattern typical of mitochondrial labeling, with dark nuclei and punctate staining of rod-like structures (**Fig. 1a$_1$**). In living cells, the expression of MitoSypHer perfectly matched the MitoTracker Red mitochondrial staining (**Fig. 1a$_{2\text{-}3}$**) and fluorescence excitation ratio was correlated with pH (**Fig. 1b$_1$**).

According to the chemioosmotic coupling hypothesis, mitochondrial matrix is expected to be more alkaline than cytosol because of the anticipated low permeability of the mitochondrial inner membrane and the constant extrusion of protons across mitochondrial inner membrane by the mitochondrial respiratory chain (Mitchell, 1979). Consistently, the resting mitochondrial matrix pH was found to be significantly higher than that of the cytosol, with pH values of 7.34±0.02 (n=46, 168 cells) and pH 7.28±0.02 (n=23, 172 cells), respectively (P<0.05 using the ANOVA procedure). However, glutamate superfusion of astrocytes caused a rapid and significant drop in mitochondrial matrix pH (**Fig. 1b$_2$**) whose amplitude was even greater than that found in the cytosol (**Fig. 1c**).

Glutamate superfusion (200μM) also induced a rapid and significant pH drop in the mitochondrial intermembrane space (**Fig. S1**) measured using the MIMS-EYFP biosensor (Porcelli et al., 2005). The intermembrane space displayed an acidification of equal amplitude compared with the glutamate-induced cytosolic acidification (**Fig. 1c**), which is consistent with the described high permeability of the outer mitochondrial membrane to ions and small solutes due to the presence of mitochondrial porins (Blachly-Dyson and Forte, 2001). Thus, we focused the rest of the study on the mitochondrial matrix compartment.

Glutamate-evoked Mitochondrial Matrix pH Acidification is Mediated by Glutamate Transporters

The observed kinetics of acidification (**Fig. 1b$_2$**) is reminiscent of a transporter-mediated process. Therefore, we investigated the concentration dependence parameters of glutamate-

evoked mitochondrial matrix acidification. Both the amplitude and initial rate of glutamate-induced mitochondrial matrix acidification followed a Michaelis and Menten relationship with glutamate concentration (**Fig. 2a**). The maximal amplitude of mitochondrial matrix acidification was observed at $200\mu M$ glutamate and the apparent EC_{50} was $13.2\pm5.1\mu M$. The initial rate of mitochondrial matrix acidification yielded an EC_{50} value of $83\pm25\mu M$. As kinetic parameters of glutamate-induced mitochondrial acidification closely matched values found previously for Na^+-dependent plasma-membrane glutamate transport (Chatton et al., 2000), we attempted to inhibit glutamate transport using DL-threo-β-benzyloxyaspartate (TBOA), a competitive inhibitor of glutamate transporters with a broad isoform selectivity. Indeed, TBOA ($500\mu M$) reversibly inhibited the glutamate-evoked mitochondrial matrix acidification by $75\pm2\%$ (**Fig. 2b** and **Fig. S2**). Astrocytic cytosolic Ca^{2+} is expected to increase in the presence of glutamate following activation of metabotropic receptors (mGluRs), and plasma membrane Na^+/Ca^{2+} antiporter activity following glutamate transport-mediated Na^+ increase. The Ca^{2+} increase itself was shown to lead to mitochondrial acidification in HeLa cells by means of plasma membrane Ca^{2+}/H^+ exchange mediated by the Ca-ATPase (Demaurex and Poburko, 2009). To test whether this mechanism was also involved in astrocytes, we simultaneously monitored pH_{mit} and cytosolic Ca^{2+} during application of the mGluR agonist t-ACPD, that is not transported, or of the glutamate transporter substrate D-aspartate. **Fig. 2c** shows that whereas both compounds lead to comparable Ca^{2+} increases, only the glutamate transporter substrate D-aspartate caused mitochondrial acidification.

Glutamate-induced Cellular Acidification Abrogates the Cytosol-to-Mitochondrial Matrix pH Gradient

The pH gradient and electrical potential across the mitochondrial inner membrane are important determinants for ATP synthesis. As cytosol and mitochondrial matrix responded to glutamate application with acidifications of different amplitudes (**Fig. 1c**), we evaluated the evolution of the pH gradient across the mitochondrial inner membrane before and during glutamate application.

We first performed a statistical analysis of distributions of mitochondrial matrix and cytosolic pH measured in separate cells and experiments. As mentioned above, under basal conditions the mitochondrial matrix was significantly more alkaline than the cytosol, consistent with an active translocation of protons across the mitochondrial inner membrane by the mitochondrial respiratory chain. However, we found that during glutamate superfusion

both the mitochondrial matrix and the cytosol reached lower pH values that were not significantly different (**Fig. S3**), suggesting that glutamate uptake abrogates cytosol-to-mitochondrial matrix pH gradient.

In order to determine the respective dynamics of mitochondrial matrix and cytosolic pH during glutamate uptake, we loaded MitoSypHer-transfected astrocytes with the cytosolic red dye SNARF-1 (**Fig. 3a**). The pattern of SNARF-1 fluorescence had typical cytosolic distribution, with nuclei and cytoplasm homogeneously stained. Only astrocytes expressing MitoSypHer exhibited the spectral signature of both fluorophores (**Fig. 3b**). Consistent with the statistical evaluation described above, the mitochondrial matrix pH was found to be significantly higher than cytosolic pH at resting state (**Fig. 3c,d**). Upon glutamate superfusion, the two compartments no longer displayed statistically different pH values, indicating that glutamate abrogated the pH gradient between the mitochondrial matrix and the cytosol. However, after glutamate washout the pH difference between both compartments was rapidly restored. The glutamate transporter substrate D-aspartate (500μM) induced mitochondrial matrix acidification which canceled the transmembrane pH difference. This result further indicated that glutamate did not induce mitochondrial acidification through intracellular metabolic reactions. The ionotropic glutamate receptor agonist kainate (500μM) induced a mild but significant acidification in both mitochondrial matrix and cytosol, however insufficient to cancel the cytosol-to-mitochondrial matrix pH gradient.

Independence of Cellular Na$^+$ and pH Responses to Glutamate

As astrocytes experience substantial changes of both cytosolic and mitochondrial Na$^+$ concentration during glutamate uptake, we investigated the possible inter-dependence of cellular Na$^+$ and pH regulation. We tested a putative role of Na$^+$/H$^+$ exchangers using ethyl-isopropyl amiloride (EIPA, 50μM), a compound known to inhibit Na$^+$/H$^+$ exchanger of both plasma membrane and mitochondria. However, EIPA neither altered resting mitochondrial matrix pH (*not shown*) nor the amplitude of glutamate-induced mitochondrial matrix acidification (**Fig. S4**), ruling out a significant contribution of the mitochondrial Na$^+$/H$^+$ exchanger in glutamate-evoked mitochondrial acidification.

We then designed a protocol to dissociate the effects of glutamate on cellular acidification from its effects on sodium concentration, by co-administering the weak base triethylammonium (TREA) together with glutamate. The concentration of TREA necessary to precisely compensate glutamate-induced cytosolic acidification was titrated by superfusing glutamate (200μM) alone, followed by successive applications of TREA at increasing

concentrations (n=4, 32 cells, *not shown*). In this series of experiments, 6mM of TREA efficiently prevented a 1.5 min glutamate-induced acidification. Under these conditions, glutamate-induced mitochondrial matrix acidification was severely impaired. In contrast, both cytosolic and mitochondrial Na^+ responses to glutamate were largely maintained, indicating that TREA did not prevent Na^+-coupled glutamate transport (**Fig. 4a**). Taken together, these experiments suggest that glutamate-induced cellular acidification and Na^+ responses are not strictly coupled. In addition, this protocol enabled producing a chemical ablation of glutamate-induced cellular acidification that has subsequently been used to highlight the signaling role of pH on glutamate-induced metabolic changes. As seen in **Fig. 4b**, the alkalinizing effect of TREA decreased during its application. Therefore, the concentration of TREA was adapted for each subsequent series of experiments and protocols.

Glutamate Induces a pH-Mediated Decrease in Oxygen Consumption Rate and Mitochondrial Reactive Oxygen Species Production

We then measured the oxygen consumption rate to investigate whether glutamate-induced mitochondrial acidification has an impact on mitochondrial physiology. Using a fluorescence-based oxygen analyzer, we measured the oxygen consumption rate in the vicinity of intact astrocytes during glutamate uptake. In these experiments, astrocytes were pre-incubated in the presence of the glycolysis inhibitor 2-deoxyglucose (2-DG) and pyruvate was added as a mitochondrial energy substrate to promote mitochondrial ATP production and avoid potential confounding effects of glycolysis activation. We found that glutamate (200µM) stably decreased the oxygen consumption rate to 88±1% of the basal level (**Fig. 5**). However, when glutamate was applied together with TREA (20mM) to prevent intracellular acidification, the oxygen consumption rate remained unchanged. Taken together, these experiments suggest that glutamate mediates a pH-mediated decrease of mitochondrial oxygen respiration in astrocytes.

During normal mitochondrial respiration, 0.2 to 2% of consumed oxygen is transformed into reactive oxygen species (mROS) from complexes I and III of the mitochondrial respiratory chain (Balaban et al., 2005). We reasoned that if glutamate induced a decrease in mitochondrial respiration, it should also decrease mROS production rate. To investigate this hypothesis, we used the mROS sensitive probe MitoSOX Red, which selectively loads into mitochondria and becomes fluorescent when oxidized by mROS. Measuring the slope of MitoSOX Red fluorescence increase enabled real time monitoring alterations of the mROS production rate. Consistent with the prevalence of glycolysis in astrocytes at resting state, the

replacement of the glucose-containing medium by a medium containing pyruvate and 2-DG enhanced the mROS production rate by ~3 fold (**Fig. 6b**).

Upon application of glutamate, mROS production was altered in a bi-phasic way (**Fig. 6a**) in which an initial increase of mROS production rate was followed by a sustained decrease to 75±3% of the initial value within 1.5 min. mROS production rate did not immediately recover to baseline after glutamate washout. When glutamate-induced acidification was compensated using TREA, glutamate no longer altered mitochondrial ROS production rate (100±2% at 5 min., **Fig 6a**). TREA alone only marginally decreased mROS production rate (**Fig. 6a**). We then reasoned that blocking glutamate uptake during glutamate application should prevent pH-mediated alteration of mROS production rate. However, TBOA not only failed to prevent the initial transient increase caused by glutamate application but led to a stable increase of mROS production rate as measured after 5 min of stimulation (**Fig. 6b**), whereas TBOA alone had no significant effect (95±4% of 2-DG condition, p=0.18, n=4, 18 cells, *not shown*). The inhibition of glutamate uptake may have actually unveiled the involvement of metabotropic glutamate receptors in the response, which involves Ca^{2+} responses (see **Fig. 2c**). To test this hypothesis, we stimulated astrocytes with glutamate in the presence of TBOA and the metabotropic glutamate receptor inhibitor (+)-α-methyl-4-carboxyphenylglycine (MCPG, 1mM). MCPG prevented the steady increase of mROS production rate in the presence of glutamate and TBOA (**Fig. 6b**). Taken together, these experiments suggest that glutamate induces a pH-mediated alteration of mROS production rate characterized by an initial transient increase of mROS production rate followed by a stable decrease of mROS production rate.

Neuronal Release of Glutamate Triggers Mitochondrial Matrix Acidification in Astrocytes

Finally, we asked whether glutamate released by neurons during activity could cause mitochondrial matrix acidification in astrocytes. To address this issue, we set up a mixed culture model resembling the *in vivo* cytoarchitecture, where astrocyte membranes are in close proximity with neuronal synapses. Cortical astrocytes previously transfected with MitoSypHer were co-cultured with neurons for two weeks. Under DIC contrast microscopy, neurons were recognizable by their pyramidal soma with several extending processes (**Fig. 7a**). Astrocytes expressing MitoSypHer were identified by their mitochondrial fluorescent pattern. Using immunohistochemistry against the synaptic vesicle protein VAMP2, we verified that in this preparation synaptic boutons were in close apposition with astrocyte

mitochondria labeled with MitoSypHer (**Fig. S5a**). In addition, we determined that a 20-second application of NMDA ($10\mu M$) reliably and selectively evoked a reversible cytosolic Ca^{2+} increase in neurons, even in the presence of TBOA, whereas in pure culture of astrocytes NMDA had no effect on cytosolic Ca^{2+} levels (**Fig. S5b,c**). Therefore, NMDA application was used to evoke neuronal excitatory responses expected to stimulate glutamate release, and mitochondrial matrix pH was measured in surrounding MitoSypHer transfected astrocytes.

Fig. 7b shows that upon a 20-second NMDA stimulation, the mitochondrial matrix pH of astrocytes declined to a maximal acidification of 0.05 ± 0.01 pH units after 112 ± 15 sec. Mitochondrial matrix pH recovered to its initial value 4-5 min later. In the absence of neurons, NMDA application did not significantly alter the mitochondrial matrix pH (**Fig. 7c**) indicating that NMDA-triggered mitochondrial matrix acidification in astrocytes is specifically linked to neuronal activity. We used TBOA to investigate whether in this situation astrocyte mitochondrial matrix acidification is mediated by plasma membrane uptake of glutamate. Consistent with experiments in pure astrocytes culture, TBOA did not significantly alter the basal mitochondrial matrix pH ($p=0.23$ using Student t test, *not shown*). However, TBOA diminished the astrocyte mitochondrial matrix acidification in response to NMDA-mediated neuronal activation (**Fig. 7c**). The extent of inhibition was however not as pronounced as in pure astrocyte cultures. Taken together, these experiments suggest that the glutamate released by neurons during synaptic activity induces a glutamate transporter-mediated mitochondrial matrix acidification in astrocytes.

Discussion

This study was designed to evaluate the impact of glutamatergic neurotransmission on mitochondrial metabolism of astrocytes. We show that glutamate uptake in astrocytes causes a pH modulation in mitochondria that rapidly impacts on their metabolic response.

Glutamate uptake through high-affinity Na^+-coupled transporters has been identified as the first step that enables astrocytes to sense the level of excitatory neuronal activity and to provide a proportionate metabolic response (Magistretti et al., 1999; Pellerin and Magistretti, 1994; Voutsinos-Porche et al., 2003). The influx of Na^+ ions and subsequent activation of the Na,K-ATPase have been shown to enhance glucose capture from the extracellular space. It has been estimated that glutamate uptake increased the overall ATP consumption by ~2 to 3-fold (Chatton et al., 2000). Astrocytes, both in primary culture and *in vivo*, possess a substantial density of mitochondria, the site of oxidative phosphorylation and energy powerhouse of cells. During glutamatergic stimulation, the increased mitochondrial concentrations of Ca^{2+} and Na^+ would be expected to stimulate mitochondrial respiration through activation of Ca^{2+}-dependent dehydrogenases (Hajnoczky et al., 1995) and through increased pyruvate dehydrogenase activity (Pawelczyk and Olson, 1995), respectively. Glutamate taken up in astrocytes could also represent a substrate of the Krebs cycle after conversion to alpha-ketoglutarate by the mitochondrial matrix enzyme glutamate dehydrogenase (Hertz et al., 2007).

The present study has investigated the impact of pH changes on astrocytic mitochondrial metabolism. In acute slices, neuronal activity was shown to induce cytosolic alkaline transients in the soma of astrocytes that follows extracellular potassium concentration increases (Chesler and Kraig, 1989). In contrast, the plasma membrane Na^+-glutamate cotransporters coupled to proton entry causes cytosolic acidification (Amato et al., 1994; Rose and Ransom, 1996). It has recently been reported that, *in situ*, hippocampal neuronal stimulation is followed by glutamate uptake in astrocytes coincident with increases of cytosolic Na^+ concentration in their fine processes (Langer and Rose, 2009). Similarly, glutamate transporter activity could potentially create local acidic cytoplasmic microdomains at the interface of plasma and mitochondrial membranes that could promote proton translocation into mitochondria. As the ionic composition of the mitochondrial intermembrane space is considered to be equivalent to that of the cytosol, cytosolic pH changes are expected to alter pH gradient across mitochondrial inner membrane. We therefore engaged in investigations of mitochondrial pH in intact astrocytes using MitoSypher, a novel

genetically-encoded pH sensor targeted to the mitochondrial matrix (Demaurex and Poburko, 2009).

We discovered that mitochondria of astrocytes undergo substantial acidification during glutamate uptake. By using an experimental model of co-cultures of neurons and astrocytes, that enabled selective monitoring of mitochondrial pH in astrocytes, we discovered that evoking neuronal activity caused a sustained acidification in astrocyte mitochondria. The experimental evidence collected in this study indicates that the mechanism of acidification involves plasma membrane glutamate transporters, as transporter inhibitors largely prevented the mitochondrial pH response. In addition, glutamate-evoked mitochondrial matrix acidification was concentration-dependent with apparent EC_{50} values close to the values found for plasma membrane transporters (Chatton et al., 2000); the shift of apparent EC_{50} value observed when measured on the amplitude versus the initial rate of the response is another signature of the plasma membrane glutamate transporter activity as described before (Chatton et al., 2000). Finally, the alternate transporter substrate D-aspartate that does not activate glutamate receptors nor is metabolized, led to a similar acidification. Interestingly, in contrast to what was observed in HeLa cells, a cytosolic Ca^{2+} increase alone caused only a mild—if any—pH_{mit} change, highlighting the role of glutamate transporter in the mitochondrial effects (Demaurex and Poburko, 2009). Data presented here did not point toward Na^+ and mitochondrial Na^+/H^+ exchangers as main contributors to the observed mitochondrial pH response, as EIPA was without effect. Compensating cellular pH changes during glutamate uptake by administration of weak base, effectively abrogated the mitochondrial pH drop, while maintaining most of the Na^+ response. Also, application of kainate, which causes a substantial Na^+ elevation (Bernardinelli et al., 2006; Chatton et al., 2000) caused only a minor mitochondrial acidification. Under the current experimental conditions, it appears that protons are translocated across the mitochondrial membranes by other transport mechanisms or possibly by mitochondrial uncoupling proteins. The observed mitochondrial proton entry may appear unexpected since the chemiosmotic hypothesis (Mitchell, 1979), widely accepted as the mechanism prevailing for oxidative ATP production, assumes that the inner mitochondrial membrane is relatively impermeable to cations in general and to protons in particular.

Several experimental data point to the fact that pH profoundly influences cellular functions, for instance by direct pH modulation of enzymes (Casey et al., 2010). At the mitochondria level, besides enzymatic pH modulation, the proton gradient across the mitochondrial membrane is central to the ability of mitochondria to synthesize ATP. Such

regulation has been recently observed in pancreatic β-cells (Wiederkehr et al., 2009), where mitochondrial matrix pH was found to be a key determinant of mitochondrial energy metabolism. We simultaneously evaluated the dynamics of cytosolic and mitochondrial matrix pH and found that the pH gradient across mitochondrial inner membrane was abrogated during glutamate uptake. Therefore, we examined whether the observed acidification in mitochondria directly influenced their metabolic function. For this purpose, we measured oxygen consumption rate and mitochondrial reactive oxygen species production in astrocytes in which glycolysis was inhibited and pyruvate was provided as an energy substrate. Under these conditions, mROS production rate was enhanced by ~3 fold compared with a glucose-containing medium indicating that glycolysis is the main energy metabolic pathway in resting cultured astrocytes. Consistently, oxygen consumption rate in glycolysis-inhibited astrocytes was approximately equal to that measured at the end of experiments in the presence of the mitochondrial uncoupler FCCP, suggesting that mitochondrial respiration was close to its maximal capacity. Direct monitoring of the oxygen consumption of astrocytes during glutamate uptake demonstrated that a significant decrease of respiration was taking place during glutamate uptake that depended on intracellular acidification. The glutamate-induced decrease of mitochondrial respiration was then confirmed by measuring the production of mROS, a side product of electron transport in the respiratory chain (Balaban et al., 2005). We found that glutamate application steadily decreased mROS output of astrocytes, an observation compatible with the notion that glutamate entry reduces the mitochondrial respiratory chain electron flow. Interestingly, as was found for oxygen consumption, glutamate uptake without concomitant intracellular acidification did not alter mROS production rate, highlighting the central role of acidification in the glutamate effects. This observation is in line with results presented with isolated mitochondria (Selivanov et al., 2008) where mROS production was strongly impaired by lowering mitochondrial matrix pH. This occurred even in a situation of zero pH gradient across the inner mitochondrial membrane. Inhibition of glutamate transport has revealed that metabotropic glutamate receptors have an opposite effect to acidification on mitochondrial metabolism, probably mediated by Ca^{2+} signaling, known to stimulate mitochondrial metabolism. Our experiments indicate that the mitochondrial acidification caused by glutamate supersedes the stimulatory effect of increased Ca^{2+} on mitochondrial metabolism. Conversely, the stimulatory effects of Ca^{2+} on mitochondrial metabolism could occur in cytoplasmic domains where pH is not affected by glutamate uptake.

Glutamate capture associated with excitatory neurotransmission has a high energy cost. Without the ability to increase their mitochondrial metabolism, astrocytes appear to resort to aerobic glycolysis as an alternative way to meet increased energy demands. Our measurements of functional mitochondrial output provide a plausible explanation for the described prevalence of the glycolytic response (Pellerin and Magistretti, 1994) as a means of providing sufficient ATP during glutamate uptake. We propose therefore that glutamate transport tunes energy metabolism in perisynaptic domains by a Na^+-mediated increase in energy demands and pH-mediated decrease in mitochondrial metabolism. The coincidence of the two phenomena promotes the release of glycolysis-derived lactate, as an energy substrate for activated neurons. In addition, by limiting mitochondrial respiration in astrocytes, uptake of glutamate may prevent excessive astrocytic mROS production while maximizing oxygen availability for neurons.

Experimental Procedures

Cell Culture and Solutions

Cortical astrocytes in primary culture were prepared from 1-3 days-old from C57 Bl 6 mice as described elsewhere (Sorg and Magistretti, 1992). Astrocytes were plated on 20mm glass coverslips and cultured for 2-4 weeks in DME medium (Sigma) plus 10% FCS. Co-cultures of neurons and astrocytes were prepared from two-week old primary cultures of astrocytes transfected with MitoSypHer (see below) on which neurons prepared from cerebral cortex of E17 embryonic mice (C57 Bl6) were plated. Briefly, neurons were prepared as follows: cortex were dissected and incubated with 200 units papain for 30 min at 34°C. Dissociated cells were plated at $0.8x10^6$ cells/dish. Co-cultures of cortical neurons were grown in B27/Neurobasal (Gibco) supplemented with 0.5mmol/L glutamine and 100 µg/mL penicillin–streptomycin for 14 days.

Experimental solutions contained (mM): NaCl 160, KCl 5.4, HEPES 20, $CaCl_2$ 1.3, $MgSO_4$ 0.8, NaH_2PO_4 0.78, glucose 5 (pH 7.4) and was bubbled with air. Solutions for dye-loading contained (mM): NaCl 160, KCl 5.4, HEPES 20, $CaCl_2$ 1.3, $MgSO_4$ 0.8, NaH_2PO_4 0.78, glucose 20 and was supplemented with 0.1% Pluronic F127 (Molecular Probes, Eugene, OR). Calibration solutions for mitochondrial matrix pH contained (mM): NaCl 20, KCl 125, $MgCl_2$ 0.5, EGTA 0.2, HEPES 20 and bubbled with air. Calibration solutions for mitochondrial intermembrane space pH contained (mM): NaCl 10, KCl 125, $CaCl_2$ 1, $MgSO_4$ 1, KH_2PO_4 1, HEPES 20.

Astrocyte Transfection

Two week old astrocytes were placed in 2ml of antibiotic-free and serum-free DMEM medium with Fugene (Roche) and DNA encoding for MitoSypHer or MIMS-EYFP. Quantities of µg DNA/µL FuGene were 2/12 and 4/8 for MitoSypHer and MIMS-EYFP, respectively. After four hours, the medium was changed with DME medium plus 10% serum and cells were used 2-3 days after transfection for pure astrocyte culture and 14 days for mixed neuron-astrocyte cultures.

Live Cell Imaging

Epifluorescence microscopy: Low-light level fluorescence imaging was performed on an inverted epifluorescence microscope (Axiovert 100M, Carl Zeiss) using a 40X 1.3 N.A. oil-immersion objective lens. Fluorescence excitation wavelengths were selected using a monochromator (Till Photonics, Planegg, Germany) and fluorescence was detected using a

12-bit cooled CCD camera (Princeton Instruments). Image acquisition and time series were computer-controlled using the software Metafluor (Molecular Devices) running on a Pentium computer.

Cells were loaded in a HEPES-buffered balanced solution and then placed in a thermostated chamber designed for rapid exchange of perfusion solutions (Chatton et al., 2000) and superfused at 35°C. To avoid phototoxicity, excitation intensity was reduced to ~10µW (as measured at the entrance pupil of the objective) by means of neutral density filters. For mitochondrial matrix pH measurement, MitoSypHer fluorescence was sequentially excited at 490 and 420nm and detected at >515nm. At the end of each experiment, *in situ* calibration was performed as described in (Demaurex and Poburko, 2009). Mitochondrial intermembrane space was investigated as previously reported (Porcelli et al., 2005). Intracellular pH measurement was performed using the pH-sensitive dye BCECF-AM and Ca^{2+} with Fura-2 AM as described previously (Chatton et al., 2001). Cytosolic and mitochondrial Na^+ concentration was investigated and calibrated as described in Bernardinelli et al. (2006). mROS production rate was measured using the mitochondrially targeted dye MitoSOX Red loaded at 0.5µM for 20 min at 37°C. MitoSOX Red fluorescence was excited at 510nm and collected above 580nm. For each experimental condition, the MitoSOX Red fluorescence slope was calculated using the software Kaleidagraph (Synergy Software) by performing the first order derivative of locally weighted least-square error fit of the original traces. Data are reported as percentage of the slope measured in 2-DG medium containing pyruvate. As a control, antimycin A (20µg/mL) was applied to verify MitoSOX Red sensitivity to mROS level.

Confocal microscopy: To verify the mitochondrial localization of the MitoSypHer and MIMS-EYFP proteins, transfected astrocytes were loaded for 20 min with MitoTracker Red (1µM, Molecular Probe) at 37°C and imaged by confocal microscopy (LSM 510 Meta, Zeiss) using excitation light at 488nm and 543nm. Fluorescence emissions were collected at 505-530nm (MitoSypHer or MIMS-EYFP) and >560nm (MitoTracker Red).

Simultaneous monitoring of cytosolic and mitochondrial pH was performed at 37°C on a TCS SP5 confocal microscope using its 8kHz Tandem resonant scanner (Leica Microsystems). The pH-sensitive cytosolic red dye SNARF-1 (AM) was loaded for 25-30 min in HEPES loading solution and then washed for 15 min in Hepes solution containing glucose. Mitochondrial and cytosolic pH-sensitive indicators were excited using 488nm low intensity laser light illumination and fluorescence was collected in three separated channels.

MitoSypHer fluorescence emission was collected in the range 500-530nm and the emission ratio (620nm-765nm)/(560nm-600nm) was used for SNARF-1. At the end of each experiment, mitochondrial and cytosolic pH were simultaneously calibrated as described before (Demaurex and Poburko, 2009).

Oxygen Consumption Rate

The oxygen consumption rate was assessed using an Extracellular Flux Analyzer (Seahorse Biosciences, North Billerica, MA). Extracellular flux analysis is a noninvasive assay which uses calibrated optical sensors which directly measures the oxygen consumption rate in cells that remain attached to the culture plate. Before experiments, astrocytes were incubated one hour at 37°C in a CO2-free incubator in a 10mM-HEPES buffered DME medium containing 10mM 2-DG, 5mM glucose, and 5mM pyruvate). Glutamate and TREA were injected in the medium at final concentrations of 200μM and 20mM, respectively. Oligomycin (5μM) and FCCP (2μM) were used as controls to inhibit and maximize mitochondrial respiration, respectively.

Statistics

Unless otherwise indicated, a paired Student's *t* test was performed for each experiment group to assess the statistical significance against respective controls and *, ** and *** refer to *p* values <0.05, 0.01, and 0.001, respectively. For the analysis of distributions of mitochondrial matrix and cytosolic pH, P value was calculated using the two tailed ANOVA on exponential transformed (SAS Institute Inc. Cary NC USA).

Materials

All chemical dyes were from Invitrogen-Molecular Probes. Glutamate, D-aspartate, kainate, CNQX and TBOA were from Tocris (ANAWA Trading). Neurobasal was from Invitrogen. Ethyl-isoporopyl amiloride was a gift from Dr. H. Lang (Aventis Pharma, Frankfurt, Germany). All other substances were from Sigma.

Supplemental Information

Supplemental Information includes five figures.

Acknowledgments

References

Alle, H., Roth, A., and Geiger, J.R. (2009). Energy-efficient action potentials in hippocampal mossy fibers. Science 325, 1405-1408.

Amato, A., Ballerini, L., and Attwell, D. (1994). Intracellular pH changes produced by glutamate uptake in rat hippocampal slices. J. Neurophysiol. 72, 1686-1696.

Balaban, R.S., Nemoto, S., and Finkel, T. (2005). Mitochondria, oxidants, and aging. Cell 120, 483-495.

Bernardinelli, Y., Azarias, G., and Chatton, J.Y. (2006). In situ fluorescence imaging of glutamate-evoked mitochondrial Na^+ responses in astrocytes. Glia 54, 460-470.

Bezzi, P., Gundersen, V., Galbete, J.L., Seifert, G., Steinhauser, C., Pilati, E., and Volterra, A. (2004). Astrocytes contain a vesicular compartment that is competent for regulated exocytosis of glutamate. Nat. Neurosci. 7, 613-620.

Blachly-Dyson, E., and Forte, M. (2001). VDAC channels. IUBMB Life 52, 113-118.

Casey, J.R., Grinstein, S., and Orlowski, J. (2010). Sensors and regulators of intracellular pH. Nat. Rev. Mol. Cell. Biol. 11, 50-61.

Chatton, J.Y., Idle, J.R., Vagbo, C.B., and Magistretti, P.J. (2001). Insights into the mechanisms of ifosfamide encephalopathy: drug metabolites have agonistic effects on alpha-amino-3-hydroxy-5-methyl-4-isoxazolepropionic acid (AMPA)/kainate receptors and induce cellular acidification in mouse cortical neurons. J. Pharmacol. Exp. Ther. 299, 1161-1168.

Chatton, J.Y., Marquet, P., and Magistretti, P.J. (2000). A quantitative analysis of L-glutamate-regulated Na^+ dynamics in mouse cortical astrocytes: implications for cellular bioenergetics. Eur. J. Neurosci. 12, 3843-3853.

Chatton, J.Y., Pellerin, L., and Magistretti, P.J. (2003). GABA uptake into astrocytes is not associated with significant metabolic cost: implications for brain imaging of inhibitory transmission. Proc. Natl. Acad. Sci. USA 100, 12456-12461.

Chaudhry, F.A., Lehre, K.P., van Lookeren Campagne, M., Ottersen, O.P., Danbolt, N.C., and Storm-Mathisen, J. (1995). Glutamate transporters in glial plasma membranes: highly

differentiated localizations revealed by quantitative ultrastructural immunocytochemistry. Neuron 15, 711-720.

Chesler, M., and Kraig, R.P. (1989). Intracellular pH transients of mammalian astrocytes. J. Neurosci. 9, 2011-2019.

Demaurex, N., and Poburko, D. (2009). Modulation of mitochondrial proton gradients by the plasma membrane calcium ATPase. J Physiol Sci 59, 348.

Grosche, J., Matyash, V., Moller, T., Verkhratsky, A., Reichenbach, A., and Kettenmann, H. (1999). Microdomains for neuron-glia interaction: parallel fiber signaling to Bergmann glial cells. Nat. Neurosci. 2, 139-143.

Hajnoczky, G., Robb-Gaspers, L.D., Seitz, M.B., and Thomas, A.P. (1995). Decoding of cytosolic calcium oscillations in the mitochondria. Cell 82, 415-424.

Haugeto, O., Ullensvang, K., Levy, L.M., Chaudhry, F.A., Honore, T., Nielsen, M., Lehre, K.P., and Danbolt, N.C. (1996). Brain glutamate transporter proteins form homomultimers. J. Biol. Chem. 271, 27715-27722.

Hertz, L., Peng, L., and Dienel, G.A. (2007). Energy metabolism in astrocytes: high rate of oxidative metabolism and spatiotemporal dependence on glycolysis/glycogenolysis. J. Cereb. Blood Flow Metab. 27, 219-249.

Langer, J., and Rose, C.R. (2009). Synaptically induced sodium signals in hippocampal astrocytes in situ. J. Physiol. 587, 5859-5877.

Lovatt, D., Sonnewald, U., Waagepetersen, H.S., Schousboe, A., He, W., Lin, J.H., Han, X., Takano, T., Wang, S., Sim, F.J., Goldman, S.A., and Nedergaard, M. (2007). The transcriptome and metabolic gene signature of protoplasmic astrocytes in the adult murine cortex. J. Neurosci. 27, 12255-12266.

Magistretti, P.J. (2009). Neuroscience. Low-cost travel in neurons. Science 325, 1349-1351.

Magistretti, P.J., Pellerin, L., Rothman, D.L., and Shulman, R.G. (1999). Energy on demand. Science 283, 496-497.

Mitchell, P. (1979). Keilin's respiratory chain concept and its chemiosmotic consequences. Science 206, 1148-1159.

Oberheim, N.A., Takano, T., Han, X., He, W., Lin, J.H., Wang, F., Xu, Q., Wyatt, J.D., Pilcher, W., Ojemann, J.G., Ransom, B.R., Goldman, S.A., and Nedergaard, M. (2009). Uniquely hominid features of adult human astrocytes. J. Neurosci. 29, 3276-3287.

Pawelczyk, T., and Olson, M.S. (1995). Changes in the structure of pyruvate dehydrogenase complex induced by mono- and divalent ions. Int. J. Biochem. Cell Biol. 27, 513-521.

Pellerin, L., and Magistretti, P.J. (1994). Glutamate uptake into astrocytes stimulates aerobic glycolysis: a mechanism coupling neuronal activity to glucose utilization. Proc. Natl. Acad. Sci. USA 91, 10625-10629.

Pellerin, L., and Magistretti, P.J. (2003). Food for thought: challenging the dogmas. J. Cereb. Blood Flow Metab. 23, 1282-1286.

Porcelli, A.M., Ghelli, A., Zanna, C., Pinton, P., Rizzuto, R., and Rugolo, M. (2005). pH difference across the outer mitochondrial membrane measured with a green fluorescent protein mutant. Biochem. Biophys. Res. Commun. 326, 799-804.

Rose, C.R., and Ransom, B.R. (1996). Mechanisms of H_+ and Na_+ changes induced by glutamate, kainate, and D-aspartate in rat hippocampal astrocytes. J. Neurosci. 16, 5393-5404.

Rouach, N., Koulakoff, A., Abudara, V., Willecke, K., and Giaume, C. (2008). Astroglial metabolic networks sustain hippocampal synaptic transmission. Science 322, 1551-1555.

Selivanov, V.A., Zeak, J.A., Roca, J., Cascante, M., Trucco, M., and Votyakova, T.V. (2008). The role of external and matrix pH in mitochondrial reactive oxygen species generation. J. Biol. Chem. 283, 29292-29300.

Serres, S., Raffard, G., Franconi, J.M., and Merle, M. (2008). Close coupling between astrocytic and neuronal metabolisms to fulfill anaplerotic and energy needs in the rat brain. J. Cereb. Blood Flow Metab. 28, 712-724.

Sibson, N.R., Dhankhar, A., Mason, G.F., Rothman, D.L., Behar, K.L., and Shulman, R.G. (1998). Stoichiometric coupling of brain glucose metabolism and glutamatergic neuronal activity. Proc. Natl. Acad. Sci. USA 95, 316-321.

Sorg, O., and Magistretti, P.J. (1992). Vasoactive intestinal peptide and noradrenaline exert long-term control on glycogen levels in astrocytes: blockade by protein synthesis inhibition. J. Neurosci. 12, 4923-4931.

Voutsinos-Porche, B., Bonvento, G., Tanaka, K., Steiner, P., Welker, E., Chatton, J.Y., Magistretti, P.J., and Pellerin, L. (2003). Glial glutamate transporters mediate a functional metabolic crosstalk between neurons and astrocytes in the mouse developing cortex. Neuron 37, 275-286.

Wiederkehr, A., Park, K.S., Dupont, O., Demaurex, N., Pozzan, T., Cline, G.W., and Wollheim, C.B. (2009). Matrix alkalinization: a novel mitochondrial signal for sustained pancreatic beta-cell activation. EMBO J. 28, 417-428.

Wyss, M.T., Weber, B., Treyer, V., Heer, S., Pellerin, L., Magistretti, P.J., and Buck, A. (2009). Stimulation-induced increases of astrocytic oxidative metabolism in rats and humans investigated with 1-11C-acetate. J. Cereb. Blood Flow Metab. 29, 44-56.

Figure legends

Fig 1. Glutamate evokes mitochondrial acidification in astrocytes. (**a**) Expression of the pH sensor MitoSypHer in the mitochondrial matrix of cortical astrocytes. Images of cortical astrocytes expressing MitoSypHer (**a₁**); image of the same cells loaded with the mitochondrial selective fluorescent marker MitoTracker Red (**a₂**), and overlay (**a₃**). Scale bar: 10μm. (**b₁**) Calibration curve of MitoSypHer fluorescence excitation ratio versus pH. (**b₂**) Glutamate (200μM) superfusion on intact astrocytes acidified the mitochondrial matrix. A typical trace from a single astrocyte is shown. (**c**) Amplitude of glutamate-induced intracellular acidifications induced by glutamate in the cytosol (n=23, 172 cells), mitochondrial intermembrane space (MIMS, n=9, 26 cells) and mitochondrial matrix (n=46, 168 cells). Data are shown as means±sem. (**d**) Scheme for the localization of mitochondrial pH sensors (MIMS-EYFP and MitoSypHer).

Fig 2. Glutamate evokes a concentration-dependent mitochondrial matrix acidification mediated by glutamate transporters. (**a**) Concentration dependence of the amplitude (open circles) and initial slope (closed triangles) of glutamate-induced mitochondrial matrix acidification. (n=24, 80 cells). (**b**) TBOA reversibly inhibited a 200μM glutamate-evoked mitochondrial matrix acidification. Amplitude of glutamate-induced mitochondrial matrix acidification before during and after TBOA (n=5, 30 cells). See also Figure S2. (**c**) Ca^{2+} (upper curves) and pH_{mit} (lower curves) responses were simultaneously monitored using Fura-2 in MitoSypher transfected astrocytes. The applications of the mGluR agonist (t-ACPD, 100μM) and glutamate transporter substrate (D-asp, 200μM) are indicated in the graph. Traces are shown as mean signals with error bars (SEM) displayed every third time point for graphical clarity (n=5, 8 cells).

Fig 3. Glutamate-induced cellular acidification abrogates the cytosol-to-mitochondrial matrix pH gradient. (**a**) Representative images of MitoSypHer transfected astrocytes loaded with the cytosolic pH-sensitive red dye SNARF-1. Scale bar: 20μm. (**b**) Spectral selectivity of both probes by measuring emission spectra in nucleus (Nuc) and cytosol (Cyt) of transfected (Tr) and untransfected (UnTr) astrocytes labeled with SNARF-1. Both fluorophores were excited at 488nm and emission fluorescence was split into three channels, for MitoSypher (Ch.1) and SNARF-1 (Ch.2 and Ch.3), repectively. Original traces (**c**) and averaged data (**d**) of cytosolic and mitochondrial matrix pH during agonist-induced acidification. Both,

glutamate and D-Aspartate, caused a collapse of cytosol-to-mitochondrial matrix pH gradient (n=7, 11 cells).

Fig 4. Independence of cellular Na$^+$ and pH responses to glutamate. (**a**) Glutamate-evoked cellular Na$^+$ response without concomitant pH change. After a first control pulse of glutamate application, glutamate was superfused together with 6mM TREA, the concentration found to compensate glutamate-induced cytosolic acidification. pH measurements in the cytosol (pH$_{cyt}$, n=4, 32 cells) and mitochondrial matrix (pH$_{matrix}$, n=6, 20 cells), and Na$^+$ measurements in the cytosol (Na$^+_{cyt}$, n=4, 30 cells) and mitochondria (Na$^+_{mit}$, n=4, 32 cells) were taken after 1.5 minutes of stimulation. Data are presented as means±SEM. (**b**) Cytosolic pH measurement during a pulse of 200μM glutamate (solid line) and during glutamate plus TREA application (dotted line). In the example shown, 10.7mM TREA effectively prevented the acidification during glutamate application, as measured after 5 minutes of glutamate application.

Fig 5. Glutamate induces a pH-mediated decrease of oxygen consumption rate. Glycolysis was inhibited using 2-deoxyglucose (10mM) to promote mitochondrial activity and glucose (5mM) and pyruvate (5mM) were given as substrates. (**a**) Time-course of oxygen consumption rate in intact astrocytes in the absence and presence of glutamate (upper graph, n=7). When glutamate-induced cellular acidification was compensated by co-administration of TREA 20mM, glutamate did no longer significantly decreased oxygen consumption rate (lower panel, n=6). As a control, mitochondrial respiration was inhibited using oligomycin (5μM) and then increased using FCCP (2μM) at the end of each experiment. (**b**) Average data of glutamate-induced decrease of oxygen consumption rate with increasing concentrations of TREA. Data were normalized to oxygen consumption rate before glutamate addition for each experiment (n=42).

Fig 6. Glutamate induced a pH-mediated alteration of mROS production rate. (**a**) After a control period, glycolysis in astrocytes was inhibited using 2-DG (10mM) to promote mitochondrial activity and pyruvate (5mM) was given as mitochondrial substrate. The mROS production rate during 2-DG plus pyruvate phase was considered as the reference rate of 100%. Time course of mROS production rate upon stimulation with glutamate, co-administration of glutamate and TREA or TREA alone. At the end of each experiment,

antimycin A (Ant. A) was used as a positive control of mROS detection. Traces are shown as mean signals with error bars (SEM) displayed every tenth time point for graphical clarity. (**b**) Mean values of mROS production rate after 5 min of stimulation. Conditions: glutamate (n=6, 34 cells) ; TREA (n=6, 34 cells) ; glutamate + TREA (n=6, 30 cells); glutamate + TBOA (n=6, 36 cells); glutamate + TBOA + MCPG (n=6, 45 cells). All data shown are means±sem.

Fig 7. Neuronal release of glutamate triggers glutamate transporter-mediated mitochondrial matrix acidification in astrocytes. Images depicting fluorescent MitoSypHer expression in astrocytes (**a$_1$**) surrounding neurons visible under DIC contrast (**a$_2$**). Scale bar: 20μm. (**b$_1$**) MitoSypHer fluorescence excitation ratio monitored in astrocytes during a 20 second stimulation of neurons using NMDA (10μM). Representative trace (**b$_1$**) and individual data (**b2**) of mitochondrial matrix pH of astrocytes at baseline and following NMDA stimulation. (**c**) Amplitudes of NMDA-evoked astrocyte mitochondrial matrix acidification in the absence or presence of TBOA and neurons. NMDA (n=9, 16 cells); NMDA + TBOA (n=5, 7 cells); NMDA without neurons (n=4, 11 cells). * $p<0.05$ and ** $p<0.01$ using unpaired Student's *t* test.

Figure 1

a

b

c
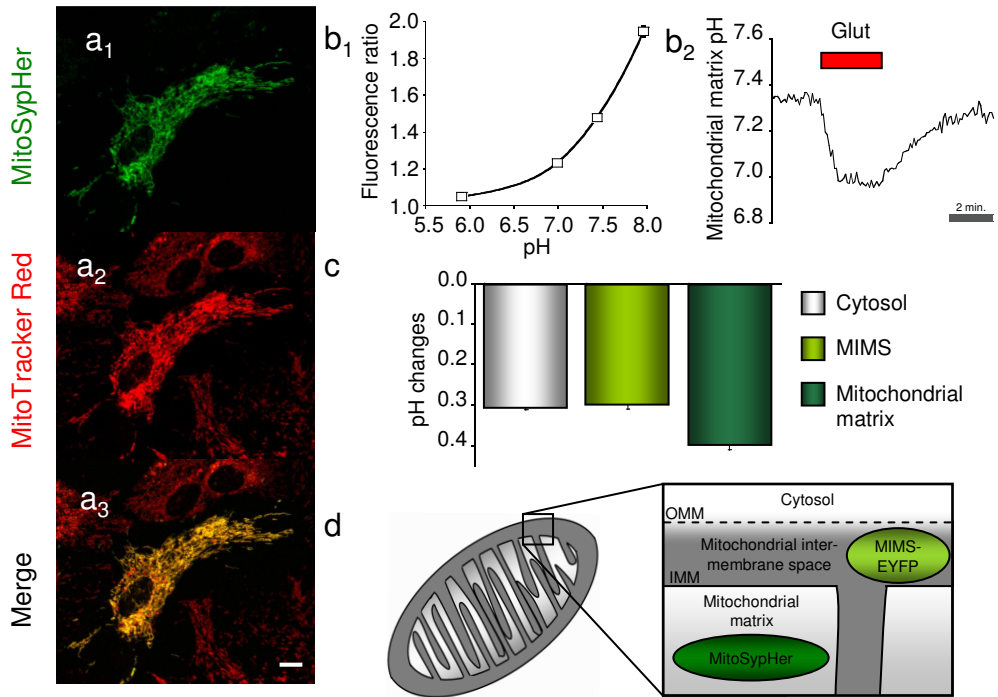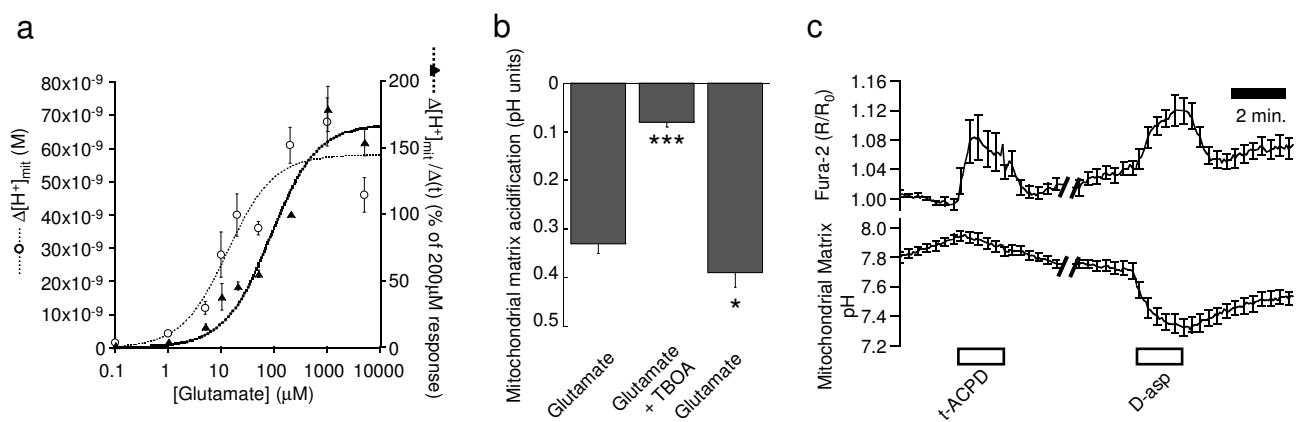
Figure 2

Figure 3

Figure 4

a

Glutamate   Oligomycin   FCCP

Glutamate +   Oligomycin   FCCP
TREA 20 mM

Oxygen consumption rate (pMoles.min^{-1})

Time (min)

b

2-DG + pyruvate + glucose medium

Oxygen consumption rate (%)

Baseline   Glutamate   Glutamate + TREA 10 mM   Glutamate + TREA 20 mM
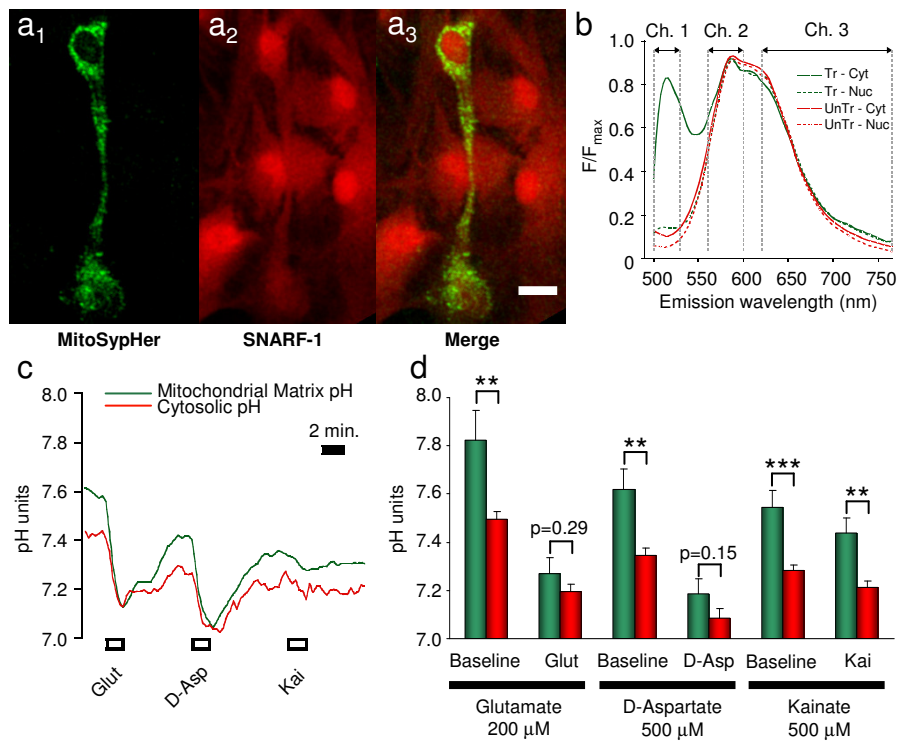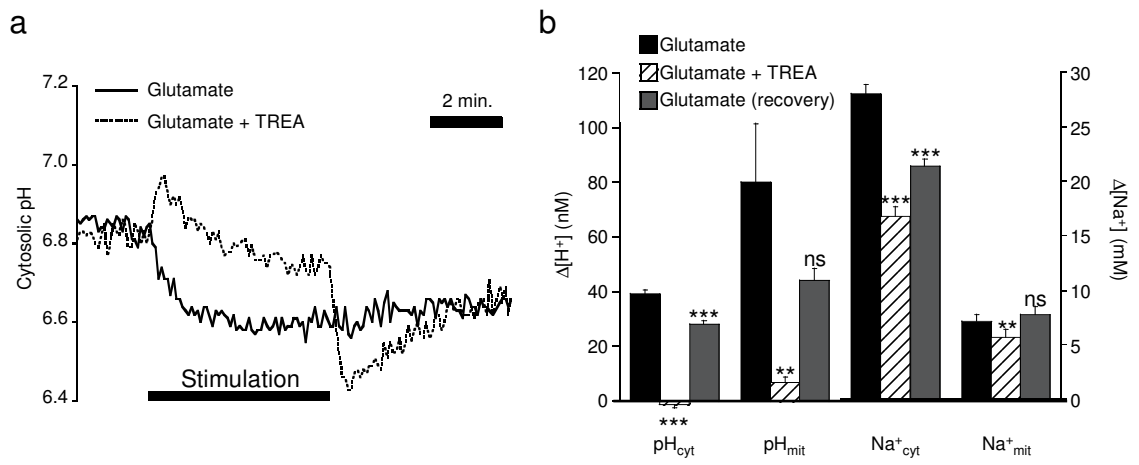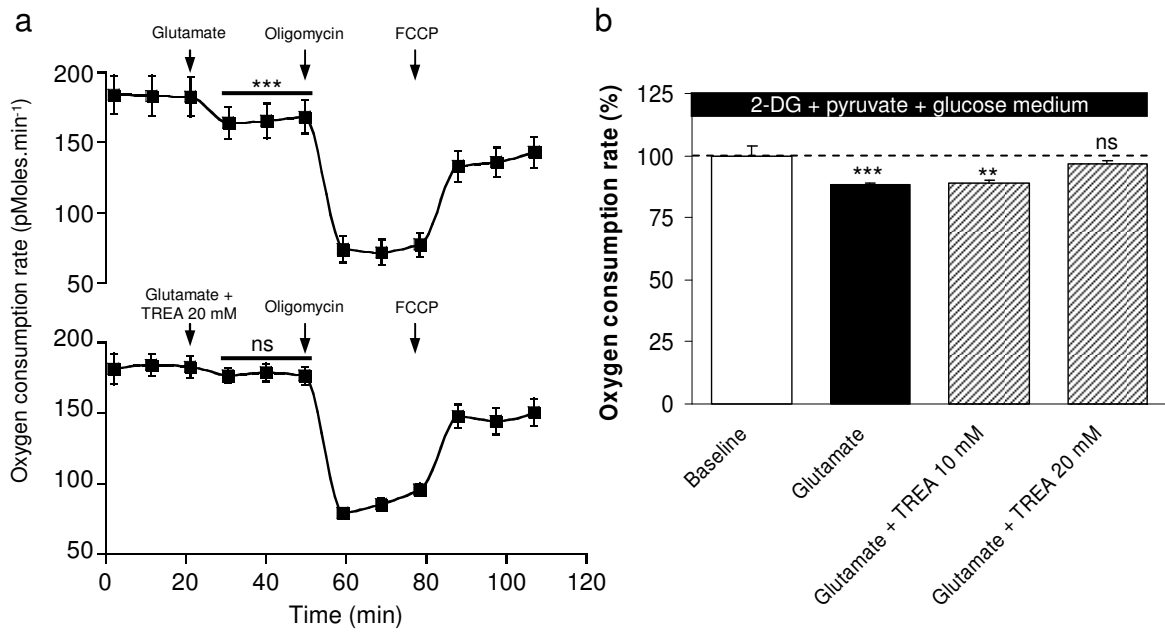
Figure 5

a
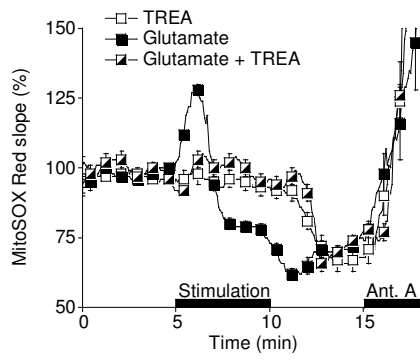
b
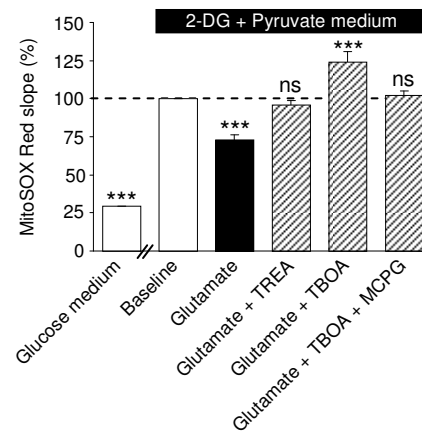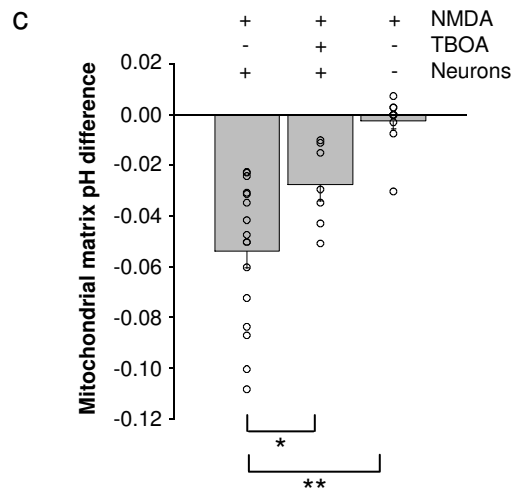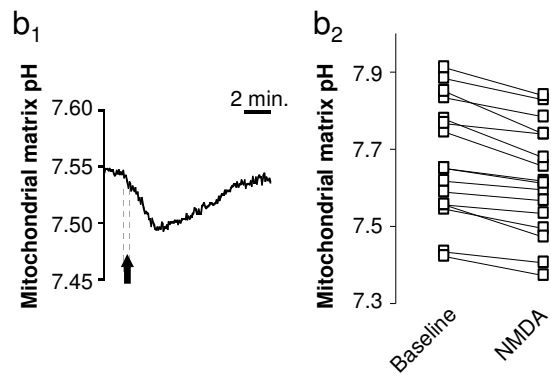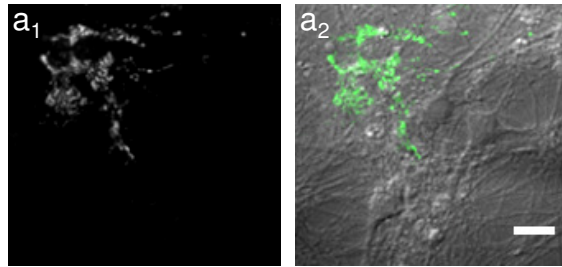
Figure 6

Figure 7

Supplemental Information

Tuning of the energy metabolic response in astrocytes by mitochondrial pH modulation

Guillaume AZARIAS, Hélène PERRETEN, Sylvain LENGACHER, Damon POBURKO, Nicolas DEMAUREX, Pierre J MAGISTRETTI and Jean-Yves CHATTON

Supplemental Data
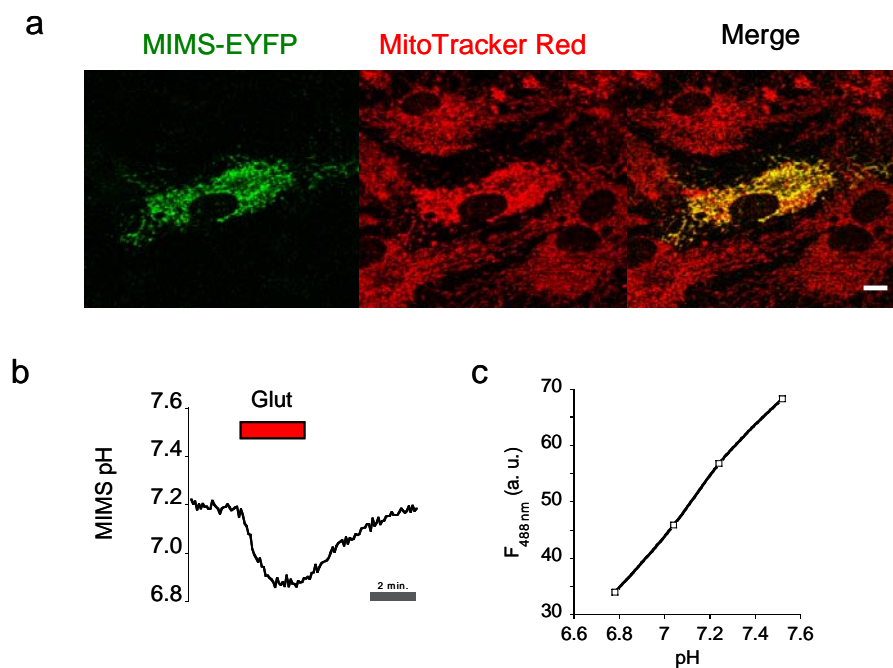
Figure S1: Glutamate induces mitochondrial intermembrane space acidification. (**a**) Cortical astrocytes transfected with MIMS-EYFP loaded with the mitochondrial specific marker MitoTracker Red. Scale bar: 10µm. (**b**) Glutamate (200µM) superfusion on intact astrocytes acidifies mitochondrial intermembrane space (MIMS). (**c**) Example of pH-sensitivity of MIMS-EYFP during the *in situ* pH calibration procedure (n=9, 26 cells).
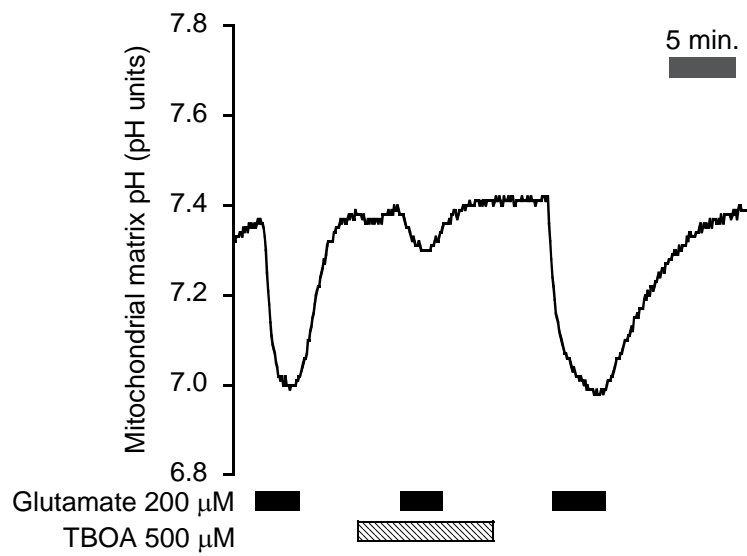
Figure S2. Glutamate-induced mitochondrial matrix acidification was inhibited using TBOA, related to Fig. 2b. Example trace of mitochondrial matrix pH dynamic during glutamate (200μM) superfusion in the presence or absence of the glutamate transporter inhitor TBOA. (n=5, 30 cells)
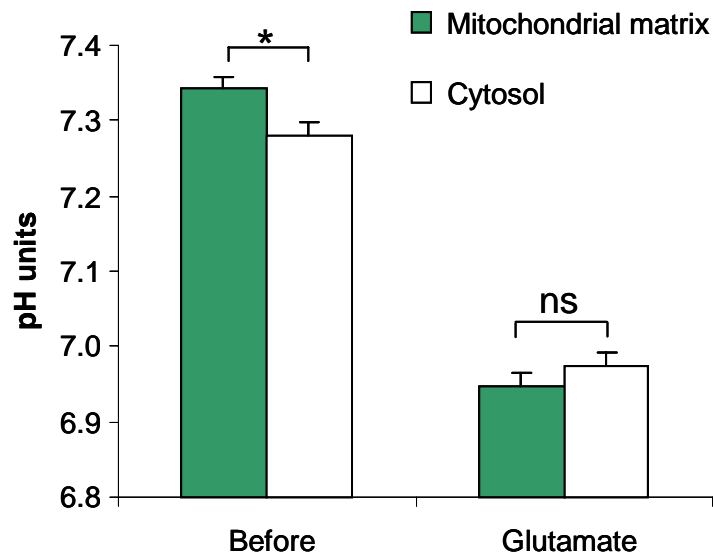
Figure S3. Glutamate cancels cytosol-to-mitochondrial matrix acidification pH gradient. Values of cytosolic and mitochondrial matrix pH measured in separate cells and experiments at resting state and during glutamate (200μM) application. Glutamate canceled any significant difference between cytosolic (n=23, 172 cells) and mitochondrial matrix pH (n=46, 168 cells). *P* value was calculated using the ANOVA procedure detailed in *Material and Methods*. *$p<0.05$.
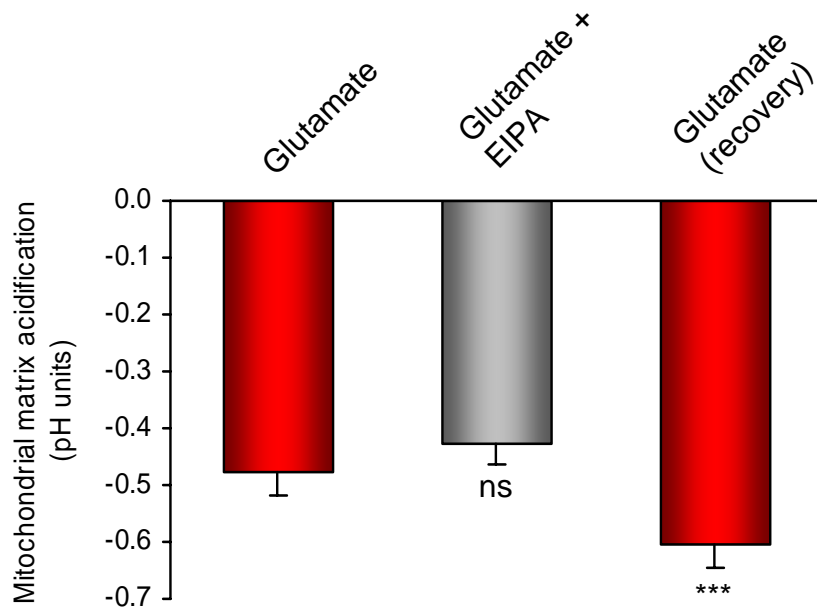
Figure S4. The Na⁺/H⁺ exchanger inhibitor EIPA did not alter glutamate-evoked mitochondrial matrix acidification. Inhibition of plasma membrane and mitochondrial Na⁺/H⁺ exchanger using 50μM EIPA did not alter the amplitude of glutamate-evoked mitochondrial matrix acidification (n=7, 29 cells).
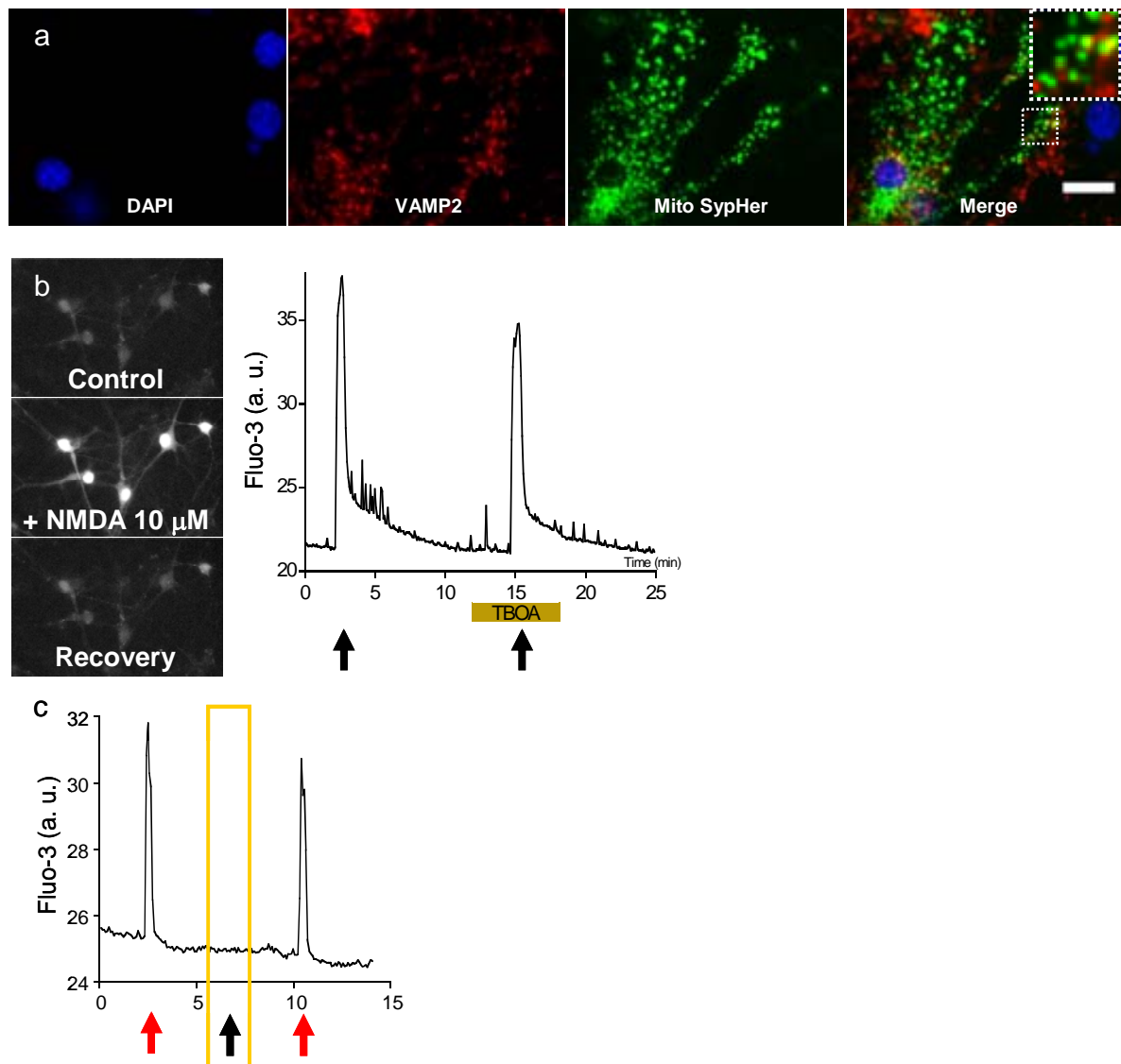
Figure S5. Selective stimulation of neurons for release of neurotransmitters on MitoSypHer transfected astrocytes, related to Fig. 7. (**a**) Close apposition between neuronal synaptic vesicles and astrocyte mitochondria in mixed neuron-astrocyte culture. Cortical embryonic neurons plated on top of primary astrocytes previously transfected with MitoSypHer were stained for the neuronal synaptic vesicle protein VAMP2. Blue: DAPI, Red: VAMP2, Green: MitoSypHer. The inset from the selected area shows the detailed distribution of neuronal VAMP2 staining and mitochondria of MitoSypHer transfected astrocytes. Scale bar: 20µm. (**b**) NMDA induces cytosolic calcium rise specifically in neurons. Representative fluorescence images (left) and experimental trace (right) of cytosolic calcium recording using Fluo-3 in mixed neuron-astrocyte culture. Black arrows indicate the NMDA (10µM) stimulation lasting 20 seconds. TBOA: 500µM. n=4, 14 cells. (**c**) NMDA stimulation (black arrow) did not alter cytosolic calcium level in pure cultures of astrocytes. Glutamate stimulation for 20 seconds (10µM, red arrow) was used as a control of calcium responses (n=4, 24 cells).

III. Discussion

A. Spontaneous individual mitochondrial transients

1. Characterization of spontaneous mitochondrial transients

Despite the prevalence of glycolysis in cultured astrocytes, we showed that astrocytes contain a high density of mitochondria in the entire cytoplasm. This high density of mitochondria suggests that they may be interconnected as a single network. However, mitochondrial network also undergoes fission and fusion in living cells that allow individual mitochondria to reach domains where ATP synthesis is needed for instance. In our culture model, mitochondria movement was negligible in the course of our experiments and no obvious correlation was found between mitochondrial transients and mitochondrial movements. Using several fluorescent probes targeted to mitochondria and sensitive to mitochondrial electrical potential, Na^+ concentration or pH, we observed that individual mitochondria display transient alterations of their ionic content whereas nearby mitochondria remained stable. The observation of individual mitochondrial transients suggests that mitochondria are functional independent units in the cells.

In a first study, we reported that mitochondrial Na^+ transients are mediated by the entry of Na^+ through an electrogenic cation uniporter. We found that mitochondrial Na^+ concentration was restored to basal level by the activity of the mitochondrial Na^+/H^+ exchanger. In further experiments, we studied the consequences of mitochondrial transients. We showed that mitochondrial Na^+ transients are coincident with mitochondrial matrix alkaline transients. Mitochondrial alkaline transients were also found as coincident with mitochondrial depolarizations. Mitochondrial alkaline transients are consistent with the involvements of electrogenic cation uniporter and mitochondrial Na^+/H^+ exchanger. Indeed, depolarizing mitochondria is expected to facilitate the extrusion of protons outside of mitochondrial matrix by the mitochondrial respiratory chain. The transient increase in mitochondrial respiratory chain activity is consistent with the mitochondrial transient increase in ROS production found in myocytes (Wang et al., 2008). In addition, simultaneous restoring of both mitochondrial matrix pH and mitochondrial Na^+ concentration is consistent with the activity of the mitochondrial Na^+/H^+ exchanger.

We reported that thapsigargin, a non competitive inhibitor of the SERCA inducing the release of Ca^{2+} from the endoplasmic reticulum, did not alter mitochondrial Na^+ transient activity (Azarias et al., 2008). Consistent with this observation, astrocytes expressing MitoSypHer and labelled with the mitochondrially targeted Ca^{2+}-sensitive dye Rhod-2 exhibited spontaneous pH transients without coincident alteration of Rhod-2 fluorescence. Similarly, mitochondrial ROS transients were not coincident with increase of mitochondrial Ca^{2+} concentration (Wang et al., 2008). Together, these data

exclude the spontaneous Ca^{2+} release from endoplasmic reticulum as an obligatory mechanism to trigger mitochondrial transients.

The fact that mitochondrial transients were detectable with specific labelling for Na^+ concentration, pH and electrical potential, but not using other mitochondrial stainings (Rhod-2, Rhod123 and red JC-1 aggregates) argues against the involvement of a mechanism of mitochondrial fusion/fission during mitochondrial transient. Mitochondrial fissions and fusions are likely to alter the fluorescence of all dyes in the same mitochondrion. Finally, the coincident increase in Na^+, decrease of H^+ (corresponding to mitochondrial matrix alkalinization) and stable mitochondrial Ca^{2+} concentrations argue for a selective entry of Na^+ into mitochondria during mitochondrial transients rather than opening of a channel with broad cation selectivity. This observation supports the hypothesis of the involvement of a mitochondrial Na^+ channel in mitochondrial transients. However, the mitochondrial Na^+ channels have been so far poorly described and their identity remains to be characterized.

The mechanism triggering mitochondrial transients remains unclear. As the cellular level of ATP was found to modulate the frequency of mitochondrial transients, we measured the magnesium concentration surrounding mitochondria exhibiting a mitochondrial Na^+ transient. We found that the free magnesium concentration decreased in the vicinity of a mitochondrion exhibiting a transient. According to the Magnesium Green technique, a decrease in free magnesium concentration suggests that the level of ATP increases. ATP microdomains has been previously reported in the islet β-cells (Kennedy et al., 1999) and might also exist in other cell types such as astrocytes (Barros and Martinez, 2007). The spatial resolution of the imaging setup used for monitoring transient ATP domains was not sufficient to distinguish if the origin of the ATP was cytosolic or mitochondrial. An attractive possibility would be that the ATP transients are generated by mitochondria because mitochondrial transients are accompanied with mitochondrial alkaline transients, increasing the chemical gradient of proton for mitochondrial ATP synthesis. However, two indications suggest that it is not the case: the mitochondrial electrical potential, which is the major driving force for the ATP synthase, is decreased during mitochondrial transients; the blocker of the ATP synthase oligomycin (1μM) did not prevent transient decreases in free magnesium (*not shown)*. The cytosolic or mitochondrial origin of transient ATP domains could be studied using a genetically encoded probe sensitive to ATP (Imamura et al., 2009) and low light level confocal microscopy. Interestingly, transient decreases of free magnesium concentration may play the role of trigger for Na^+-permissive mitochondrial cation uniporter opening as it was described to be opened in low divalent cation containing medium and its open-state could be induced by ATP (Bernardi, 1999).

During mitochondrial transient, the alkalinization of mitochondrial matrix is expected to increase the pH gradient across mitochondrial inner membrane, thereby increasing the chemical gradient in the total electrochemical gradient. However, the mitochondrial electrical potential also increased as revealed by the mitochondrial electrical potential sensitive dyes JC-1 and TMRE. As a consequence,

the total electrochemical force probably remains relatively stable during a mitochondrial transient. To address this issue, we need to calibrate both mitochondrial pH gradient and mitochondrial electrical potential. The calibration of mitochondrial electrical potential *in situ* has been attempted before with mixed success (Ubl et al., 1996). These experiments remain even more difficult to perform because such measurements need the calibration of both mitochondrial pH value and mitochondrial electrical potential in the same mitochondrion. In **Fig. 20,** I summarized the data obtained during our studies on mitochondrial transients.
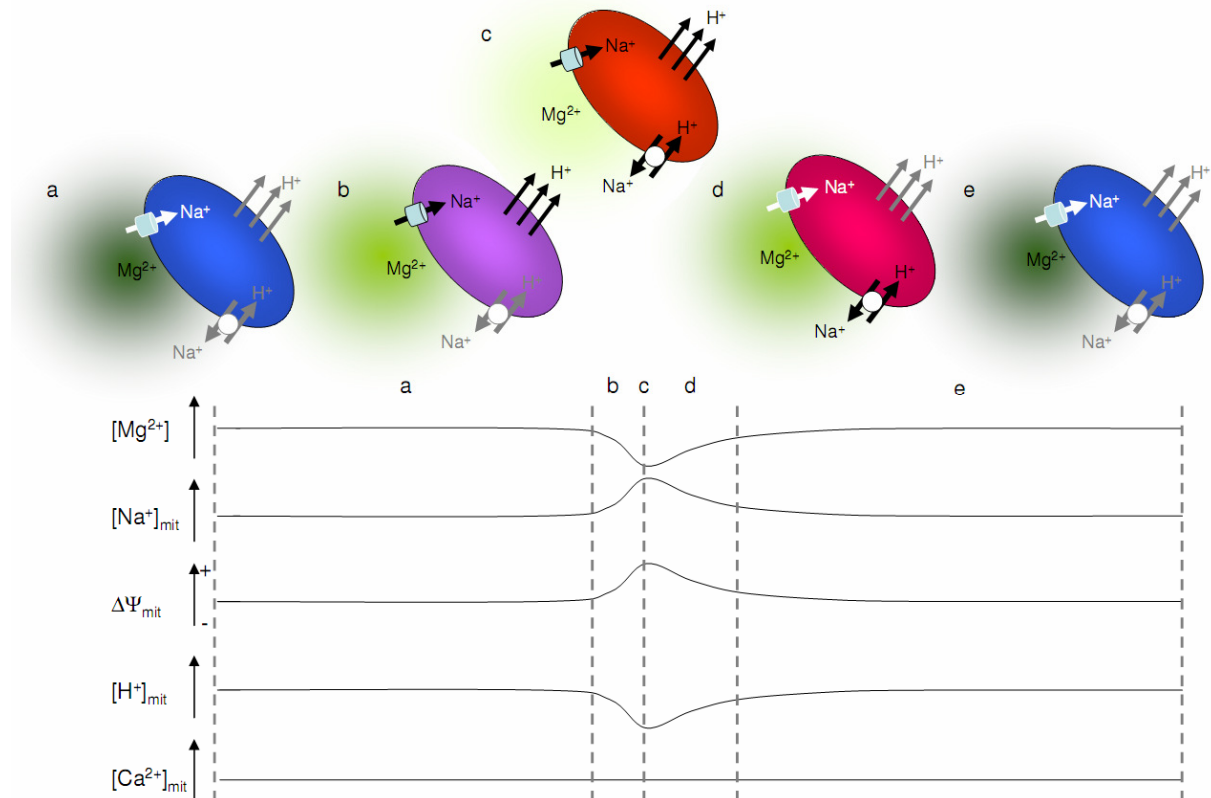
Fig. 20: Working model of ionic alterations occurring during a mitochondrial transient. The colors of the mitochondria illustrate the mitochondrial electrical potential. (a) and (e) are resting mitochondria in the cytosol with a basal free magnesium level.

Our working model suggests that an unknown mechanism, possibly ATP changes, decreases the free magnesium level activating the electrogenic and Na^+-permeable mitochondrial cation uniporter (**Fig. 20b**). The mitochondrial depolarization facilitates the extrusion of protons by the mitochondrial respiratory chain. The increasing of mitochondrial Na^+ concentration and mitochondrial alkalinization enhance the activity of the mitochondrial Na^+/H^+ exchanger (**Fig. 20c**). **Fig. 20d** illustrates the closure of the mitochondrial cation uniporter which stops the mitochondrial depolarization, whereas the mitochondrial Na^+/H^+ exchanger restores Na^+ and H^+ concentrations to basal level. This model is admittedly speculative inasmuch as the temporal resolution reached by the methods used in our studies did not allow us to define the sequence by which events occurred during the transients.

2. Mitochondrial transients in pathological context

As mitochondrial transients occur spontaneously in cells, they probably have a physiological significance within the cells. Therefore, one might expect that mitochondrial Na^+ activity might be impaired in pathological condition and conversely, impairment of mitochondrial transient activity could participate to the progression of disease states.

Several pieces of evidence already pointed out the inverse relationship between the frequency of mitochondrial transients and oxidative stress (Jacobson and Duchen, 2002; Chalmers and McCarron, 2008; Wang et al., 2008). Namely, the frequency of mitochondrial transients decreased during oxidative stress. In unpublished experiments, we deprived astrocytes of organic substrates for a total time of 2 hours, during which noradrenaline (100µM) was first applied for 1 hour in order to induce maximal glycogenolysis (Tsacopoulos and Magistretti, 1996). Then D-aspartate (200µM), a non-metabolized substrate of the Na^+/glutamate co-transporter was applied to increase the Na^+/K^+-ATPase activity and rapidly deplete the cellular energy pools (Magistretti and Chatton, 2005). This protocol mimicked a glucose deprivation that is expected to induce oxidative stress in astrocytes (Ouyang et al., 2007). After this pre-incubation, the mitochondrial Na^+ transient frequency was considerably reduced compared to cells in glucose-containing media. Re-addition of glucose caused rapid increase of mitochondrial Na^+ transient frequency (*not shown*). Similar experiments on cultured myocytes also shown that the frequency mitochondrial ROS transients was related to oxidative stress (Wang et al, 2008). Therefore, in agreement with previous studies, these experiments suggest that the frequency of mitochondrial Na^+ transients is also linked to the level of oxidative stress.

In Alzheimer disease, early neuropathological changes are characterized by accumulation of astrocytes near the amyloid-β plaques (Wyss-Coray et al., 2003). Several studies showed that Alzheimer disease is related to dysregulation of brain energy metabolism, including mitochondrial metabolism of astrocytes (Abramov et al., 2004; Zhu et al., 2006). In particular, the β-amyloid peptide (25-35) was shown to induce oxidative stress and mitochondrial dysfunction in astrocytes (Abramov et al., 2004). Therefore, we investigated the putative link between oxidative stress in astrocytes and the spontaneous mitochondrial Na^+ transient activity. We performed experiments indicating that superfusing astrocytes with the β-amyloid peptide (25-35) rapidly decreased the frequency of mitochondrial Na^+ transients (*not shown*).

Taken together, these results suggest that modulation of mitochondrial transient activity may be related to the oxidative stress in the cells. Therefore, the mechanisms underlying mitochondrial transients may be putative targets to fight oxidative stress in pathological conditions. The evaluation of the impact of increasing mitochondrial transient activity (by inducing intracellular alkalinization for instance) on oxidative stress may help to answer this question.

3. Relevance of results

Our data provided robust indications that mitochondrial transients occur in cultured cells. However, the observation of mitochondrial transients *in vivo* is a critical step to ensure the physiological relevance of mitochondrial transients. These investigations may also provide information about where mitochondrial transients occur in the cells. As mentioned above, cultured astrocytes exhibit dramatically different morphology from *in vivo*. This morphology may explain why mitochondrial transients appeared without obvious correlation in space and time. It is likely that mitochondrial transients occur preferentially in specialized cell compartments *in vivo* (astrocyte endfeet, processes or soma). The identification of a cellular compartment with a higher mitochondrial transient activity may help to unravel the regulatory mechanism as well as the physiological roles of mitochondrial transients.

Unfortunately, the measurement of mitochondrial Na^+ remains so far not possible *in situ* and *in vivo*. Indeed, as a cationic dye, diffusion of CoroNa Red is not cell specific because it crosses plasma membrane and accumulates within tissues without mitochondrial selectivity (Yann Bernardinelli, personal communication). The difficulty regarding the specificity of loading could be circumvent by the use of genetically encoded fluorescent dye sensitive but this kind of probe is currently not available for Na^+. In contrast, MitoSypHer which is encoded in a plasmid may be easier to use for the monitoring of mitochondrial transients because the sequence encoding for this probe is known and the signal-to-noise ratio of MitoSypHer is excellent. For instance, viral vector-mediated gene delivery is an attractive procedure for introducing MitoSypHer in astrocytes of intact brain and monitor *in vivo* mitochondrial alkaline transients.

4. Future directions of research

Despite our efforts to understand the triggering mechanisms and functions of mitochondrial transients, many questions remain unsolved. In this section, I listed the most relevant experiments that may help to better understand mitochondrial transients:

- Different pathways may mediate different types of mitochondrial transients. For instance, Na^+ might not be the exclusive ion responsible for mitochondrial depolarization. This issue could be addressed by perfusing astrocytes with a Na^+-free solution and measuring the frequency of mitochondrial transient depolarizations and mitochondrial alkaline transients. Importantly, mitochondrial alkaline transients occurred at a frequency which was obviously smaller than mitochondrial Na^+ transients. During the experiments of simultaneous monitoring of mitochondrial Na^+ and mitochondrial pH, many detectable mitochondrial Na^+ transients were not accompanied with detectable mitochondrial alkaline transients. This discrepancy

might be explained by the fact that several mechanisms lead to mitochondrial transients and only part of mitochondrial transients are coincident with mitochondrial alkaline transients.

- Our observation of mitochondrial alkaline transients also suggests that mitochondrial transients are coincident with the increase of the mitochondrial respiratory chain activity, which is compatible with a localized increase in ROS production as reported in myocytes (Wang et al., 2008). However, this is in contradiction with the lack of effect of the inhibitor of the mitochondrial respiratory chain (rotenone, inhibitor of the complex I of the mitochondrial respiratory chain) on mitochondrial Na^+ transient frequency. Similarly, we found cyclosporine A had no significant effect on mitochondrial Na^+ transient activity in agreement with a previous study on mitochondrial transient depolarizations (Buckman and Reynolds, 2001). In myocytes, the superoxide flashes frequency was severely impaired by cyclosporine A suggesting the involvement of the mitochondrial transition pore (Chalmers and McCarron, 2008; Wang et al., 2008). These discrepancies could be addressed by monitoring mitochondrial Na^+ transients and mitochondrial ROS production. In addition, it is possible to monitor mitochondrial alkaline transients using MitoSypHer and mitochondrial ROS production using MitoSOX Red in the same mitochondrion. It is noteworthy that the biosensor used to monitor the mitochondrial ROS transients also exhibited significant pH sensitivity (Wang et al., 2008). Therefore, it might be that part of the mitochondrial transients interpreted as increase of ROS transients corresponded in fact to mitochondrial alkaline transients.

- If mitochondrial alkaline transients are due to increase of the mitochondrial respiratory chain, it is expected that mitochondrial alkaline transients are coincident with transient acidification of the mitochondrial intermembrane space. This issue could be addressed by monitoring mitochondrial Na^+ concentration in astrocytes transfected with a pH sensitive probe targeted to mitochondrial intermembrane space such as MIMS-EYFP (Porcelli et al., 2005).

- The metabolic cascade leading to local ATP microdomain formation and regulation remains to be solved. In our hands, local ATP transient increases were not inhibited by oligomycin (1μM, *not shown*) suggesting that cytosolic enzymes are responsible for ATP production. The use of inhibitors of enzymes producing ATP (phosphoglycerate kinase and pyruvate kinase for instance) may help to tackle this issue.

- The specific effect of β-amyloid peptide should be confirmed by application of the reverse peptide Aβ 35-25 as negative control, application of the full-length peptide 1-42, as well as the fibrillar versus monomeric forms of the peptide. Some of the effects of Aβ peptides appear to be related to their endocytosis. This hypothesis can be tested either by inhibiting endocytotic pathways or by competition with the polycation heparin and simultaneously measuring mitochondrial Na^+ transient activity.

- An alternative link between mitochondrial Na^+ transient and surrounding transient decrease in free magnesium concentration may be supported by the involvement of a mitochondrial Na^+/Mg^{2+} exchanger. Na^+/Mg^{2+} exchanger have been reported as expressed at the plasma-membrane of PC12 cells (Kubota et al., 2003) and cardiac myocytes (Tashiro et al., 2006). The involvement of Na^+/Mg^{2+} may provide a link between opposite alterations of Na^+ and Mg^{2+} mitochondrial levels during mitochondrial Na^+ transient. However, evidence demonstrating mitochondrial localization of this exchanger is hitherto lacking. The involvement of a putative Na^+/Mg^{2+} exchanger can be tested by using its potent inhibitor imipramine (200µM), also known as antidepressant.

B. *Mitochondrial ionic alterations evoked by glutamate*

1. Mitochondrial Na^+ changes and putative consequences

Astrocytes experience significant changes in Na^+ concentration in the cytosol during glutamate uptake, therefore we investigated if mitochondrial Na^+ was also altered during glutamate uptake. We observed that mitochondrial Na^+ concentration increased with a kinetic similar to the cytosolic Na^+ increase. The mitochondrial Na^+ concentration measured by using the Na^+-sensitive mitochondrial dye CoroNa Red (10-20mM) fell in a similar range to what was found in other studies using the technique of X-Ray analysis (8-15mM, Pozzo-Miller et al., 1997; Pivovarova et al., 1999; Pivovarova et al., 2002; Pivovarova et al., 2004). In contrast, Baron and colleagues also used CoroNa Red to monitor mitochondrial Na^+ concentration in Madin-Darby canine kidney cells and found a significantly higher value at resting state nearing 50mM (Baron et al., 2005). This discrepancy may be explained by the use of the mitochondrial uncoupler FCCP during their calibration procedure. However, FCCP as a mitochondrial uncoupler abrogates the mitochondrial electrical potential which appears not appropriate for the use of a dye, whose specificity of mitochondrial labelling is based on the existence of a mitochondrial electrical potential. In our hands, the use of FCCP at a concentration higher than 100nM induced a very strong increase in CoroNa Red fluorescence, the loss of specific mitochondrial staining and the loss of sensitivity to Na^+ concentration of the calibration solutions (*not shown*).

So far, except for a pyruvate dehydrogenase whose conformational changes are determined by the Na^+ concentration (Pawelczyk and Olson, 1995), few data may directly link mitochondrial Na^+ concentration to mitochondrial metabolism. Our data suggest that mitochondrial Na^+/Ca^{2+} exchanger is involved in the entry of Na^+ into mitochondria during glutamate uptake, as its inhibitor CGP-37157 decreased the amplitude of the glutamate-evoked mitochondrial response by 20%. However, it is also important to mention that inhibition of the mitochondrial Ca^{2+} uniporter using Ruthenium Red, did not significantly alter the amplitude of glutamate-evoked mitochondrial Na^+ response (*not shown*). Therefore, an unknown route of Na^+ into mitochondria remains to be explored. Mitochondrial

uncoupling proteins might be a potential pathway for Na^+ into mitochondria as they are permissive to monovalent cations such as protons (Andrews et al., 2005). This issue could be addressed by silencing or overexpressing mitochondrial uncoupling proteins UCP4 and UCP5 expressed in astrocytes.

During our investigation of glutamate effect on mitochondrial matrix pH (Azarias et al., *submitted*), we found mitochondrial Na^+ and pH are independent raising the question of the role of the mitochondrial Na^+/H^+ exchanger. We showed that the inhibitor EIPA had no effect on mitochondrial pH at resting state or during glutamate uptake. In addition, using triethylammonium (TREA), we were able to compensate the intracellular acidification induced by glutamate and found that mitochondrial Na^+ response was mainly conserved. In addition, the initial slope of the mitochondrial matrix acidification during glutamate uptake was similar in the presence or absence EIPA (*not shown*). Therefore, it appears that the mitochondrial Na^+/H^+ exchanger plays a crucial role in maintaining the mitochondrial Na^+ concentration, whereas the mitochondrial matrix pH is regulated by other pathways and changes in mitochondrial Na^+ concentration has a negligible impact on mitochondrial pH. The physiological effects of increasing mitochondrial Na^+ in astrocytes remain unclear. A simple explanation for the increase in mitochondrial Na^+ concentration in parallel with increasing the cytosolic Na^+ concentration would be to maintain the Na^+ chemical gradient across mitochondrial inner membrane ($\Delta\mu_{Na^+} = RT \ln [Na^+]_{matrix}/[Na^+]_{mims}$, where R, T, matrix and mims have the meanings defined in the introduction section I.B.3.a). Importantly, the dysregulation of mitochondrial Na^+ concentration has been linked to pathological conditions such as ischemia and heart failure in cardiac muscle cells (Murphy and Eisner, 2009) suggesting that an abnormal level of mitochondrial Na^+ has an impact on mitochondrial output.

2. Mitochondrial pH changes and putative consequences

According to the chemiosmotic coupling hypothesis, proton pumping by the mitochondrial respiratory chain is responsible for the pH gradient across the mitochondrial inner membrane. Using the measurement of cytosolic and mitochondrial matrix pH in different cells, we showed that the mitochondrial matrix is significantly more alkaline than cytosol. However, we found that the value of pH gradient was small (about 0.06 pH units). In contrast, the pH gradient measured in the same cells by labelling MitoSypHer transfected astrocytes with the pH-sensitive cytosolic red dye SNARF-1 was estimated at 0.55 ± 0.06 pH units. This discrepancy could be explained by the wide distribution of pH values among cells. This variability may also indicate differences in mitochondrial respiratory activity among cell cultures.

As mentioned above, mitochondrial oxidative metabolism might be higher in astrocytes *in vivo* (Lovatt et al., 2007) than in cultured cells. For instance, we noted that inhibiting glycolysis using 2-deoxyglucose increased the rate of mROS production by ~3 fold suggesting that the contribution of mitochondrial oxidative metabolism in energy metabolism is limited in cultured astrocytes. Therefore,

the effects of glutamate on mitochondrial metabolism of astrocytes were studied in astrocytes whose glycolysis was inhibited using 2-deoxyglucose to better highlight the impact of glutamate on mitochondrial metabolism.

Our study showed that the main mechanism responsible for mitochondrial matrix acidification during glutamate stimulation was the Na^+-dependent glutamate transporter. Three pieces of evidence supported this conclusion: the concentration-dependence of mitochondrial matrix acidification closely matched the values found for the glutamate transporter, glutamate-evoked mitochondrial matrix acidification was prevented by inhibiting the glutamate transporters using DL-threo-β-benzyloxyaspartate (TBOA) and D-aspartate, a substrate of the glutamate transporter evoked mitochondrial matrix acidification similar to glutamate. Simultaneous monitoring of cytosolic calcium concentration and mitochondrial matrix pH indicated that mitochondrial matrix acidification was poorly affected by intracellular increase of cytosolic calcium concentration. In contrast, in HeLa cells histamine evokes a mitochondrial matrix acidification dependent on the activity of plasma membrane Ca^{2+} ATPase (PMCA, Demaurex and Poburko, 2009). Although PMCA are also expressed in cultured astrocytes (Fresu et al., 1999), our data exclude a major role of PMCA in the glutamate-evoked mitochondrial matrix acidification.

3. Relevance of results regarding astrocyte morphology and glutamate stimulus

The role of astrocytes in modulation of glutamatergic transmission is currently the matter of intensive debate (Agulhon et al., 2010; Hamilton and Attwell, 2010). Attwell put emphasis on the relevance of the methodology used to highlight the role of astrocytes in modulation of neurotransmission. Similarly the use of continuous superfusion of glutamate for 20min (Pellerin and Magistretti, 1994), or 2min (our studies) is not physiological. Therefore, we set up a culture model where astrocytes expressing the biosensor MitoSypHer were in close apposition with neurons. Selective stimulation of neurons induced a mitochondrial matrix acidification in astrocytes that was smaller in the presence of the glutamate transporter inhibitor TBOA. Although we validated the impact of neuronally-released glutamate on mitochondrial matrix pH in astrocytes, monitoring the effect of glutamate on mitochondrial matrix pH *in vivo* is a critical step to validate our hypothesis.

According to the model that we propose, mitochondrial metabolism of astrocytes is decreased in mitochondria close to the glutamate transporters. In contrast, our data also support the notion that Ca^{2+} signalling may be involved in the up-regulation of mitochondrial metabolism. Indeed, we found that the stimulation of astrocytes in the presence of the inhibitor of metabotropic glutamate receptors (+)-α-methyl-4-carboxyphenylglycine (MCPG) decreased the rate of mROS production. Therefore, it is conceivable that *in vivo*, the mitochondrial metabolism is differentially regulated between the soma and fine processes. The glutamate-evoked cytosolic Ca^{2+} increase mediated by metabotropic glutamate

receptors is expected to stimulate the mitochondrial oxidative metabolism, whereas this effect is prevented by the pH changes in mitochondria found in the vicinity of glutamate transporters. As the ionic alterations induced by glutamate transport are mainly localized to fine processes of astrocytes (Langer and Rose, 2009), the large proportion of mitochondria in the cell body of astrocytes would be stimulated by Ca^{2+} signals. The compartmentalized regulation of astrocytes metabolism may explain why measurements of mitochondrial metabolism *in vivo* indicated an increase in the mitochondrial oxidative metabolism of astrocytes (Wyss et al., 2009). A working model of the compartmentalized tuning of astrocyte energy metabolism is summarized in **Fig. 21**.
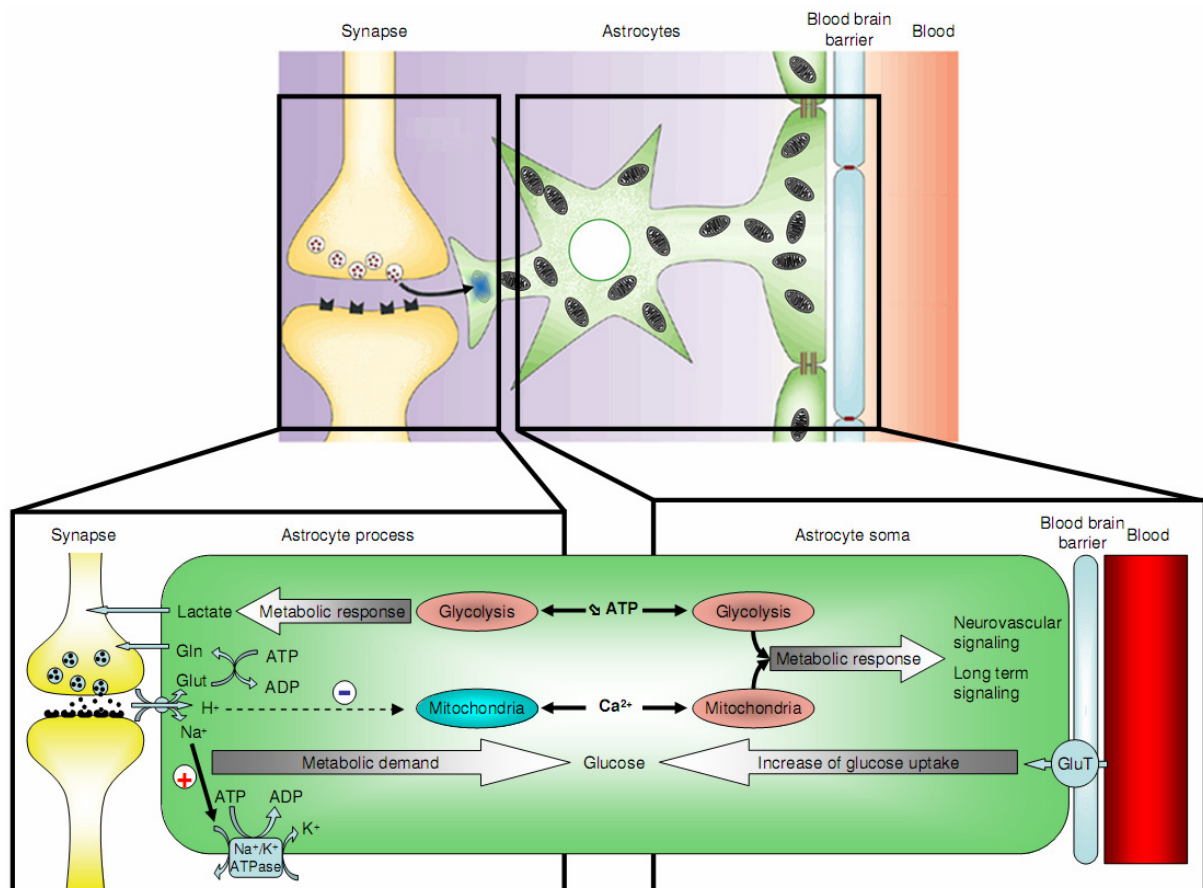
Fig. 21: Proposed model for the compartmentalized tuning of energy metabolism in astrocytes by neuronally released glutamate. The blue region in the upper graph indicates the acidic microdomain. The signalling pathways responsible for cytosolic Ca^{2+} increase are not represented for reasons of clarity. Glut: Glutamate, Gln: glutamine, GluT: glucose transporter. The upper image was modified from Nedergaard et al., 2002.

Taken together our results support a putative pH-mediated regulation of mitochondrial metabolism occurring during glutamate uptake and localized to the vicinity of glutamate transporters. We propose that glutamate uptake induces a metabolic demand in astrocyte processes which is mediated by Na^+ and tunes the metabolic response towards an increase of glycolysis in perisynaptic astrocyte processes.

The glutamate released by presynaptic neuron induces a cytosolic Ca^{2+} rise that may stimulate the mitochondrial oxidative metabolism in the cell body of astrocytes. In parallel, glutamate uptake

increases a cytosolic Na$^+$ concentration which enhances an increase of ATP consumption by the Na$^+$/K$^+$ ATPase responsible for a metabolic demand. The metabolic demand induced glucose uptake from blood. In astrocyte soma, both mitochondria and glycolysis are responsible for metabolic response for neurovascular coupling and long term metabolic adaptations, whereas in astrocyte processes, the activity of glutamate transporters induces an acidic microdomain that prevent mitochondrial contribution to metabolic response.

4. Future directions of research

Our data strongly suggest that glutamate decreases mitochondrial matrix pH in astrocytes and decreases mitochondrial metabolism. According to the astrocyte-neuron lactate shuttle hypothesis, the lactate released by the astrocytes is taken up and used by nearby neurons. It could be interesting to check if mitochondrial matrix pH is also altered in neurons stimulated with glutamate. A previous study showed that glutamate induces a transient alkalinization of mitochondrial matrix in cultured neurons (Abad et al., 2004), which suggests that glutamate stimulates mitochondrial ATP synthesis as found in pancreatic β cells (Wiederkehr et al., 2009). Future challenges of the astrocyte-neuron lactate may be to investigate if lactate transport into the cytosol of neurons (by monocarboxylate transporters coupled to the proton gradient) do not acidify mitochondrial matrix and if glutamate still induce mitochondrial matrix alkalinization in neurons.

In an effort to stimulate astrocytes with a more physiological stimulus than glutamate superfusion, we evaluated the impact of neuronal release of neurotransmitters on mitochondrial matrix pH in astrocytes. The step ahead to validate our hypothesis on the role of pH signalling on mitochondrial metabolism of astrocytes is to perform *in vivo* transfection of astrocytes using an astrocyte specific promoter (GFAP for instance) and evoke neuronal response by whisker stimulation for instance. In this kind of experiments, the use of 2-photon microscopy is particularly important because the mitochondrial matrix acidification may occur only in mitochondria in the immediate vicinity of glutamate transporters.

It is conceivable that the dynamic regulation of astrocyte metabolism (oxidative *versus* glycolytic) and therefore the release of lactate could participate in memory processes. In *Drosophila*, a new mutant strain named *Megad*, whose expression of a brain monocarboxylate transporter is impaired, has recently been described in a study to which I contributed (Isabel et al., *submitted*). This *Drosophila* mutant showed a specific impairment of a consolidated form of memory independent from the classical cAMP-dependent long term memory. Several other elements provide a putative link between neuronal ability to take up energy equivalent and formation of a memory trace: 1) Lactate is an energy substrate for neurons (Schurr et al, 1988, Izumi et al, 1997, Rouach et al, 2008) ; 2) The density of monocarboxylate transporters is upregulated by neuronal stimulation (Pierre et al, 2009) ; 3) The density of monocarboxylate is rate limiting for lactate transport (Bliss et al. 2004) ; 4) The neuronal

energy status is a constraint on coding and processing of sensory information (Laughlin, 2001). Further use of adequate genetic models and pharmacological investigations may unravel a new molecular cascade relying on a lactate-dependent pathway and supporting the construction of memory traces.

C. General conclusions

Whereas astrocyte energy metabolism was previously thought to be almost exclusively glycolytic, recent investigations emphasized the relevance of mitochondrial oxidative metabolism. Our work has provided new insights into the regulation of mitochondrial metabolism. We have shown that mitochondria exhibit spontaneous, transient, and selective alterations of their ionic content. We also provided evidence for the coexistence of microdomain with low free magnesium concentration which will help to unravel the mechanisms triggering mitochondrial transients. The physiological significance of mitochondrial transients remains unclear but may open new perspectives to tackle pathological issues such as Alzheimer disease and cerebral ischemia.

Our work contributed to a better understanding of the regulation of astrocyte energy metabolism during neurometabolic coupling. The astrocyte-neuron lactate shuttle hypothesis initially provided strong evidence for the mobilization of glycolysis during glutamate uptake without critically addressing the contribution of mitochondrial oxidative metabolism. Here, we provided experimental work that should help deciphering the astrocyte energy metabolism during neurometabolic coupling. The glutamate-mediated steering of astrocyte energy metabolism toward glycolysis has three implications: save oxygen for neuronal metabolism, strengthen the control the astrocyte reactive oxygen species production in the vicinity of neurons, and producing lactate to meet neuronal energy demands.

IV.References

Abad MF, Di Benedetto G, Magalhaes PJ, Filippin L, Pozzan T (2004) Mitochondrial pH monitored by a new engineered green fluorescent protein mutant. J Biol Chem 279:11521-11529.

Abbott NJ, Ronnback L, Hansson E (2006) Astrocyte-endothelial interactions at the blood-brain barrier. Nat Rev Neurosci 7:41-53.

Abramov AY, Canevari L, Duchen MR (2004) Beta-amyloid peptides induce mitochondrial dysfunction and oxidative stress in astrocytes and death of neurons through activation of NADPH oxidase. J Neurosci 24:565-575.

Agulhon C, Fiacco TA, McCarthy KD (2010) Hippocampal short- and long-term plasticity are not modulated by astrocyte Ca^{2+} signaling. Science 327:1250-1254.

Alle H, Roth A, Geiger JR (2009) Energy-efficient action potentials in hippocampal mossy fibers. Science 325:1405-1408.

Amato A, Ballerini L, Attwell D (1994) Intracellular pH changes produced by glutamate uptake in rat hippocampal slices. J Neurophysiol 72:1686-1696.

Andrews ZB, Diano S, Horvath TL (2005) Mitochondrial uncoupling proteins in the CNS: in support of function and survival. Nat Rev Neurosci 6:829-840.

Attwell D, Laughlin SB (2001) An energy budget for signaling in the grey matter of the brain. J Cereb Blood Flow Metab 21:1133-1145.

Azarias G, Van de Ville D, Unser M, Chatton JY (2008) Spontaneous Na^+ transients in individual mitochondria of intact astrocytes. Glia 56:342-353.

Azarias G, Perreten H, Lengacher S, Poburko D, Demaurex N, Magistretti PJ, Chatton JY Tuning of the energy metabolic response in astrocytes by mitochondrial pH modulation. *Submitted*.

Balaban RS, Nemoto S, Finkel T (2005) Mitochondria, oxidants, and aging. Cell 120:483-495.

Baron S, Caplanusi A, van de Ven M, Radu M, Despa S, Lambrichts I, Ameloot M, Steels P, Smets I (2005) Role of mitochondrial Na^+ concentration, measured by CoroNa red, in the protection of metabolically inhibited MDCK cells. J Am Soc Nephrol 16:3490-3497.

Barres BA (2008) The mystery and magic of glia: a perspective on their roles in health and disease. Neuron 60:430-440.

Barros LF, Martinez C (2007) An enquiry into metabolite domains. Biophys J 92:3878-3884.

Bergersen LH (2007) Is lactate food for neurons? Comparison of monocarboxylate transporter subtypes in brain and muscle. Neuroscience 145:11-19.

Bernardi P (1999) Mitochondrial transport of cations: channels, exchangers, and permeability transition. Physiol Rev 79:1127-1155.

Bernardi P, Angrilli A, Azzone GF (1990) A gated pathway for electrophoretic Na^+ fluxes in rat liver mitochondria. Regulation by surface Mg^{2+}. Eur J Biochem 188:91-97.

Bernardinelli Y, Azarias G, Chatton JY (2006) In situ fluorescence imaging of glutamate-evoked mitochondrial Na^+ responses in astrocytes. Glia 54:460-470.

Bezzi P, Gundersen V, Galbete JL, Seifert G, Steinhauser C, Pilati E, Volterra A (2004) Astrocytes contain a vesicular compartment that is competent for regulated exocytosis of glutamate. Nat Neurosci 7:613-620.

Blachly-Dyson E, Forte M (2001) VDAC channels. IUBMB Life 52:113-118.

Boulland JL, Jenstad M, Boekel AJ, Wouterlood FG, Edwards RH, Storm-Mathisen J, Chaudhry FA (2009) Vesicular glutamate and GABA transporters sort to distinct sets of vesicles in a population of presynaptic terminals. Cereb Cortex 19:241-248.

Buckman JF, Reynolds IJ (2001) Spontaneous changes in mitochondrial membrane potential in cultured neurons. J Neurosci 21:5054-5065.

Busciglio J, Pelsman A, Wong C, Pigino G, Yuan M, Mori H, Yankner BA (2002) Altered metabolism of the amyloid beta precursor protein is associated with mitochondrial dysfunction in Down's syndrome. Neuron 33:677-688.

Cahoy JD, Emery B, Kaushal A, Foo LC, Zamanian JL, Christopherson KS, Xing Y, Lubischer JL, Krieg PA, Krupenko SA, Thompson WJ, Barres BA (2008) A transcriptome database for astrocytes, neurons, and oligodendrocytes: a new resource for understanding brain development and function. J Neurosci 28:264-278.

Casey JR, Grinstein S, Orlowski J (2010) Sensors and regulators of intracellular pH. Nat Rev Mol Cell Biol 11:50-61.

Chalmers S, McCarron JG (2008) The mitochondrial membrane potential and Ca^{2+} oscillations in smooth muscle. J Cell Sci 121:75-85.

Chatton JY, Marquet P, Magistretti PJ (2000) A quantitative analysis of L-glutamate-regulated Na^+ dynamics in mouse cortical astrocytes: implications for cellular bioenergetics. Eur J Neurosci 12:3843-3853.

Chaudhry FA, Reimer RJ, Edwards RH (2002) The glutamine commute: take the N line and transfer to the A. J Cell Biol 157:349-355.

Chaudhry FA, Lehre KP, van Lookeren Campagne M, Ottersen OP, Danbolt NC, Storm-Mathisen J (1995) Glutamate transporters in glial plasma membranes: highly differentiated localizations revealed by quantitative ultrastructural immunocytochemistry. Neuron 15:711-720.

Chesler M, Kraig RP (1989) Intracellular pH transients of mammalian astrocytes. J Neurosci 9:2011-2019.

D'Antoni S, Berretta A, Bonaccorso CM, Bruno V, Aronica E, Nicoletti F, Catania MV (2008) Metabotropic glutamate receptors in glial cells. Neurochem Res 33:2436-2443.

Danbolt NC (2001) Glutamate uptake. Prog Neurobiol 65:1-105.

De Giorgi F, Lartigue L, Ichas F (2000) Electrical coupling and plasticity of the mitochondrial network. Cell Calcium 28:365-370.

De Vos KJ, Sheetz MP (2007) Visualization and quantification of mitochondrial dynamics in living animal cells. Methods Cell Biol 80:627-682.

Deitmer JW, Rose CR (2009) Ion changes and signalling in perisynaptic glia. Brain Res Rev.

Demaurex N, Poburko D (2009) Modulation of mitochondrial proton gradients by the plasma membrane calcium ATPase. J Physiol Sci 59:348.

Demaurex N, Poburko D, Frieden M (2009) Regulation of plasma membrane calcium fluxes by mitochondria. Biochim Biophys Acta 1787:1383-1394.

Fresu L, Dehpour A, Genazzani AA, Carafoli E, Guerini D (1999) Plasma membrane calcium ATPase isoforms in astrocytes. Glia 28:150-155.

Hajnoczky G, Robb-Gaspers LD, Seitz MB, Thomas AP (1995) Decoding of cytosolic calcium oscillations in the mitochondria. Cell 82:415-424.

Halassa MM, Florian C, Fellin T, Munoz JR, Lee SY, Abel T, Haydon PG, Frank MG (2009) Astrocytic modulation of sleep homeostasis and cognitive consequences of sleep loss. Neuron 61:213-219.

Hamilton NB, Attwell D (2010) Do astrocytes really exocytose neurotransmitters? Nat Rev Neurosci 11:227-238.

Haugeto O, Ullensvang K, Levy LM, Chaudhry FA, Honore T, Nielsen M, Lehre KP, Danbolt NC (1996) Brain glutamate transporter proteins form homomultimers. J Biol Chem 271:27715-27722.

Hertz L, Peng L, Dienel GA (2007) Energy metabolism in astrocytes: high rate of oxidative metabolism and spatiotemporal dependence on glycolysis/glycogenolysis. J Cereb Blood Flow Metab 27:219-249.

Imamura H, Nhat KP, Togawa H, Saito K, Iino R, Kato-Yamada Y, Nagai T, Noji H (2009) Visualization of ATP levels inside single living cells with fluorescence resonance energy transfer-based genetically encoded indicators. Proc Natl Acad Sci U S A 106:15651-15656.

Isabel G, Sejourne J, Trannoy S, Azarias G, Tchenio P, Preat T Gating long term memory. *Submitted*.

Ito U, Hakamata Y, Kawakami E, Oyanagi K (2009) Degeneration of astrocytic processes and their mitochondria in cerebral cortical regions peripheral to the cortical infarction: heterogeneity of their disintegration is closely associated with disseminated selective neuronal necrosis and maturation of injury. Stroke 40:2173-2181.

Jacobson J, Duchen MR (2002) Mitochondrial oxidative stress and cell death in astrocytes - requirement for stored Ca^{2+} and sustained opening of the permeability transition pore. J Cell Sci 115:1175-1188.

Jiang D, Zhao L, Clapham DE (2009) Genome-wide RNAi screen identifies Letm1 as a mitochondrial Ca^{2+}/H^+ antiporter. Science 326:144-147.

Jou MJ (2008) Pathophysiological and pharmacological implications of mitochondria-targeted reactive oxygen species generation in astrocytes. Adv Drug Deliv Rev 60:1512-1526.

Jung DW, Baysal K, Brierley GP (1995) The sodium-calcium antiport of heart mitochondria is not electroneutral. J Biol Chem 270:672-678.

Kennedy HJ, Pouli AE, Ainscow EK, Jouaville LS, Rizzuto R, Rutter GA (1999) Glucose generates sub-plasma membrane ATP microdomains in single islet beta-cells. Potential role for strategically located mitochondria. J Biol Chem 274:13281-13291.

Kettenmann H, Verkhratsky A (2008) Neuroglia: the 150 years after. Trends Neurosci 31:653-659.

Kirichok Y, Krapivinsky G, Clapham DE (2004) The mitochondrial calcium uniporter is a highly selective ion channel. Nature 427:360-364.

Kolomeets NS, Uranova N (2009) Ultrastructural abnormalities of astrocytes in the hippocampus in schizophrenia and duration of illness: A postortem morphometric study. World J Biol Psychiatry 11:282-292.

Lalo U, Pankratov Y, Kirchhoff F, North RA, Verkhratsky A (2006) NMDA receptors mediate neuron-to-glia signaling in mouse cortical astrocytes. J Neurosci 26:2673-2683.

Langer J, Rose CR (2009) Synaptically induced sodium signals in hippocampal astrocytes in situ. J Physiol 587:5859-5877.

Laughlin SB (2001) Energy as a constraint on the coding and processing of sensory information. Curr Opin Neurobiol 11:475-480.

Levy LM, Warr O, Attwell D (1998) Stoichiometry of the glial glutamate transporter GLT-1 expressed inducibly in a Chinese hamster ovary cell line selected for low endogenous Na^+-dependent glutamate uptake. J Neurosci 18:9620-9628.

Lovatt D, Sonnewald U, Waagepetersen HS, Schousboe A, He W, Lin JH, Han X, Takano T, Wang S, Sim FJ, Goldman SA, Nedergaard M (2007) The transcriptome and metabolic gene signature of protoplasmic astrocytes in the adult murine cortex. J Neurosci 27:12255-12266.

Magistretti PJ (2006) Neuron-glia metabolic coupling and plasticity. J Exp Biol 209:2304-2311.

Magistretti PJ (2009) Neuroscience. Low-cost travel in neurons. Science 325:1349-1351.

Magistretti PJ, Chatton JY (2005) Relationship between L-glutamate-regulated intracellular Na^+ dynamics and ATP hydrolysis in astrocytes. J Neural Transm 112:77-85.

Magistretti PJ, Pellerin L, Rothman DL, Shulman RG (1999) Energy on demand. Science 283:496-497.

Matute C, Perez-Cerda F (2005) Multiple sclerosis: novel perspectives on newly forming lesions. Trends Neurosci 28:173-175.

Maxwell DS, Kruger L (1965) The Fine Structure of Astrocytes in the Cerebral Cortex and Their Response to Focal Injury Produced by Heavy Ionizing Particles. J Cell Biol 25:141-157.

Mitchell P (1979) Keilin's respiratory chain concept and its chemiosmotic consequences. Science 206:1148-1159.

Morgenthaler FD, Kraftsik R, Catsicas S, Magistretti PJ, Chatton JY (2006) Glucose and lactate are equally effective in energizing activity-dependent synaptic vesicle turnover in purified cortical neurons. Neuroscience 141:157-165.

Murphy E, Eisner DA (2009) Regulation of intracellular and mitochondrial sodium in health and disease. Circ Res 104:292-303.

Nedergaard M, Takano T, Hansen AJ (2002) Beyond the role of glutamate as a neurotransmitter. Nat Rev Neurosci 3:748-755.

Nicholls DG, Budd SL (2000) Mitochondria and neuronal survival. Physiol Rev 80:315-360.

Ouyang YB, Voloboueva LA, Xu LJ, Giffard RG (2007) Selective dysfunction of hippocampal CA1 astrocytes contributes to delayed neuronal damage after transient forebrain ischemia. J Neurosci 27:4253-4260.

Pawelczyk T, Olson MS (1995) Changes in the structure of pyruvate dehydrogenase complex induced by mono- and divalent ions. Int J Biochem Cell Biol 27:513-521.

Pellerin L, Magistretti PJ (1994) Glutamate uptake into astrocytes stimulates aerobic glycolysis: a mechanism coupling neuronal activity to glucose utilization. Proc Natl Acad Sci U S A 91:10625-10629.

Pellerin L, Magistretti PJ (2003) Food for thought: challenging the dogmas. J Cereb Blood Flow Metab 23:1282-1286.

Pellerin L, Pellegri G, Bittar PG, Charnay Y, Bouras C, Martin JL, Stella N, Magistretti PJ (1998) Evidence supporting the existence of an activity-dependent astrocyte-neuron lactate shuttle. Dev Neurosci 20:291-299.

Petravicz J, Fiacco TA, McCarthy KD (2008) Loss of IP_3 receptor-dependent Ca^{2+} increases in hippocampal astrocytes does not affect baseline CA1 pyramidal neuron synaptic activity. J Neurosci 28:4967-4973.

Pfrieger FW, Barres BA (1996) New views on synapse-glia interactions. Curr Opin Neurobiol 6:615-621.

Pierre K, Pellerin L (2005) Monocarboxylate transporters in the central nervous system: distribution, regulation and function. J Neurochem 94:1-14.

Pierre K, Magistretti PJ, Pellerin L (2002) MCT2 is a major neuronal monocarboxylate transporter in the adult mouse brain. J Cereb Blood Flow Metab 22:586-595.

Pierre K, Pellerin L, Debernardi R, Riederer BM, Magistretti PJ (2000) Cell-specific localization of monocarboxylate transporters, MCT1 and MCT2, in the adult mouse brain revealed by double immunohistochemical labeling and confocal microscopy. Neuroscience 100:617-627.

Pinton P, Rimessi A, Romagnoli A, Prandini A, Rizzuto R (2007) Biosensors for the detection of calcium and pH. Methods Cell Biol 80:297-325.

Pinton P, Brini M, Bastianutto C, Tuft RA, Pozzan T, Rizzuto R (1998) New light on mitochondrial calcium. Biofactors 8:243-253.

Pivovarova NB, Hongpaisan J, Andrews SB, Friel DD (1999) Depolarization-induced mitochondrial Ca accumulation in sympathetic neurons: spatial and temporal characteristics. J Neurosci 19:6372-6384.

Pivovarova NB, Pozzo-Miller LD, Hongpaisan J, Andrews SB (2002) Correlated calcium uptake and release by mitochondria and endoplasmic reticulum of CA3 hippocampal dendrites after afferent synaptic stimulation. J Neurosci 22:10653-10661.

Pivovarova NB, Nguyen HV, Winters CA, Brantner CA, Smith CL, Andrews SB (2004) Excitotoxic calcium overload in a subpopulation of mitochondria triggers delayed death in hippocampal neurons. J Neurosci 24:5611-5622.

Poburko D, Liao CH, Lemos VS, Lin E, Maruyama Y, Cole WC, van Breemen C (2007) Transient Receptor Potential Channel 6 Mediated, Localized Cytosolic [Na^+] Transients Drive Na^+/Ca^{2+} Exchanger Mediated Ca^{2+} Entry in Purinergically Stimulated Aorta Smooth Muscle Cells. Circ Res.

Porcelli AM, Ghelli A, Zanna C, Pinton P, Rizzuto R, Rugolo M (2005) pH difference across the outer mitochondrial membrane measured with a green fluorescent protein mutant. Biochem Biophys Res Commun 326:799-804.

Pozzo-Miller LD, Pivovarova NB, Leapman RD, Buchanan RA, Reese TS, Andrews SB (1997) Activity-dependent calcium sequestration in dendrites of hippocampal neurons in brain slices. J Neurosci 17:8729-8738.

Ramon y Cajal S (1913) Contribución al conocimiento de la neuroglia del cerebro humano. Trab Lab Invest Biol 11:255-315.

Rich P (2003) Chemiosmotic coupling: The cost of living. Nature 421:583.

Rieger A, Deitmer JW, Lohr C (2007) Axon-glia communication evokes calcium signaling in olfactory ensheathing cells of the developing olfactory bulb. Glia 55:352-359.

Rose CR, Ransom BR (1996) Mechanisms of H^+ and Na^+ changes induced by glutamate, kainate, and D-aspartate in rat hippocampal astrocytes. J Neurosci 16:5393-5404.

Rouach N, Koulakoff A, Abudara V, Willecke K, Giaume C (2008) Astroglial metabolic networks sustain hippocampal synaptic transmission. Science 322:1551-1555.

Serres S, Raffard G, Franconi JM, Merle M (2008) Close coupling between astrocytic and neuronal metabolisms to fulfill anaplerotic and energy needs in the rat brain. J Cereb Blood Flow Metab 28:712-724.

Simpson IA, Carruthers A, Vannucci SJ (2007) Supply and demand in cerebral energy metabolism: the role of nutrient transporters. J Cereb Blood Flow Metab 27:1766-1791.

Stavrianeas S, Silverstein T (2005) Teaching glycolysis regulation to undergraduates using an electrical power generation analogy. Adv Physiol Educ 29:128-130.

Tashiro M, Tursun P, Miyazaki T, Watanabe M, Konishi M (2006) Effects of intracellular and extracellular concentrations of Ca^{2+}, K^+, and Cl^- on the Na^+-dependent Mg^{2+} efflux in rat ventricular myocytes. Biophys J 91:244-254.

Tsacopoulos M, Magistretti PJ (1996) Metabolic coupling between glia and neurons. J Neurosci 16:877-885.

Ubl JJ, Chatton JY, Chen S, Stucki JW (1996) A critical evaluation of in situ measurement of mitochondrial electrical potentials in single hepatocytes. Biochim Biophys Acta 1276:124-132.

Verkhratsky A, Steinhauser C (2000) Ion channels in glial cells. Brain Res Brain Res Rev 32:380-412.

Volterra A, Meldolesi J (2005) Astrocytes, from brain glue to communication elements: the revolution continues. Nat Rev Neurosci 6:626-640.

Voutsinos-Porche B, Bonvento G, Tanaka K, Steiner P, Welker E, Chatton JY, Magistretti PJ, Pellerin L (2003) Glial glutamate transporters mediate a functional metabolic crosstalk between neurons and astrocytes in the mouse developing cortex. Neuron 37:275-286.

Wang W, Fang H, Groom L, Cheng A, Zhang W, Liu J, Wang X, Li K, Han P, Zheng M, Yin J, Mattson MP, Kao JP, Lakatta EG, Sheu SS, Ouyang K, Chen J, Dirksen RT, Cheng H (2008) Superoxide flashes in single mitochondria. Cell 134:279-290.

Wiederkehr A, Park KS, Dupont O, Demaurex N, Pozzan T, Cline GW, Wollheim CB (2009) Matrix alkalinization: a novel mitochondrial signal for sustained pancreatic beta-cell activation. EMBO J 28:417-428.

Witcher MR, Kirov SA, Harris KM (2007) Plasticity of perisynaptic astroglia during synaptogenesis in the mature rat hippocampus. Glia 55:13-23.

Witte ME, Bo L, Rodenburg RJ, Belien JA, Musters R, Hazes T, Wintjes LT, Smeitink JA, Geurts JJ, De Vries HE, van der Valk P, van Horssen J (2009) Enhanced number and activity of mitochondria in multiple sclerosis lesions. J Pathol 219:193-204.

Wyss-Coray T, Loike JD, Brionne TC, Lu E, Anankov R, Yan F, Silverstein SC, Husemann J (2003) Adult mouse astrocytes degrade amyloid-beta *in vitro* and *in situ*. Nat Med 9:453-457.

Wyss MT, Weber B, Treyer V, Heer S, Pellerin L, Magistretti PJ, Buck A (2009) Stimulation-induced increases of astrocytic oxidative metabolism in rats and humans investigated with 1-11C-acetate. J Cereb Blood Flow Metab 29:44-56.

Zhou N, Gordon GR, Feighan D, Macvicar BA (2010) Transient Swelling, Acidification, and Mitochondrial Depolarization Occurs in Neurons but not Astrocytes during Spreading Depression. Cereb Cortex.

Zhu D, Lai Y, Shelat PB, Hu C, Sun GY, Lee JC (2006) Phospholipases A2 mediate amyloid-beta peptide-induced mitochondrial dysfunction. J Neurosci 26:11111-11119.